VYSOKÉ UČENÍ TECHNICKÉ V BRNĚ

BRNO UNIVERSITY OF TECHNOLOGY

FAKULTA STAVEBNÍ
ÚSTAV STAVEBNÍ MECHANIKY

FACULTY OF CIVIL ENGINEERING

INSTITUTE OF STRUCTURAL MECHANICS

INVERSE PROBLEMS IN STRUCTURAL ENGINEERING SOLVED BY SOFT COMPUTING METHODS

HABILITAČNÍ PRÁCE

HABILITATION THESIS

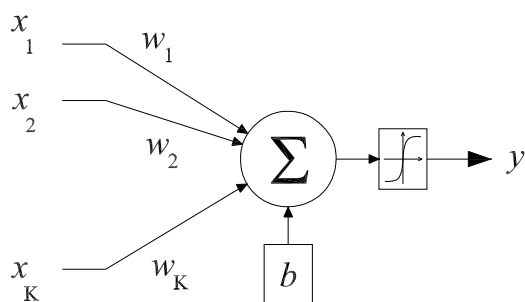AUTOR PRÁCE   DAVID LEHKÝ

AUTOR

BRNO 2016

Brno University of Technology

Faculty of Civil Engineering
Institute of Structural Mechanics

Inverse problems in structural engineering solved by soft computing methods

by

David Lehký

Habilitation thesis

Brno 2016

To my family.

Preface

This habilitation thesis deals with the utilization of soft computing methods in the solution of selected inverse problems from the civil and structural engineering fields. My interest in inverse analysis and artificial intelligence first started during my Ph.D. studies with the identification of material parameters based on the results of fracture tests. Since then, the developed basic methodology has been significantly improved and extended to other types of inverse problems, some of which are shown in this work.

Inverse problems are an integral part of a wide range of engineering tasks. The development of a generally applicable methodology for their solutions is therefore more than desirable. Artificial neural networks and genetic algorithms are very interesting soft computing models inspired by biological processes and natural evolution. A wide range of fascinating possibilities exists for their utilization, and in combination with traditional mathematical models and methods they can offer an efficient and powerful solution for many engineering tasks.

First of all I would like to express my gratitude to my colleagues and friends, namely Prof. Ing. Drahomír Novák, DrSc., Prof. Ing. Zbyněk Keršner, CSc., Assoc. Prof. Ing. Petr Frantík, Prof. Ing. Břetislav Teplý, CSc., and Assoc. Prof. Dr. Alfred Strauss for their valuable advice, the discussions we have had and the inspiration they have provided for my work. I also owe thanks to Ing. Martina Šomodíková, Ph.D., Ing. Ondřej Slowik, Bc. Martin Lipowczan, Bc. Petra Jonášová, Ing. Jiří Doležel, and many other colleagues and students from the Institute of Structural Mechanics for their help and cooperation in carrying out research and teaching activities. My deepest obligation is to my family for their love and support.

David Lehký

Brno University of Technology
Brno, September 2016

Inverse problems in structural engineering solved by soft computing methods

Ing. David Lehký, Ph.D.

Brno University of Technology, Brno

Abstract

The habilitation thesis introduces a general methodology for solving inverse problems and presents its utilization while dealing with selected tasks from civil and structural engineering – inverse reliability problems, structural damage detection, and the identification of material model parameters. The proposed methodology combines an artificial neural network-based surrogate model with a small-sample simulation method utilized for the efficient stochastic preparation of the network training set. During its development, special emphasis was placed on the implementation of the most effective and powerful methods, models and procedures with respect to its primary focus on time-consuming tasks solved via nonlinear finite element method analysis. The successful solution of these tasks required the development and integration of several software tools, such as a general-purpose tool for working with artificial neural networks, and also programs with a specific focus on individual inverse problems. The proposed methodology was verified on a number of numerical examples, both theoretical ones obtained from the available literature as well as examples of real structures. The results were evaluated and discussed together with the advantages and disadvantages of the methodology and its utilization in solving the specified types of inverse problems. At the end of the thesis, suggestions are made regarding the possibilities for future development.

Contents

vi

Chapter 1

Introduction

Inverse problems can be found in various forms in civil and structural engineering. This work presents three specific inverse problems – (1) the identification of design parameters that enable the attainment of a desired reliability level defined by reliability indicators; (2) damage detection based on changes in structural vibration; and (3) the identification of fracture–mechanical parameters based on the results of laboratory tests. Other typical inverse problems include, e.g. identification of the size and shape of a fracture process zone via the analysis of strain wave signals measured by acoustic emission sensors (e.g. Kral et al. [34]), identification of load action based on the measured structural response (e.g. Lehký [41]), etc.

A common feature of all inverse problems is generally the search for the input parameters of the system $\mathbf{X}$ based on the given responses $\mathbf{Y}$ while the forward relationship between the input data (parameters) and output data (response) is often known. This can take the form of an analytical or numerical model which describes the input–output relationship and allows comparison of the numerical and real response.

$$\mathbf{Y} = f(\mathbf{X}). \tag{1.1}$$

Determination of the inverse relationship

$$\mathbf{X} = f^{-1}(\mathbf{Y}) \tag{1.2}$$

is usually very difficult or practically impossible. One example of complicated functional dependence is the utilization of nonlinear finite element method (FEM) modeling, in which the functional relationship between the input and output data is given in implicit form. In the proposed methodology which is discussed in this work, instead of finding the original inverse function (1.2) a surrogate model is created in the form of an artificial neural network (ANN):

$$\mathbf{X} = f_{\text{ANN}}^{-1}(\mathbf{Y}). \tag{1.3}$$

The main advantages of employing an ANN are its robustness, extensibility and ability to adapt to new conditions. Theoretical details regarding artificial neural networks are described in Section 1.2.

The structure of the habilitation thesis is as follows. With the exception of the introduction and conclusions it consists of three main parts related to analyzed inverse problems – inverse reliability analysis, damage detection, and fracture–mechanical parameter determination.

Chapter 2 introduces inverse reliability analysis. It can be categorized as structural design, i.e. the identification of design parameters that enable the achievement of the desired reliability described by reliability indicators related to particular limit states. Here, the parameters to be identified are deterministic or random design parameters related to the structure itself, the acting load or the surrounding environment. The known (in this case desired) response is the safety level described by reliability indicators. As shown in the application section, the functional relationship between design parameters and reliability indicators can take the form of an analytical formulation or a stochastic nonlinear FEM model.

The proposed methodology has been verified and applied to various classes of inverse reliability problems. Selected examples with *a priori* known results taken from the literature were utilized for basic verification. The presented examples included both linear and nonlinear cases with single as well as multiple design parameters, and with independent basic random variables as well as random variables with prescribed statistical correlations. After verification, the proposed methodology was utilized in the structural design of a reinforced concrete slab and for the determination of uncertain design parameters of an existing prestressed concrete bridge.

Chapter 3 is focused on damage detection in dynamically loaded structures. The aim is to detect damage in the structure, localize it and identify its size. From the dynamic point of view, the cracking/crushing of concrete or rupture of reinforcement/prestress tendons leads to changes in the stiffness of the affected structural part. Damage detection therefore means the identification of stiffness distribution along the structure and its comparison with the original stiffness. The response of the structure is expressed by changes in structural vibration. The functional relationship between structural stiffness and the corresponding dynamic response is often modeled by a multi-degree-of-freedom system and subsequent modal analysis.

Since the type of input information (dynamic response) is very important for successful damage identification, the influence of local decreases in stiffness on modal properties (eigenfrequencies and mode shapes) was studied using both experimental measurements and numerical analyses. Subsequently, damage identification was carried out for selected simple beams and for the Z24 Bridge in Switzerland.

Chapter 4 describes the procedure of material parameter identification using experimental data from fracture tests. Here, the aim of identification is to acquire a set of selected fracture–mechanical parameters describing the quasi-brittle behavior of concrete, including crack initiation and propagation. In this case, the known

response is represented by a load vs. deflection or load vs. crack mouth opening displacement diagram recorded during specimen testing. The functional relationship between the structural and material parameters and the above-mentioned response is given in the form of a nonlinear FEM model of the tested specimen.

The proposed methodology and developed software were utilized for the evaluation of the fracture–mechanical parameters of specimens manufactured from standard concrete types of various strength classes as well as of several concrete mixtures in which Portland cement was partially or fully replaced with low-calcium fly-ash. The determination of the statistical characteristics of fracture–mechanical parameters is also presented.

Since the procedures needed to deal with all the above-mentioned inverse problems are time-consuming and demanding in terms of data manipulation, several software tools have been developed to automate the whole process. In Chapter 5 all of the individual software tools developed by the author are briefly described.

1.1 Goals and objectives

The specific goals of this habilitation thesis were set as follows:

1. Development of a general methodology for solving arbitrary inverse problems in civil and structural engineering. The proposed methodology should respect all important aspects related to the analyzed problems, those mainly being the time and computational demands of structural analyses. It should be robust, reliable and efficient, and should incorporate advanced models and methods in order to provide sufficiently accurate results.

2. Modification and adjustment of the proposed methodology, and its application to selected inverse problems associated with structural design, damage detection, load-bearing capacity and reliability assessment.

3. Development of software tools allowing the analysis of inverse problems to be automated.

4. Verification of the applicability and effectiveness of the proposed methodology and software tools; discussion of their advantages and disadvantages.

1.2 Artificial neural networks

A cornerstone of the proposed methodology for solving inverse problems is the use of an artificial neural network, which can be classified as a soft computing method. Soft computing, as defined by Zadeh [89], is a collection of methodologies which aim to exploit tolerance for imprecision, uncertainty and partial truth so as to achieve

tractability, robustness and low solution cost. The principal constituents of soft computing are fuzzy logic, neural computing, evolutionary computation, machine learning and probabilistic reasoning, with the latter incorporating belief networks, chaos theory and parts of learning theory. Soft computing is a partnership in which each of the partners contributes a distinct methodology for addressing problems in its domain. From this perspective, the principal constituent methodologies in soft computing are complementary rather than competitive.

In contrast to analytical methods, soft computing methodologies mimic consciousness and cognition in several important respects: they can learn from experience; they can universalize into domains where direct experience is absent; and, through parallel computer architectures that simulate biological processes, they can perform mapping from inputs to outputs faster than inherently serial analytical representations. The trade-off, however, is a decrease in accuracy. If a tendency towards imprecision could be tolerated, then it should be possible to extend the scope of such applications even to those problems where analytical and mathematical representations are readily available.

Soft computing differs from conventional (hard) computing in many ways. For example, as mentioned above, soft computing exploits tolerance of imprecision, uncertainty, partial truth, and approximation. In effect, the role model for soft computing is the human mind. In this work, in addition to the use of artificial neural networks, which are described in detail in this section, genetic algorithms (GA) and evolution strategies (ES) are utilized as powerful optimization techniques employed for ANN training in DLNNET software; see Chapter 5.

An artificial neural network (e.g. Cichocki and Unbehauen [7]) is a mathematical model inspired by biological neural networks (Figure 1.1). Generally speaking, an ANN is an information or signal processing system composed of a large number of simple processing elements, called artificial neurons (or nodes). These are interconnected by direct links called connections and cooperate to perform parallel distributed processing in order to solve a desired computational task. One of the attractive features of ANNs is their ability to adapt themselves to special environmental conditions by changing their connection strengths or structure.

In the proposed ANN-based inverse reliability method a feed-forward multi-layer network type is used. In this type of network artificial neurons are organized into different layers and the information only moves in the forward direction: data leaves the input nodes and passes through hidden nodes (if any) to the output nodes (Figure 1.2). Such a network is a great mathematical tool for modeling complex relationships between inputs and outputs. The output from a single neuron can be calculated as:

$$y = f(u) = f(\sum_k (w_k x_k + b)), \tag{1.4}$$

where k indicates the input number, w_k is the synaptic weight of the connecting path
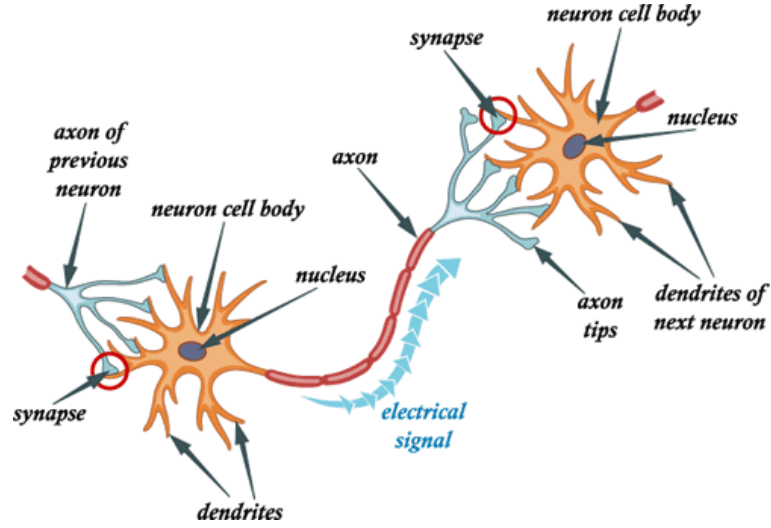
Figure 1.1: Schematic structure of a biological neuron (adopted from [51])

from the kth neuron of previous layer, x_k is the input signal coming from the kth neuron of previous layer, b is the bias of the neuron and f is the transfer function of the neuron; see Figure 1.3. If the output of the whole ANN is required, the outputs of all previous layers must be calculated layer by layer starting from the input layer. The output of the kth neuron in the uth layer of the network is:

$$y_k^u = f^u \left(\sum_{j=1}^J (w_{kj}^u y_j^{u-1}) + b_k^u \right) = f^u \sum_{j=1}^J (x_j^u), \qquad (1.5)$$

where w_{kj}^u is the synaptic weight of the connection between the kth neuron in the uth layer (current) and the jth neuron in the $(u-1)$th layer (previous), y_j^{u-1} is the output of jth neuron in the previous layer, b_k^u is the bias of the kth neuron in the current layer, and f^u is the transfer function of the current layer. If the current layer u is the last one then the vector $\mathbf{y}^u$ is the output vector of the ANN.

1.2.1 ANN training

The behavior of an ANN is determined by its structure (i.e. the number of hidden layers and the corresponding number of neurons), the types of transfer functions and the values of synaptic weights and biases. The later parameters are adjusted during the training process. A feed-forward type network is trained using "supervised" learning, where a set of example pairs of inputs and corresponding outputs (x, y), $x \in \mathbf{X}$, $y \in \mathbf{Y}$ is introduced to the network. The aim of the subsequent optimization procedure is to find a neural network function $f_{\text{ANN}} : \mathbf{X} \to \mathbf{Y}$ in the allowed class of functions that matches the examples. This is performed by minimizing the following
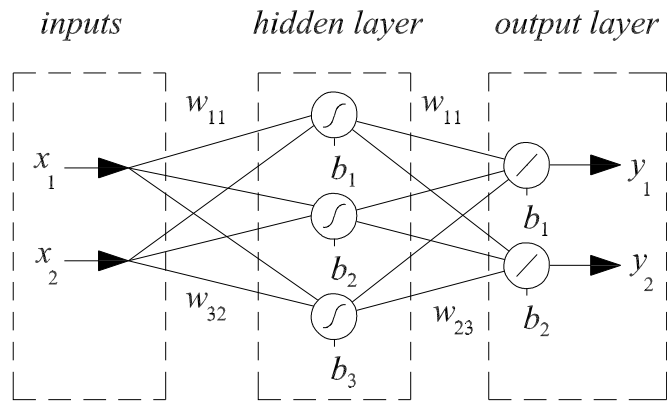
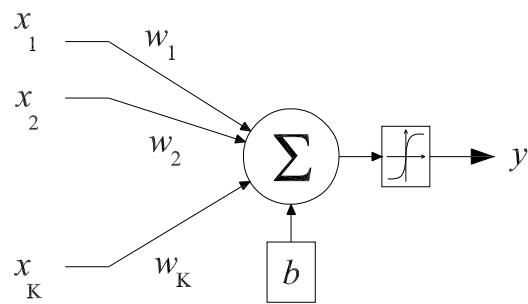Figure 1.2: Diagram of a feed-forward multi-layer network

Figure 1.3: Diagram of a single neuron

error function:

$$E = \frac{1}{2} \sum_{i=1}^{N} \sum_{k=1}^{K} (y_{ik}^{\mathrm{o}} - y_{ik}^{\mathrm{t}})^2,$$ (1.6)

where N defines the size of the training set, y_{ik}^{t} is the desired (target) output of the kth output neuron for the ith input signal and y_{ik}^{o} is the real output of the same neuron for the same input signal, which depends on the current network parameters. In the proposed inverse method, the Latin hypercube sampling simulation technique is used for the efficient preparation of the training set (Section 1.3). ANN training is an optimization task which can be solved via an appropriate minimization method.

Minimization algorithms can be classified into two types: local minimization and global minimization. Local minimization algorithms such as gradient descent and Newton's methods are fast but usually converge to local minima. In contrast, global minimization algorithms have strategies to help the search escape from local minima. Local minimization algorithms mainly have difficulties when the surface is flat (the gradient is close to zero), when there is a large range of gradients, or when the surface is very rugged. To overcome the deficiencies in local search methods, global minimization methods have been developed. These methods rely on local searches to determine local minima, and focus on bringing the search out of a local minimum once it gets there. Global algorithms can be classified as being either deterministic or probabilistic. Deterministic methods include covering, trajectory and penalty methods. These methods do not work well when the problem has more than a few variables. Probabilistic methods include clustering methods, random search methods and methods based on stochastic models. Some of these algorithms, especially genetic algorithms, have been found to work well for ANN training problems.

Genetic algorithms were combined with gradient descent methods for the purpose of training all the ANNs mentioned later in this work. Genetic algorithms are powerful global optimization tools. They were used here to avoid local minima and get as close as possible to the region near the global minimum. Subsequently, the gradient descent method was used to quickly find the global minimum in order to speed up the optimization process. For more details on the gradient descent method see, e.g. Cichocki and Unbehauen [7], Gurney [18]; a description of genetic algorithms can be found in Spall [77].

1.2.2 ANN structure

An important step before the training process begins is the design of an appropriate ANN structure, which is generally dependent on the type of inverse task to be solved. The number of inputs to the ANN, N_{inp}, and the number of output neurons, N_{out}, are known in advance and are related to the analyzed problem. The number of hidden layers and the number of neurons in them are other parameters of the ANN.

According to Kolmogorov's theorem [35], two hidden layers with a sufficient number of neurons are enough to compute any reliability task. The best practice is to start with one hidden layer. If the neural network cannot be trained, then a second hidden layer is added. The number of neurons in the ith hidden layer, $N_{i,\text{hidden}}$, needs to be adjusted according to the problem being solved, and in most cases it is necessary to "experiment" with them and to check the convergence during the training process (optimization task). As a first rough estimate, the following equation for a neural network with one hidden layer can be used:

$$N_{\text{hidden}} = \sqrt{N_{\text{inp}} N_{\text{out}}}. \tag{1.7}$$

The number of neurons in the first and second layer of the neural network with two hidden layers can be estimated as:

$$N_{1,\text{hidden}} = N_{\text{out}} \left(\sqrt[3]{\frac{N_{\text{inp}}}{N_{\text{out}}}} \right)^2, N_{2,\text{hidden}} = N_{\text{out}} \left(\sqrt[3]{\frac{N_{\text{inp}}}{N_{\text{out}}}} \right). \tag{1.8}$$

1.2.3 Transfer functions

The performance and usability of a particular ANN also depends on the choice of transfer (activation) functions. The early McCulloch-Pitts neuron model only used the **binary (hard-limiting) function**:

$$y = f(u) = \begin{cases} -1(0) & \text{for } u \leq 0 \\ 1 & \text{for } u > 0 \end{cases} \tag{1.9}$$

The greatest advantage of using binary elements is the high speed of computation. Generally, the hard-limit function can be replaced by more general linear or nonlinear functions and consequently the output of the neuron can either assume one value from a discrete set (e.g. $\{-1, 1\}$) or vary continuously (e.g. between -1 and 1 or generally between y_{min} and y_{max}). The **linear transfer function** can be described as:

$$y = f(u) = au, \tag{1.10}$$

where a is a positive constant which controls the "steepness" of the function. Typically, a nonlinear function is a monolithically increasing sigmoid (S-shaped) function. The **hyperbolic tangent function** can be used to obtain a symmetrical (bipolar) representation:

$$y = f(u) = \tanh au = \frac{1 - e^{-2au}}{1 + e^{-2au}}. \tag{1.11}$$

If an unsymmetrical unipolar representation is required, the **logistic function** can be employed:
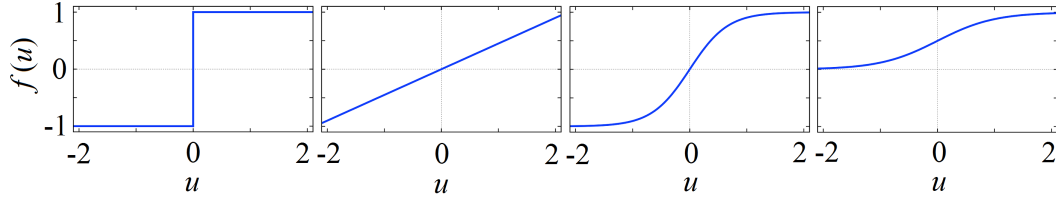
Figure 1.4: Typical transfer functions used in artificial neural networks: hard-limit, linear, hyperbolic tangent, logistic

$$y = f(u) = \frac{1}{1 + e^{-au}}. \tag{1.12}$$

The aforementioned types of transfer functions are depicted in Figure 1.4

1.3 Small-sample simulation

In all three engineering problems described in this work time-consuming calculations need to be performed. Even with the increasing speed of computers and the possibilities offered by parallel computing, efficient techniques must be employed in order to reduce computational effort. For time-consuming stochastic calculations, small-sample simulation techniques based on stratified sampling of the Monte Carlo type represent a rational compromise between feasibility and accuracy. Because of this, Latin Hypercube Sampling (McKay et al. [53], Novák et al. [57]), which today is well known, has been selected as a key fundamental technique. LHS can be categorized as an advanced stratified sampling method, i.e. a method which results in a very good estimate of statistical moments of response if small-sample simulation is used. More precisely, LHS is considered to be a variance reduction technique because it yields statistical moment estimates with a lower variance compared to crude Monte Carlo sampling for the same sample size; see e.g. Koehler and Owen [32]. This is the reason the technique has become very attractive when dealing with computationally intensive problems such as complex finite element simulations.

The basic feature of LHS is that the region of each random variable X_i is divided into N_{sim} intervals (N_{sim} is the number of simulations) of equal probability, indexed by $k = 1, ..., N_{\text{sim}}$, in consistency with the corresponding distribution function F_i; see Figure 1.5. This is achieved by dividing the unit probability interval into N_{sim} probability intervals of identical length. There are several alternative ways of selecting the sample values from these intervals. The most commonly used strategy is to select the median of each unit probability interval. Its sampling probability is:

$$p_k = \frac{k - 0.5}{N_{\text{sim}}}. \tag{1.13}$$
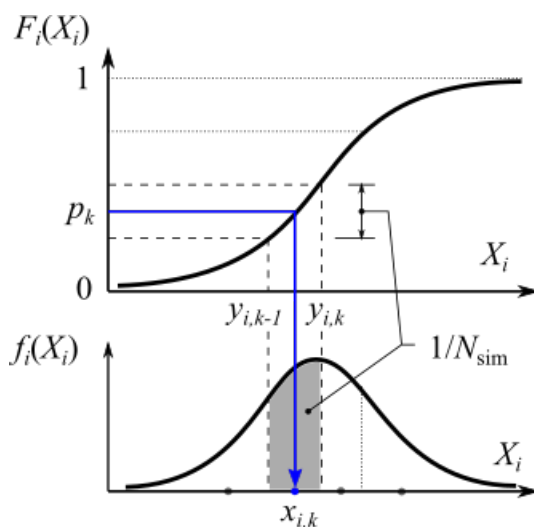
Figure 1.5: Sample value selection from the probabilistic means of the intervals

The second option is to generate a random sampling probability for each unit probability interval:

$$p_k = \frac{i - 1 + rand(0,1)}{N_{\text{sim}}}. \tag{1.14}$$

The samples of arbitrary continuously distributed variable X_i are then selected using the inverse transformation of the probabilities:

$$x_{i,k} = F_i^{-1}(p_k). \tag{1.15}$$

The third option for selecting the sample values is the approach suggested in Keramat and Kielbasa [30] and Hungtington and Lyrintzis [24], where the representative value of each interval is its mean value (interval centroid, see the shaded area in Figure 1.5):

$$x_{i,k} = \frac{\int_{y_{i,k-1}}^{y_{i,k}} x f_i(x) \mathrm{d}x}{\int_{y_{i,k-1}}^{y_{i,k}} f_i(x) \mathrm{d}x} = N_{sim} \int_{y_{i,k-1}}^{y_{i,k}} x f_i(x) \mathrm{d}x. \tag{1.16}$$

Here, f_i is the probability density function of variable X_i, and the integration limits are:

$$y_{i,k} = F_i^{-1}\left(\frac{k}{N_{\text{sim}}}\right), \quad k = 1, ..., N_{\text{sim}}. \tag{1.17}$$

The average of samples $x_{i,k}$ generated according to Equation (1.16) exactly equals the mean value of the variable X_i: the variance of the sample set is much closer to
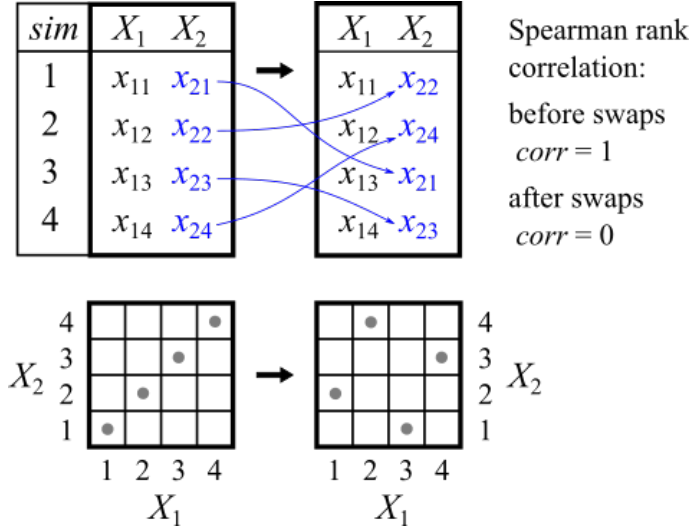
Figure 1.6: Illustration of sampling plans for two random variables and four simulations – Left: Original plan with undesired correlation between variables; Right: Updated plan after sample swaps determined by a simulated annealing algorithm

the target variance compared with other selection schemes; see Vořechovský and Novák [86].

The generated samples form a *sampling plan*: a matrix of the dimensions $N_{\text{sim}} \times N_{\text{var}}$ (N_{var} is the number of variables); see an example sampling plan diagram for two random variables and four simulations in Figure 1.6. At the beginning of the process, sample values from Equations (1.15) and (1.16) are sorted in ascending order, which leads to undesired correlation between variables. To diminish it, the mutual ordering of the samples must be changed; see the illustration of swaps in Figure 1.6. A common procedure is to use random permutations of the samples, though this method has been shown to deliver relatively large errors in correlation with small sample sizes (Vořechovský [84]). Vořechovský and Novák [86] therefore proposed a combinatorial optimization algorithm based on simulated annealing. Its aim is to minimize the difference between the target correlation matrix, $\mathbf{T}$, and the actual correlation matrix, $\mathbf{A}$, which is estimated from the generated samples. The difference between these two matrices can be quantified by a suitable matrix norm. This matrix norm can be minimized by changing the mutual ordering of the samples in the sampling plan.

Due to the stratification principle of the LHS method, the addition of new sample subsets to an existing set is problematic. This is a disadvantage of this method compared to the crude Monte Carlo method. In many analyses it is impossible to determine the sample size needed to provide adequate data *a priori*. A small sample size may not give acceptable results, while a large sample size may not be feasible

from the point of view of time. Consequently, the ability to extend and refine the
design of an experiment without needing to discard the results of the previous sample
set(s) may be important. Vořechovský [85] proposed the concept of the hierarchical
Latin hypercube sampling method (HLHS). In this method, the previously selected
sampling probabilities from Equation (1.13) constitute the parent subset, $\mathbf{p}_{\text{old}}$. Its
child subset, $\mathbf{p}_{\text{add}}$, is constructed in such a manner that each sampling probability
of $\mathbf{p}_{\text{old}}$ will "generate" t offspring sampling probabilities. The additional subsets
themselves are not LH-samples. However, if such a subset is combined with the
previous subset, one obtains an exact LH-sample set, $\mathbf{p}_{\text{tot}}$:

$$\mathbf{p}_{\text{tot}} = \mathbf{p}_{\text{old}} \cup \mathbf{p}_{\text{add}}. \tag{1.18}$$

This means that new sampling probabilities are added in such a way that the
aggregated vector of sampling probabilities will form a regular grid. The total sample
size of one refinement is:

$$N_{\text{sim}} = N_{\text{old}} + N_{\text{add}} = (t+1)N_{\text{old}}, \tag{1.19}$$

where t is a positive even integer and denotes the refinement factor with the smallest
possible value equal to two. The total sample size is then $N_{\text{sim}} = 3N_{\text{old}}$. The new
subset of sampling probabilities, $\mathbf{p}_{\text{add}}$, is obtained from Equation (1.13), excluding
those that were already used in subset $\mathbf{p}_{\text{old}}$, i.e. indices $k = 1, ..., N_{sim}$ that follow
the equality

$$(k-1) \bmod (t+1) = t/2 \tag{1.20}$$

must be ignored. Here, "mod" is the modulo operation, which finds the remainder
after the division of one number by another. For $t = 2$, the following indices are
skipped: $k = 2, 5, 8, 11, 14, ...$ The new sampling probabilities are then used in
Equation (1.15) to obtain the additional sample set. The optimal reordering of the
additional sample set for each random variable is achieved via application of the
above-mentioned combinatorial optimization algorithm described in Vořechovský
and Novák [86]. The only difference is that mutual ordering can only be changed
for the new sampling points.

Chapter 2

Inverse reliability analysis

To achieve desired level of reliability in limit state design is generally not an easy task. Uncertainties are involved in every part of structural system (e.g. material properties, geometrical imperfections, dead load, live load, wind, snow, corrosion rate, etc.). Traditional approaches simplified the problem by considering the uncertain parameters to be deterministic, and accounted for the uncertainties through the use of empirical safety factors. These are usually derived based on the past experience. But, they cannot guarantee required reliability level; they do not provide information on the influence of individual parameters on reliability. Also it is difficult (almost impossible) to design structures with uniform reliability levels among components.

When performing either reliability assessment or advanced engineering design, it is essential to take uncertainties into account using a probabilistic analysis. Reliability assessment requires forward reliability methods for estimating the reliability. On the other hand, the engineering design requires an inverse reliability approach to determine the design parameters to achieve desired target reliabilities.

A "trial and error" procedure is generally used to determine the values of design parameters related to the design of particular limit states (both ultimate and serviceability, according to current standards). Design parameters (material properties, geometry, etc.) are changed step by step in order to satisfy specified limit states. This problem leads to the use of optimization methods. The task of achieving target reliability levels, expressed by theoretical failure probabilities or reliability indices, is much more difficult. The reliability problem is generally described by the limit state function and basic random variables. Design parameters can be deterministic or they can be associated with random variables described by statistical moments and a suitable model of probability distribution function (PDF). They affect the theoretical failure probability – a reliability indicator which cannot be easily calculated and requires an approximation method or the application of simulation techniques. The "trial and error" approach can also be used for the task of achieving target

reliability levels, but its shortcomings are obvious.

While forward reliability methods have been applied widely and successfully in reliability engineering in various fields, inverse reliability approaches have not received the same degree of both attention and application, although they are particularly useful due to their important role in engineering design. The reason is that they are mathematically much more difficult – it is necessary to amalgamate forward reliability methods with other mathematical approaches of the optimization type. Inverse reliability problems appear when, for example:

1. Target reliability is specified in a design (ultimate and/or serviceability limit states). In this case, the design parameters must be determined to achieve the given reliability level.

2. Reliability-based design code is being calibrated. Code design procedures usually include performance and load safety factors, which are used to account for uncertainties and to produce a design with the desired reliability. To achieve this objective, the performance and load factors may be calculated using the inverse reliability approach.

3. A target quality is specified for a manufactured product. Several design parameters in the manufacturing process, ranging from material properties to process implementation, may have to be obtained in order to ensure that the processed product meets a pre-specified quality or tolerances with a desired reliability.

Some sophisticated approaches have been proposed that are termed "inverse reliability methods". Reliability calculation is usually based on approximation methods like the first order reliability method (FORM) as these inverse techniques require repetitive calculation of reliability – and calculation of reliability even by advanced simulation techniques of the Monte Carlo type is generally extremely time-consuming. Therefore FORM, originally proposed by Hasofer and Lind [19], is a very feasible alternative for inverse reliability tasks despite its inaccuracy for highly nonlinear problems.

Winterstein et al. [88] were probably the first to overcome the tedious "trial and error" method; they suggested a more efficient solution based on a reliability contour method where only one parameter was treated as a deterministic design variable. Der Kiureghian et al. [13] proposed an iterative algorithm based on the modified Hasofer–Lind–Rackwitz–Fiessler scheme used in reliability analysis. A direct algorithm for the single-parameter inverse problem using a Newton–Raphson iterative algorithm to find multiple design parameters was proposed by Li and Foschi [48], [49]. This general technique could solve inverse reliability problems with multiple design points and constraints and the design parameters could be treated as random variables too. Sadovský [67] proposed the improvement of the algorithm

in the sense of improving the convergence of the design parameter. Minguez et al. [55] used a decomposition technique to solve inverse reliability problems; the proposed algorithm detects unsolvable cases and the existence of infinite solutions. An inverse reliability strategy that uses percentile performance was proposed by Sherali and Ganesan [71].

An artificial neural network-based (ANN) version of FORM was proposed by Cheng et al. [26]. The authors utilized ANN to approximate the limit state function first and then FORM was used for the ANN approximation obtained. The paper only shows single design parameter cases. An extension and investigation of two implicit response surface functions with respect to their efficiency regarding inverse reliability problems was performed by Cheng and Li [27]. An ANN methodology based on an evolutionary learning process was developed by António and Hoffbauer [1].

The methodology proposed in this work attempts to overcome the shortcomings of existing inverse reliability methods. It utilizes ANN too, but in a different way: Computational time is reduced by using a small-sample LHS simulation technique in ANN-based inverse problem proposed by Novák and Lehký [58], Lehký and Novák [37].

2.1 Problem definition

2.1.1 Reliability problem formulation

Classical reliability theory introduces the basic concept of structural reliability more formally, treating it as a response variable (e.g. deflection, stress, ultimate capacity, etc.) or safety margin Z (in the case that the function expresses a failure condition) which is the function of basic random variables $\mathbf{X} = X_1, X_2, \ldots, X_n$ (or random fields):

$$Z = g(X_1, X_2, ..., X_n), \tag{2.1}$$

where the function $g(\mathbf{X})$ represents a functional relationship between elements of vector $\mathbf{X}$ (computational model). Elements of vector $\mathbf{X}$ can be statistically correlated. If $g(\mathbf{X})$ represents a failure condition then it is called the limit state function or the performance function. The structure is considered to be safe if:

$$Z = g(\mathbf{X}) = g(X_1, X_2, ..., X_n) > 0. \tag{2.2}$$

The limit state function can be an explicit or implicit function of basic random variables and it can take a simple or rather complicated form. Usually, the convention is that it takes a negative value if a failure event occurs; $Z \leq 0$, and the survival event is defined as $Z > 0$. The performance of the system and its components is described considering a number of limit states (multiple limit state functions). The aim
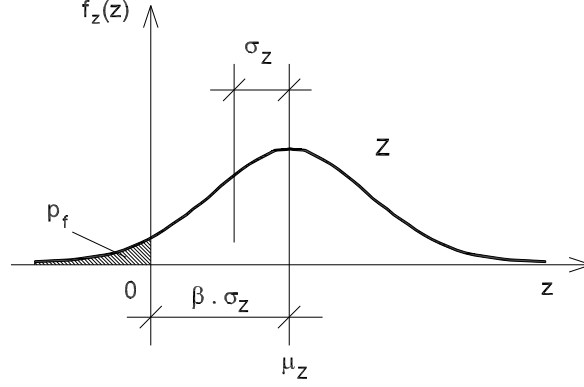
Figure 2.1: Safety margin, failure probability and Cornell's reliability index

of reliability analysis is the estimation of unreliability using a probability indicator called the theoretical failure probability, defined as:

$$p_\mathrm{f} = \mathrm{P}(Z \leq 0). \tag{2.3}$$

More formally, this probability is defined as:

$$p_\mathrm{f} = \int_{D_\mathrm{f}} f_\mathbf{X}(\mathbf{X}) \,\mathrm{d}\mathbf{X}, \tag{2.4}$$

where the domain of integration is limited to the failure domain D_f where $g(\mathbf{X}) \leq 0$, $f_\mathbf{X}(\mathbf{X})$ is the joint probability density function of basic random variables (and also of other, deterministic quantities), and in general, its marginal variables can be statistically correlated. The explicit calculation of integral in Equation (2.4) is generally impossible. Therefore a large number of efficient stochastic analysis methods have been developed during the last decades.

For practical calculations failure probability p_f can be substituted by the reliability index β, which makes the inverse reliability problem numerically more feasible to solve. The variable safety margin in the original space of random variables is shown in Figure 2.1.

2.1.2   Inverse reliability problem formulation

The inverse reliability problem is the problem to find design parameters corresponding to specified reliability levels expressed by reliability index or by theoretical failure probability. In general, an inverse problem involves finding either a single design parameter to achieve a given single reliability constraint or multiple design parameters to meet specified multiple reliability constraints. The design parameters can be deterministic or they can be associated with random variables. Therefore, we include in addition to the vector of basic random variables $\mathbf{X} = X_1, X_2, \ldots, X_i, \ldots, X_n$ the

Table 2.1: Design parameters alternatives

Variable	Deterministic	Random	
		Mean	CoV
d_1	?	–	–
r_1	–	?	prescribed
r_2	–	prescribed	?
r_3, r_4	–	?	?

Note: d_1 is deterministic design parameter, $r_1 - r_4$ are
design parameters associated with random variables.

vector of design deterministic parameters $\mathbf{d} = d_1, d_2, \ldots, d_k, \ldots, d_p$ and the vector of the design parameters of random variables $\mathbf{r} = r_1, r_2, \ldots, r_l, \ldots, r_q$. Note that the design parameters of random variables can be statistical moments of the first and/or second order. To consider higher statistical moments as design parameters is mathematically possible but useless from the practical point of view. In case of mean value one need to choose if either standard deviation or coefficient of variation will be fixed.

In the case of multiple limit states we have several safety margins Z_j and target failure probabilities $p_{\mathrm{f},j}$ or reliability indices β_j, where $j = 1, 2, ..., m$ is number of limit state functions. The inverse problem can be stated generally as:

$$
\begin{aligned}
\text{Given}: &\quad p_{\mathrm{f},j} \text{ or } \beta_j \\
\text{Find}: &\quad \mathbf{d} \text{ or/and } \mathbf{r} \\
\text{Subject to}: &\quad Z_j = g(\mathbf{X}, \mathbf{d}, \mathbf{r})_j = 0, \text{ for } j = 1, 2, ..., m.
\end{aligned}
\tag{2.5}
$$

Table 2.1 shows alternatives which can occur for one variable (deterministic or random); design parameters to be found are marked by question mark.

2.2 ANN-based inverse reliability method

A general soft computing-based inverse method is proposed and applied for solving inverse reliability problem, which aim is determination of the design parameters in order to achieve the prescribed reliability level. The inverse analysis is based on the coupling of a stratified LHS simulation method and an ANN. ANN, as a cornerstone of the method, is used as a surrogate model of unknown inverse function describing relation between the design parameters and corresponding reliability indicators.

$$
\mathbf{P} = f_{\mathrm{ANN}}^{-1}(\mathbf{I}),
\tag{2.6}
$$

where $\mathbf{P} = \mathbf{d} \cup \mathbf{r}$ is the vector of all design parameters (deterministic and random ones) and $\mathbf{I} = \boldsymbol{\beta} \vee \mathbf{p_f}$ is the vector of reliability indicators.

ANN has already been used for inverse reliability problems by some authors (Shayanfar et al. [70]; Cheng et al. [26]). A novelty of the approach suggested here is the utilization of the efficient small-sample simulation method LHS (see Section 1.3) used for the stochastic preparation of the training set utilized in training the ANN. For that purpose, the design parameters (e.g. mean values or standard deviations of selected random variables) are considered as random variables with a scatter reflecting the physical range of design values. Subsequently, the calculation of reliability is performed using appropriate simulation or approximation method, e.g. FORM. Once the ANN has been trained, it represents an approximation consequently utilized in a following way: To provide the best possible set of design parameters corresponding to prescribed reliability. The whole procedure is illustrated by a simple flow chart as shown in Figure 2.2 and is implemented as follows:

1. The limit state functions $g(\mathbf{X}, \mathbf{P})_j$ have to be defined first. This can be done at the level of explicitly defined formula or at the level of a computational model using the appropriate FEM software. The functions have to be approximately calibrated via "trial and error" procedure using design parameters $\mathbf{P}$; the initial calculation uses a set of the initial design parameters resulting in a rough agreement with the target reliability indicators $\mathbf{I}$. An initial estimation of the design parameters has to be made based on engineering judgment and computational simulation. The parameters are estimated only roughly and therefore identification should follow as the next step.

2. Design parameters are considered as random variables described by a probability distribution; the rectangular distribution is a "natural choice" as the lower and upper limits represent the bounded range of the physical existence of design parameters. However, other distributions can also be used, e.g. Gaussian. Random realizations of design parameters are generated using LHS simulation method (see vector $\mathbf{P}$ in Figure 2.3).

3. A multiple calculation of reliability indicators related to the limit state functions using random realizations of design parameters is performed and a statistical set of the reliability indicators $\mathbf{I}$ is obtained (see Figure 2.3). Note that the selection of an appropriate number of simulations is driven by many factors, mainly by the complexity of the problem (computational demands), the structure of the neural network and the variability of design parameters. No general rule can be therefore suggested.

4. Random realizations $\mathbf{P}$ (outputs of ANN) and the random responses – reliability indicators related to the limit states $\mathbf{I}$ (inputs of ANN) – serve as the basis for the training of an appropriate ANN. This key point of the whole procedure
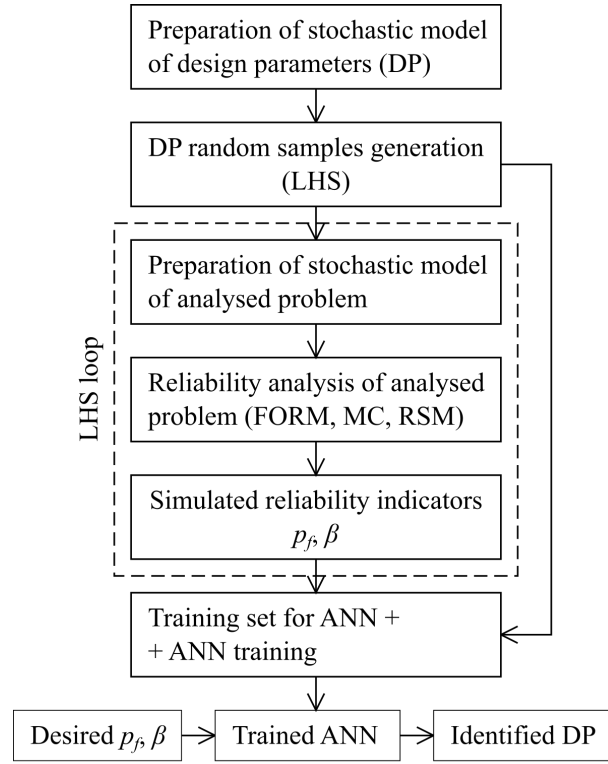
Figure 2.2: A flow chart of proposed inverse reliability method

is illustratively sketched in Figure 2.3 for $m = 2$ and $p + q = 2$ according to Section 2.1.2.

5. The trained ANN is ready to provide an answer to the key task: To give the best design parameters so that the stochastic calculation may result in the best agreement with target reliability indicators, which is performed by means of a network simulation using target reliability indicators as an input. This results in an optimal set of design parameters $\mathbf{P}_{opt}$.

6. The last step is the verification of the results – the calculation of reliability indicators related to limit state functions using the optimal parameters $\mathbf{P}_{opt}$. A comparison with target reliability indicators will show the extent to which the inverse analysis was successful.

Note that the important step of the ANN-based inverse reliability method is the design of appropriate ANN structure (step 4), i.e. selection of the appropriate number of hidden layers and the corresponding number of neurons, the choice of transfer functions, etc. For more details about ANN design see Section 1.2.2. Let's just mention here that the number of inputs (reliability indicators corresponding to

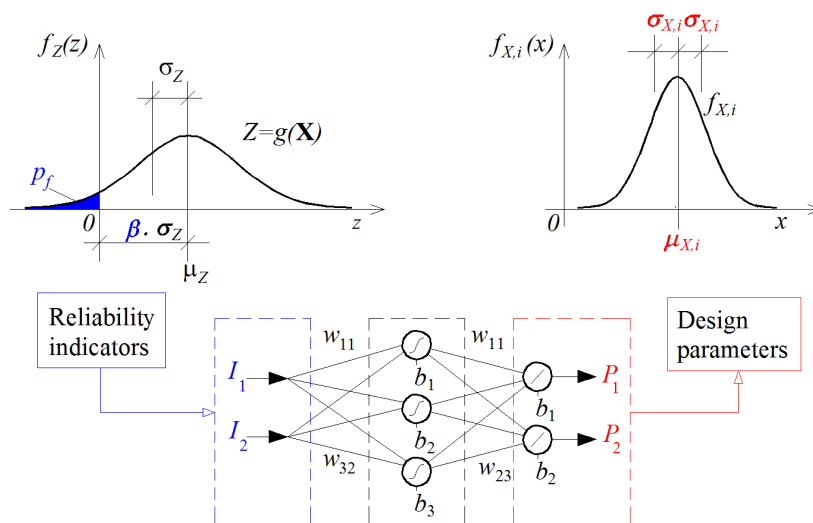Figure 2.3: A schematic view of the artificial neural network-based inverse
reliability method

limit states) and the number of output neurons (design parameters) are known in advance.

Importance of the training sample preparation has been emphasized and tested by Tong and Liu [82], including the LHS scheme. In spite of the fact that these authors concluded that the number-theoretic methods appear to be the most efficient, the LHS scheme also provided very good results. Moreover, the focus on LHS is also determined by the general applicability of this small-sample simulation technique for practical statistical, sensitivity and reliability analyses in many fields of engineering. For inverse reliability problems a small-sample simulation is extremely important as a multiple calculation of reliability indicators (as described in step 3) is needed.

In the case of inverse reliability analysis a double stochastic analysis is needed for the training set preparation for ANN (steps 2 and 3 of the procedure). In the outer loop random realizations of design parameters are generated using the LHS simulation technique. The inner loop represents the reliability calculation for one particular realization of design parameters. Here, the FORM or other approximation method (see e.g. Lehký and Šomodíková [47]) is recommended due to computational demands, as Monte Carlo type simulation techniques require a very high number of simulations for small failure probabilities (thousands, millions).The number of simulations in outer loop is driven by ANN and only tens of simulations are usually needed.

Since inverse reliability analysis combines ANN with multiple stochastic calculations, two software tools named DLNNET (Lehký [44] and IRel (Lehký [45]) has been developed to automate such time-consuming tasks. DLNNET is the artificial neural network software which is combined with the FReET software for statistical,

sensitivity and reliability analyses (Novák et al. [59], [60]). Inverse reliability software IRel works as a master program which manages the whole process of inverse reliability analysis and controls communication between DLNNET and FReET. For more details see Chapter 5.

2.3 Statistical correlation

In the inverse reliability problem a statistical correlation can appear in two alternatives: (1) correlation among random variables of stochastic system; (2) correlation among design parameters (e.g. mean values of selected material parameters, etc.). In the first case the statistical correlation is related to a joint probability distribution function $f_{\mathbf{X}}(\mathbf{X})$ of Equation (2.4). It is related to reliability technique for calculation of theoretical failure probability. E.g. in case of approximation technique FORM, correlation is solved using Nataf's transformation.

The second case is usually related to statistical correlation among design parameters represented by statistical small-sample simulation LHS which is used for training of ANN, as described in previous section. Statistical correlation has to be imposed in simulation scheme. A robust technique to impose statistical correlation based on the stochastic method of optimization called simulated annealing has been proposed by Vořechovský and Novák in [86]. As mentioned in Section 1.3, the imposition of the prescribed correlation matrix into the sampling scheme can be understood as a combinatorial optimization problem: The difference between the prescribed (target) $\mathbf{T}$ and the generated (actual) $\mathbf{A}$ correlation matrices should be as small as possible. Let's denote the difference matrix (error matrix) $\mathbf{E}$:

$$\mathbf{E} = \mathbf{T} - \mathbf{A} \tag{2.7}$$

To gain a scalar measure of the error a suitable norm of the matrix $\mathbf{E}$ is introduced. The norm has to be minimized, from the definition of the optimization problem point of view; the objective function is the error norm and the design variables are related to the ordering in the sampling scheme. The method is implemented in reliability software FReET [59] which was utilized for reliability-based purposes in this work.

2.4 Numerical examples

The proposed methodology has been tested and applied to the various classes of inverse reliability problems – both linear and nonlinear cases with single as well as multiple design parameters, and with independent basic random variables as well as random variables with prescribed statistical correlations. In general, the method can be applied to the inverse reliability task of whatever complexity but it must not be ill-posed problem. But, this is not the limitation of this particular method but

of optimization techniques in general. Some selected examples are shown in this section.

2.4.1 A single design parameter problem

A limit state function with a single design parameter, as shown in Li and Foschi [48], is used first to show the applicability of the proposed methodology and to offer comparison with published results in the literature. The limit state function g is defined as:

$$g = \exp\left[-\theta\left(u_1 + 2u_2 + 3u_3\right)\right] - u4 + 1.5, \tag{2.8}$$

where the vector of random variables $\mathbf{u} = (u_1, u_2, u_3, u_4)^{\mathrm{T}}$ is in standard normal space and uncorrelated. Target reliability index $\beta = 2.0$.

Case 1: Parameter θ is treated as a deterministic design parameter.

Case 2: Parameter θ is treated as a two-parametric lognormal random variable with a coefficient of variation of 0.30. Its mean value is considered as a design parameter.

Table 2.2 summarizes all basic random variables. Reliability analysis was carried out using the FORM method. The starting values were means; the tolerance for convergence was 10^{-4}. For training set preparation parameter θ (case 1) or the mean value of θ (case 2) was considered as random variable with rectangular distribution, see Table 2.3. Forty-one simulations were used here. In case 2, the coefficient of variation of θ was considered as fixed while the standard deviation changed with the mean value.

In both cases, the ANN (see Figure 2.4) consisted of one hidden layer with two nonlinear neurons (hyperbolic tangent transfer function) and an output layer with one output neuron (linear transfer function) which corresponds to one design parameter θ (case 1) or mean(θ) (case 2). The network has one input which corresponds to one specified reliability index β.

The resulting values of parameter θ or mean(θ) are given in Table 2.4. To check their accuracy the resulting values of design parameters were used in Equation (2.8) and reliability indices β were calculated; see the comparison with target β_{target} in Table 2.4. Parameter θ (case 1) and mean value of parameter θ (case 2) agree with those given in Li and Foschi [48].

Table 2.2: Random variables and design parameters

Variable	Distribution	Mean	Std	CoV
u_1	Normal	0	1	–
u_2	Normal	0	1	–
u_3	Normal	0	1	–
u_4	Normal	0	1	–
θ – case 1	Deterministic	?	–	–
θ – case 2	Lognormal (2 par.)	?	–	0.30

Table 2.3: Randomization of design parameters for training set preparation

Variable	Distribution	Mean	Std	a	b
θ – case 1	Rectangular	0.30	0.0577	0.20	0.40
mean(θ) – case 2	Rectangular	0.30	0.0577	0.20	0.40
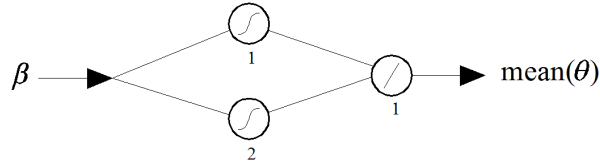
Figure 2.4: A schematic view of the artificial neural network in example 1 (both cases)

Table 2.4: Resulting values of parameter θ (case 1) and the mean value of parameter θ (case 2) and reliability indices β

Case 1		Case 2		
θ	β	mean(θ)	β	β_{target}
0.36717	1.9999	0.37245	2.0000	2.0

2.4.2   A multiple design parameters problem

A set of three limit state functions are given involving four random variables, x_1, x_2, x_3 and x_4 (Li and Foschi [48]):

$$
\begin{aligned}
g_1 &= x_1^2 - 4x_2 - 2x_3x_4 \\
g_2 &= 2x_1x_4 - x_2x_3 \\
g_3 &= x_1x_2x_4 - 2x_3
\end{aligned}
\tag{2.9}
$$

with the given target reliability indices $\beta_1 = 3.0, \beta_2 = 3.5$ and $\beta_3 = 4.0$.

Case 1: The aim of inverse reliability analysis is to identify the mean values of three variables, x_1, x_2 and x_3, for given target reliability indices. All variables are assumed uncorrelated.

Case 2: The aim of inverse reliability analysis is to identify the standard deviation of variable x_1 and the mean values of variables x_2 and x_3 for the given target reliability indices. All variables are assumed uncorrelated.

Case 3: The design parameters are the same as in case 2, i.e. the standard deviation of variable x_1 and the mean values of variables x_2 and x_3. Here, to show the effect of correlation, the first two variables were assumed to have a correlation; see correlation matrix in Table 2.6.

Table 2.5 summarizes all basic random variables. Reliability analysis was carried out using the FORM method; the starting values were means and the tolerance for convergence was 10^{-4}. For training set preparation the design parameters were considered as random variables with rectangular distribution; see Tables 2.7–2.9. One hundred simulations were used here. The ANN (see Figure 2.5) consisted of one hidden layer with five (case 1), eight (case 2) or ten (case 3) nonlinear neurons (hyperbolic tangent transfer function) and an output layer with three output neurons (linear transfer function) which correspond to three design parameters – the mean values of variables x_1, x_2 and x_3 (case 1) or the standard deviation of variable x_1 and the mean values of variables x_2 and x_3 (cases 2, 3). The ANN has three inputs which correspond to the three specified reliability indices β_1, β_2 and β_3. The resulting design parameter values are given in Tables 2.10–2.12. To check their accuracy these values were used in Equation (2.9) and reliability indices were calculated; see their comparison with target reliability indices in Tables 2.10–2.12.

Table 2.5: Random variables and design parameters

Variable	Distribution	Mean	Std	CoV
x_1 – case 1	Normal	?	–	0.01
x_1 – cases 2, 3	Normal	6	?	–
x_2	Normal	?	–	0.2
x_3	Normal	?	–	0.1
x_4	Normal	1.0	0.1	0.1

Table 2.6: Correlation matrix in case 3

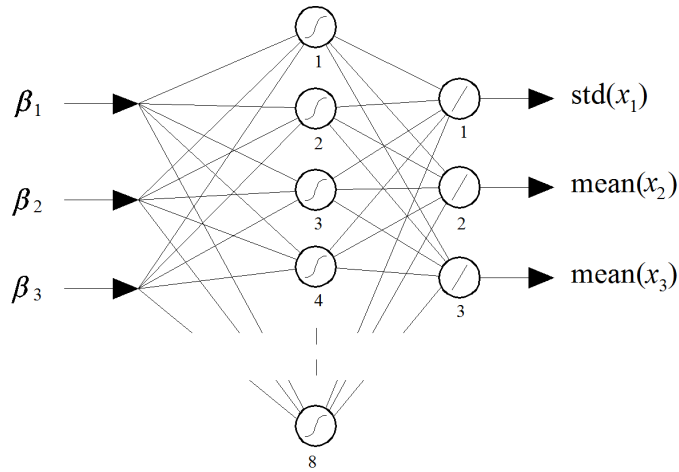|	x_1	x_2	x_3	x_4
x_1	1	0.8	0	0
x_2	0.8	1	0	0
x_3	0	0	1	0
x_4	0	0	0	1

Figure 2.5: A schematic view of the artificial neural network in example 2 (case 2)

Table 2.7: Randomization of design parameters for training set preparation in case 1

Variable	Distribution	Mean	Std	a	b
mean(x_1)	Rectangular	4.5	0.2887	4.0	5.0
mean(x_2)	Rectangular	2.5	0.2887	2.0	3.0
mean(x_3)	Rectangular	1.5	0.2887	1.0	2.0

Table 2.8: Randomization of design parameters for training set preparation in case 2

Variable	Distribution	Mean	Std	a	b
std(x_1)	Rectangular	1.0	0.2887	0.5	1.5
mean(x_2)	Rectangular	2.5	0.2887	2.0	3.0
mean(x_3)	Rectangular	1.5	0.2887	1.0	2.0

Table 2.9: Randomization of design parameters for training set preparation in case 3

Variable	Distribution	Mean	Std	a	b
std(x_1)	Rectangular	1.0	0.2887	0.5	1.5
mean(x_2)	Rectangular	3.5	0.2887	3.0	4.0
mean(x_3)	Rectangular	2.5	0.2887	2.0	3.0

Table 2.10: Resulting values of design parameters and reliability indices in case 1

mean(x_1)	mean(x_2)	mean(x_3)	β_1 ($\beta_{1,\text{target}}$)	β_2 ($\beta_{2,\text{target}}$)	β_3 ($\beta_{3,\text{target}}$)
4.3636	2.1619	1.7836	2.999 (3.0)	3.498 (3.5)	4.001 (4.0)

Table 2.11: Resulting values of design parameters and reliability indices in case 2

std(x_1)	mean(x_2)	mean(x_3)	β_1 ($\beta_{1,\text{target}}$)	β_2 ($\beta_{2,\text{target}}$)	β_3 ($\beta_{3,\text{target}}$)
0.7688	2.1950	2.0779	2.999 (3.0)	3.502 (3.5)	3.998 (4.0)

Table 2.12: Resulting values of design parameters and reliability indices in case 3

std(x_1)	mean(x_2)	mean(x_3)	β_1 ($\beta_{1,\text{target}}$)	β_2 ($\beta_{2,\text{target}}$)	β_3 ($\beta_{3,\text{target}}$)
0.8295	3.3071	1.9912	2.999 (3.0)	3.500 (3.5)	4.001 (4.0)

2.4.3 A timber beam design

This application originates from the civil engineering field of structural mechanics. The aim is to design the dimensions of a rectangular cross-section with width b and height h of a simply supported beam made of timber (Figure 2.6). Both dimensions are considered as random variables with a variation of $5\,\%$. The mean values of b and h are design parameters in the inverse reliability problem. The design is performed fully according to Eurocode 5 [14]. The ultimate limit state as well as the serviceability limit state is taken into account. The limit states are described by the following limit state functions g_1 and g_2:

$$
\begin{aligned}
g_1 &= M_{\mathrm{R}} - M_{\mathrm{E}} \\
g_2 &= u_{\mathrm{lim,fin}} - u_{\mathrm{net,fin}}
\end{aligned}
\tag{2.10}
$$

where M_{R} is the bending moment of resistance, M_{E} is the bending moment of load action, $u_{\mathrm{lim,fin}}$ is the final limit deflection and $u_{\mathrm{net,fin}}$ is the final deflection caused by load action. Bending moments M_{R} and M_{E} are calculated as:

$$
\begin{aligned}
M_{\mathrm{R}} &= \theta_{\mathrm{R}} \frac{1}{6} b h^2 k_{\mathrm{mod}} f_{\mathrm{m}} \\
M_{\mathrm{E}} &= \theta_{\mathrm{E}} \frac{1}{8} (g + q) l^2
\end{aligned}
\tag{2.11}
$$

where b and h are the width and height of rectangular cross-section, l is the length of the beam, f_{m} is flexural strength, k_{mod} is the modification factor taking into account the effect on the strength parameters of the duration of the load and the moisture content in the structure, g is permanent load, q is variable load and θ_{R} and θ_{E} are the model uncertainties of resistance and load action respectively. Deflections in the
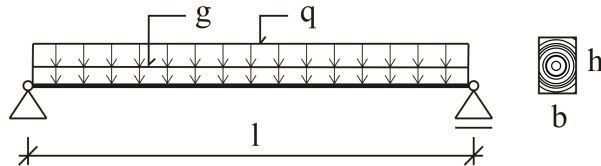

Figure 2.6: Scheme of a simply supported beam with a rectangular cross-section)

second limit state function g_2 are calculated as:

$$
\begin{aligned}
u_{\text{lim,fin}} &= \frac{l}{200} \\
u_{\text{net,fin}} &= \theta_{\text{E}}(u_{1,\text{fin}} + u_{2,\text{fin}}) \\
u_{1,\text{fin}} &= \frac{5}{384}\frac{gl^4}{E\frac{1}{12}bh^3}(1 + k_{1,\text{def}}) \\
u_{2,\text{fin}} &= \frac{5}{384}\frac{ql^4}{E\frac{1}{12}bh^3}(1 + k_{2,\text{def}})
\end{aligned}
\tag{2.12}
$$

where $u_{1,\text{fin}}$ and $u_{2,\text{fin}}$ are the final deflections caused by the permanent load and variable load, E is the modulus of elasticity of timber, $k_{1,\text{def}}$ is a factor which takes into account the increase in deflection with time due to the combined effect of creep and moisture and it belongs to permanent load and $k_{2,\text{def}}$ is the same factor but for variable load. Table 2.13 summarizes all random variables and their randomization. The values of the material parameters correspond to spruce timber. Randomization was carried out according to the recommendations of JCSS model code [28].

Reliability analysis was carried out using the FORM method; the starting values were means; the tolerance for convergence was 10^{-4}. For training set preparation the design parameters were considered as random variables with rectangular distribution, see Table 2.14. One hundred simulations were used here. The ANN (see Figure 2.7) consisted of one hidden layer with four nonlinear neurons (hyperbolic tangent transfer function) and an output layer with two output neurons (linear transfer function) which correspond to two design parameters – the mean values of width b and height h. The ANN has two inputs which correspond to two specified reliability indices, β_1 and β_2. The resulting design parameter values are given in Table 2.15. To check their accuracy these values were used in Equations (2.10–2.12) and reliability indices were calculated; see the comparison with the target reliability indices in Table 2.15. In the case of practical design the dimensions of cross-section should be selected from available set of dimensions. In our example, the resulting width and height would be $b = 0,140\,\text{m}$ and $h = 0,220\,\text{m}$ which gives the final reliability indices $\beta_{1,\text{fin}} = 4.068$ and $\beta_{2,\text{fin}} = 1.912$.

The same example has been also solved using small-sample double-loop reliability-based optimization method (Slowik [75]). In this method, inverse reliability problem is considered as an optimization task and an Aimed Multilevel Sampling strategy for the reduction of sampling space is utilized. Resulting values of desired dimensions and corresponding reliability indices were: mean(b) = 0.13116 m, mean(h) = 0.21514 m, $\beta_{1,\text{fin}} = 3.7930$ and $\beta_{2,\text{fin}} = 1.5001$, see Lehký et al. [43] for more details.

Table 2.13: Random variables and design parameters

Variable	Distribution	Mean	Std	CoV
l [m]	Normal	3.5	0.175	0.05
b [m]	Normal	?	–	0.05
h [m]	Normal	?	–	0.05
E [GPa]	Lognormal (2 par)	10	1.3	0.13
f_m [MPa]	Lognormal (2 par)	34	8.5	0.25
g [kN/m]	Gumbel Max EV 1	1.686	0.169	0.10
q [kN/m]	Gumbel Max EV 1	2.565	0.770	0.30
θ_R [–]	Lognormal (2 par)	1	0.10	0.10
θ_E [–]	Lognormal (2 par)	1	0.10	0.10

Table 2.14: Randomization of design parameters for training set preparation

Variable	Distribution	Mean	Std	a	b
mean(h) [m]	Rectangular	0.125	0.0144	0.10	0.15
mean(b) [m]	Rectangular	0.225	0.0144	0.20	0.25

Table 2.15: Resulting values of design parameters and reliability indices

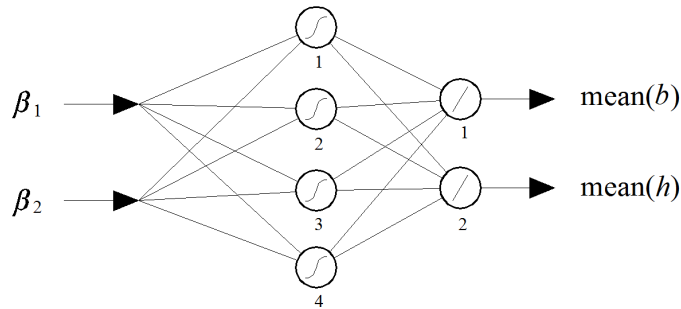| mean(b) [m]	mean(h) [m]	β_1 ($\beta_{1,\text{target}}$)	β_2 ($\beta_{2,\text{target}}$)
0.13244	0.21432	3.8001 (3.8)	1.5001 (1.5)

Figure 2.7: A schematic view of the artificial neural network in example 3

2.4.4   Post-tensioned composite bridge

The structure in question is a single-span post-tensioned composite bridge, carrying a main road across a single-track railway, situated near the village of Uherský Ostroh in the Czech Republic. A diagnostic survey conducted in 2007 ascertained that the bridge is made of twelve precast post-tensioned concrete MPD 3 (outer) and MPD 4 (intermediate) type girders, which have been used from 1955 for the construction of slab bridges with clear spans of up to 18 m. Each of the MPD girders is composed of six segments that are connected to each other by transverse joints. See Figure 2.8 for the bridge composition.

A numerical model of the bridge was created in ATENA software (Červenka et al. [8]). The "3D NonLinear Cementitious 2" material model was used for the concrete. Pre-stressing tendons and shear reinforcement were modeled as discrete and smeared reinforcement, respectively, by means of a bilinear stress-strain diagram with hardening. The following load cases were modeled: the dead load of the structure, longitudinal pre-stressing, secondary dead load, and traffic load for the assessment of normal load-bearing capacity. The loading scheme related normal loading class consists of a three-axle vehicle in each traffic lane and a continuous load over the bridge width. For details see [11]. A computational model of the bridge, including the loading scheme described above, is shown in Figure 2.9. In the figure the load imposed by the front axle of each three-axle vehicle is replaced by the equivalent value of continuous load for each individual traffic lane.

The material properties of the concrete were randomized for the purposes of stochastic modeling. The stochastic parameters of random input variables were defined using FReET software according to the recommendations of JCSS [28] and TP 224 [37] and updated based on the tested material parameters gained from the aforementioned diagnostic survey. Definitions of the random input variables are summarized in Table 2.16. Alongside the concrete material parameters, the dead load of the structure and the weight of the road layers were also randomized; see concrete mass density and secondary dead load, respectively, in Table 2.16. The values of pre-stress forces were defined by their mean values with respect to short-term as well as long-term losses of initial tension according to ČSN EN 1992-2 [10]. Considering their substantial effect on the global level of load bearing capacity when the serviceability limit states were reached, the applied stochastic model was also defined in a manner that is fully in agreement with JCSS recommendations. Finally, traffic load was defined as deterministic.

Statistical correlation between the material parameters of the concrete used in the bridge segments and transverse joints and the parameters of pre-stressing tendons was also considered and imposed using a simulated annealing approach. Correlation matrices (see Figure 2.10) were defined with respect to previously-performed tests and the recommendations of the JCSS.

According to the diagnostic survey, the mean value of concrete compressive
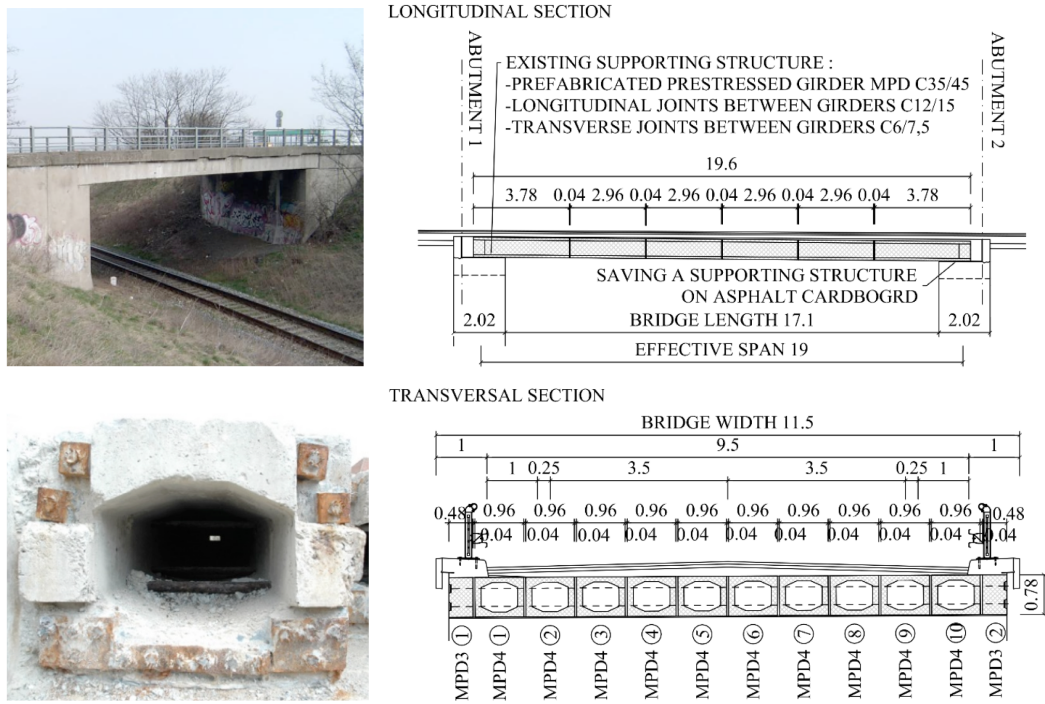
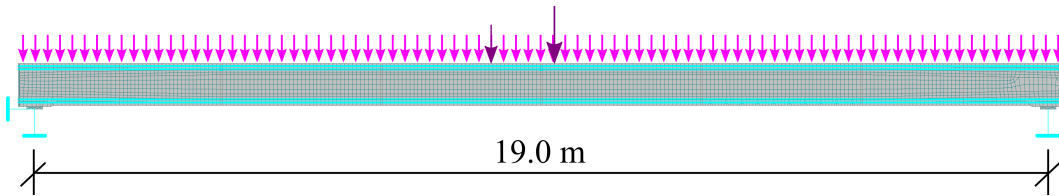Figure 2.8: Views, longitudinal and transverse sections of the analyzed bridge

Figure 2.9: Computational model of the bridge, including the traffic load related normal loading class

	E_c	f_t	f_c	G_f	ρ
E_c	1	0	0.3	0	0
f_t	0	1	0.4	0.8	0
f_c	0.3	0.4	1	0	0
G_f	0	0.8	0	1	0

	$f_{y,p}$	$f_{u,p}$	E_p	P_1–P_4
$f_{y,p}$	1	0.9	0.5	0
$f_{u,p}$	0.9	1	0.5	0
E_p	1	0	1	0
P_1–P_4	0	0	0	1

(a) Concrete of segments and transverse joints   (b) Pre-stressing tendons

Figure 2.10: Correlation matrices of material parameters

Table 2.16: Definition of input random variables

| Variable	Symbol	Unit	Distribution	Mean	CoV
Concrete of segments:					
Elastic modulus	$E_{c,s}$	[GPa]	Lognormal (2-par.)	37.20	0.10
Tensile strength	$f_{t,s}$	[MPa]	Weibull min (2-par.)	3.301	0.15
Compressive strength	$f_{c,s}$	[MPa]	Lognormal (2-par.)	43.35	0.08
Specific fracture energy	$G_{f,s}$	[N/m]	Weibull min (2-par.)	82.51	0.15
Mass density	ρ_s	[kN/m^3]	Normal	23.80	0.04
Concrete of transverse joints:					
Elastic modulus	$E_{c,j}$	[GPa]	Lognormal (2-par.)	26.81	0.15
Tensile strength	$f_{t,j}$	[MPa]	Weibull min (2-par.)	1.913	0.35
Compressive strength	$f_{c,j}$	[MPa]	Triangular	19.13	0.23
Specific fracture energy	$G_{f,j}$	[N/m]	Weibull min (2-par.)	47.82	0.25
Mass density	ρ_j	[kN/m^3]	Normal	23.80	0.04
Pre-stressing tendons:					
Elastic modulus	E_p	[GPa]	Normal	190.0	0.03
Yield strength	$f_{y,p}$	[MPa]	Normal	1248	0.03
Ultimate strength	$f_{u,p}$	[MPa]	Normal	1716	0.03
Prestress force 1	P_1	[MN]	Normal	14.20	0.09
Prestress force 2	P_2	[MN]	Normal	10.05	0.09
Prestress force 3 and 4	P_3, P_4	[MN]	Normal	3.449	0.09
Other:					
Secondary dead load	g_1	[kN/m]	Normal	65.55	0.05
Traffic load	V_n	[t]	Deterministic	V_n	–
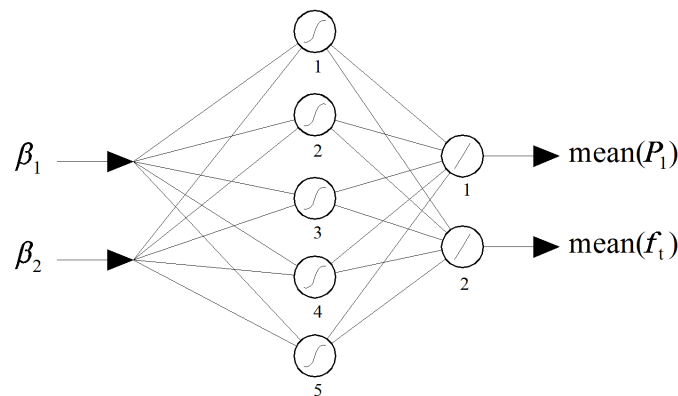
Figure 2.11: A schematic view of the artificial neural network in example 4

Table 2.17: Randomization of design parameters for training set preparation

Variable	Distribution	Mean	Std	a	b
mean(P_1) [MN]	Rectangular	15	0.115	12	18
mean($f_{t,j}$) [MPa]	Rectangular	2.4	0.144	1.8	3.0

Table 2.18: Resulting values of design parameters and reliability indices

mean(P_1) [MN]	mean($f_{t,j}$) [MPa]	β_1 ($\beta_{1,\text{target}}$)	β_2 ($\beta_{2,\text{target}}$)
15.077	3.04	0.0734 (0)	1.2767 (1.3)

strength of the joints was $40.5\,\text{MPa}$, but the concrete was only classified as strength class C6/7.5 due to high variability in the measurements, which was probably caused by the spatial deterioration of the bridge. This also introduces uncertainty to the current loss of prestress. The value for this loss was roughly estimated according to code specifications as $17\,\%$, which corresponds to the prestress force $P_1 = 14.20\,\text{MN}$, including current loss of prestress. Since the tensile strength of the transverse joints and the bridge prestress has a significant effect on the bridge's load-bearing capacity, mean values of both were considered as uncertain design parameters with the aim of finding their critical values corresponding to the desired reliability level and load-bearing capacity. Two limit states were taken into account – the serviceability limit state of decompression (SLSD) and the serviceability limit state of crack initiation (SLSC). Both of these limit states have an implicit form – structural resistance is calculated using the nonlinear finite element model, and load action is considered as a deterministic variable placed according to the normal loading scheme. The target reliability indices were considered as $\beta_1 = 0$ for the SLSD and $\beta_2 = 1.3$ for the SLSC. According to the diagnostic survey and the needs of the bridge administrator, the desired load-bearing capacity related to the normal loading class was considered as $25\,\text{t}$.

Reliability analysis was carried out using the LHS simulation method. Due to the high computational demands of the nonlinear model, 30 simulations were used in order to generate random samples of the design parameters (outer loop – size of the training set), and 32 simulations were used to calculate Cornell's reliability indices for both limit states (inner loop). The inverse task was treated as a multiple design parameter and multiple reliability constraint problem. The ANN (see Figure 2.11) consisted of one hidden layer having five nonlinear neurons (hyperbolic tangent transfer function) and an output layer having two output neurons (linear transfer function) which correspond to two design parameters – mean(P_1) and mean(f_t). The ANN has two inputs which correspond to two specified reliability indices, β_1 and β_2. For training set preparation the design parameters were considered as random variables with rectangular distribution, see Table 2.17.

The resulting design parameter values are summarized in Table 2.18. To validate

the results a stochastic analysis was carried out that included the determined design parameters, and reliability indices were calculated; see the comparison with the target reliability indices in Table 2.18. The results show that the required mean value of concrete tensile strength in transverse joints is relatively high, but, due to high variability, the corresponding characteristic value (quantile 5 %) is 1.64 MPa. Based on this value, concrete can be roughly classified as of C20/25 class according to recommendations in Eurocode 2 [9]. This demand is lower than what was the original finding of the diagnostic survey, where the mean value and standard deviation of compressive strength were 40.5 MPa and 15.5 MPa, respectively. Let's note that the requirement for reliability index $\beta_2 = 1.3$ in the case of the SLSC is relatively strict. Lower reliability index values would result in an even lower mean concrete strength requirement being obtained.

The resulting requirement as regards prestress force value is slightly stricter compared to that estimated according to code specifications where prestress loss was considered as 17 % for an infinite lifetime (9 % is immediate loss; coefficient of variation is 0.09). The identified mean prestress force value indicates a current loss of prestress of 12 %. From the results we can conclude that a requirement for a normal load-bearing capacity of $V_{\mathrm{n}} = 25$ t is adequate for the SLSC. In the case of the SLSD, a more detailed investigation of prestress loss and its variability would be necessary to confirm the required load-bearing capacity for a given level of safety.

2.5 Summary

Finding a more realistic optimum structural design in the presence of uncertainties is not an easy or straightforward task. The main reason for this is the increasing computational effort required when dealing with optimization and reliability concepts. Proposed approach to solving reliability-based design problems utilizes small-sample simulation LHS to reduce computational effort. It provides very good results, as is indicated in the numerical examples. Some advantages and disadvantages of the method can be highlighted:

- The method is general and can be easily used for almost any inverse reliability problem. In case of the structural design it allows identification of design parameters of both existing as well as new structure.

- The procedure yields to "exact" values of required reliability indicators for individual limit states given in code specifications.

- In combination with FORM or response surface method it enables to perform the inverse reliability analysis also for the time-consuming FEM applications.

- Its efficiency is proving especially when dealing with a multiple design parameter and multiple reliability constraint problem. As demonstrated by the

example in Section 2.4.2, it is no problem to combine different statistics of random variables in one inverse task.

- The main disadvantage of the method is the fact that the design and training of ANN require the knowledge and deeper involvement of the user, which can make the approach difficult to use.

- In addition, an initial estimation of the design parameters is required – the better estimation, the faster solution and more accurate results.

Chapter 3

Damage detection

The second class of inverse problems, which has recently become a very topical issue among bridge owners and operators, is damage identification in aging bridges. Civil engineering structures such as bridges must be periodically inspected to ensure they maintain structural integrity since many of these structures have reached the end of their projected service life and may have become damaged. The conventional approaches of visual inspection and local non-destructive evaluation are expensive, subjective, inconsistent, labor and time-consuming, and need easy access to the damage zone. That is the reason substantial research and development has recently been taking place in the area of structural health monitoring (SHM) techniques (e.g. Wenzel and Pichler [87]). Among these, modal-based techniques have been extensively investigated due to their global nature and simplicity. They can be used for automated damage localization and provide consistent damage assessment. From the practical point of view, damage assessment can be categorized into four levels:

1. Detecting if the structure is damaged;

2. finding the location of damage;

3. estimating the magnitude of damage, and

4. evaluating the remaining service life of the structure.

Modal-based techniques use ambient vibration measurements and can be used for damage identification in structures while they are in use. Experimental measurements typically provide data on the dynamic response of the structure in the form of time series (accelerations, velocities). Consequently, modal properties (mode shapes and corresponding eigenfrequencies – "characteristic" frequencies at which a system vibrates), damping characteristics and assurance criteria (MAC, COMAC, DLAC, etc.), are evaluated (e.g. Salgado et al. [68], Koh and Dyke [33]). During the last decade, both academic and industrial research groups have been involved

in research into the utilization of this kind of structural response information for damage localization and structural health assessment.

The efficiency of the identification procedure depends on the accuracy of the placement of sensors on the structure. Sensors placed closer to the damaged part of the structure show higher sensitivity (Spencer et al. [78]). Besides the effects of structural damage, what are termed operative conditions (e.g. temperature changes) should also be taken into account during inverse analysis (Feltrin [16]). The term "model updating method" is frequently used in connection with SHM and damage detection (Link [50], Teughels et al. [81], Deix and Geier [12], Fang et al. [15], Huth et al. [25], Wenzel and Pichler [87]). "Updating" means that individual parameters of the FEM model are iteratively changed in order to minimize the difference between experimentally measured and calculated responses. Here, the sensitivity of model parameters to the structural response is frequently utilized for improving efficiency of the updating process (Strauss et al. [79] and [80]).

An important part of the damage detection procedure is the proper selection of input information. For that purpose, several numerical and experimental studies of modal properties were carried out using simple laboratory beam specimens as well as real bridge structures; see Section 3.2. The aim of these studies was to find out which eigenfrequencies, mode shapes or assurance criteria are affected by changes in stiffness at a certain position in the structure. In short, the results show that if the damage is reasonably large, eigenfrequencies are sufficient for damage detection. Lower eigenfrequencies are affected more than higher ones, but not consistently along the structure. Their shift corresponds to mode shapes. That is the reason higher eigenfrequencies must be used for the detection of damage at some positions in the structure. If mode shapes are available, their utilization can be helpful for damage detection. When compared to eigenfrequencies, higher mode shapes are more affected by stiffness change than lower ones. Unfortunately, obtaining higher mode shapes from ambient vibration measurements is often difficult. For more detailed results, see Section 3.2.

Extensive research has been performed by other authors, who suggest other quantities which can be used for damage detection using various methods. Among them, the assurance criteria MAC, COMAC, DLAC and MDLAC (Salgado et al. [68], Koh and Dyke [33]), the rank ordering of eigenfrequency shifts (Armon et al. [2]), and the damage index (Salgado et al. [68]) can be mentioned.

3.1   ANN-based damage detection

Referring to Equation (1.1) in the introduction to this work, the classical (forward) problem in structural and bridge engineering is defined in the following way: for a given set of structural, material, loading, and environmental parameters $\mathbf{X}$, the corresponding structural response $\mathbf{Y}$ is obtained experimentally or by numerical sim-

ulation. If we focus our attention on dynamic analysis and the dynamic response of the structure, the most important input parameters are mass and stiffness distribution along the structure $\mathbf{S}$. The structural response is then represented by vibration data and/or structural modal properties $\mathbf{M}$ (eigenfrequencies and mode shapes).

The damage detection discussed in this chapter is the inverse task of the above mentioned forward problem. The aim is to identify damage in certain parts of the structure based on measured changes in its vibration. Finding such an inverse relationship in an analytical form is once again extremely complicated. Therefore, an ANN is employed as an appropriate surrogate model.

$$\mathbf{S} = f_{\mathrm{ANN}}^{-1}(\mathbf{M}), \tag{3.1}$$

The main idea of the proposed inverse analysis method is based on the fact that a damaged structure has smaller stiffness in some parts, which will affect vibration and modal properties. The differences between the vibration of a damaged structure in comparison with that of a virgin (undamaged) structure are utilized for damage detection and localization. The damage is defined as a stiffness reduction (bending or torsional) in certain parts of the structure. The ANN then serves as an approximation of the following inverse task: to determine what damage has caused the given changes in vibration and/or modal properties? The whole procedure of inverse analysis can be itemized as follows:

1. First, a dynamic computational model of the analyzed structure has to be developed using FEM software. For the purpose of subsequent damage detection, the structure is divided into smaller parts, each with independent stiffness.

2. The stiffness values in individual parts of the structure are considered random variables described by a rectangular distribution. Random realizations of stiffness in individual parts are generated using the LHS simulation method (see vector $\mathbf{S}$ in Figure 3.1).

3. A multiple dynamic modal analysis of the FEM model using random realizations of stiffness is performed, resulting in a statistical set of responses (eigenfrequencies and mode shapes; see vector $\mathbf{M}$ in Figure 3.1). The selection of an appropriate number of simulations depends on many factors, but mainly on the complexity of the problem (the size of the structure, the number of parts with individual stiffness, and computational demands). In general, only tens of simulations are usually needed.

4. The random realizations of stiffness $\mathbf{S}$ (outputs of the ANN) and the random responses from the computational model $\mathbf{M}$ (inputs to the ANN) serve as the basis for the training of an appropriate ANN; see Figure 3.1 (here for the response in the form of eigenfrequencies).
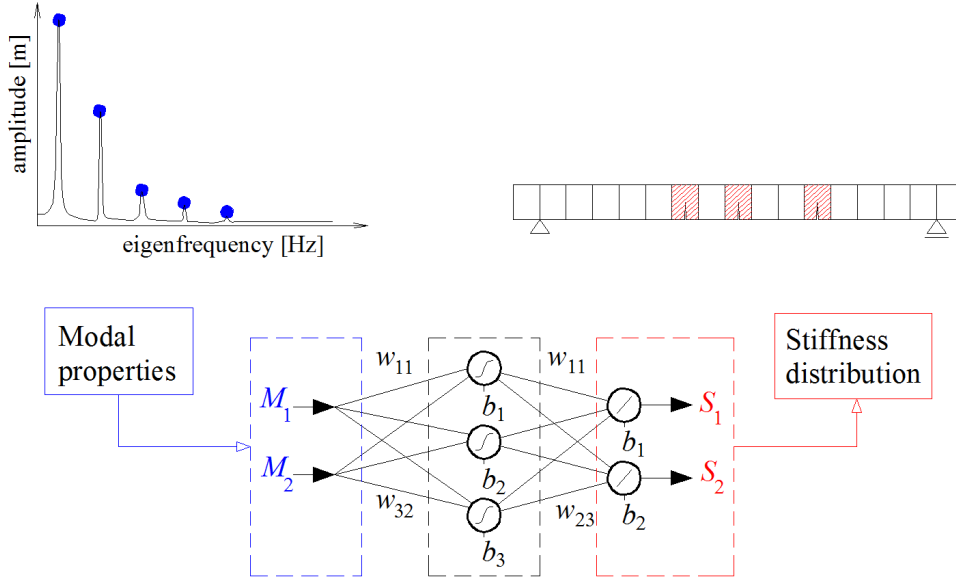
Figure 3.1: Schematic view of ANN-based damage detection

5. The trained ANN is ready to provide an answer to the question posed by the key task: What is the best stiffness distribution so that the dynamic calculation may result in the best agreement with an experimentally measured response? The answer is supplied by means of a network simulation using the measured response as an ANN input.

6. The last step is the verification of the results via dynamic analysis using identified stiffness values and the comparison of experimental and numerical responses.

The damage detection procedure requires a combination of efficient statistical simulation techniques, an artificial neural network and FEM structural dynamics analysis. For this purpose, several software tools were combined to provide a powerful package for fast and effective inverse analysis. It includes SOFiSTiK [76] – FEM software which performs the structural dynamics analysis of the given problem; FReET software [59] – a probabilistic engine based on LHS simulation, which is employed in the preparation of random stiffness samples; and DLNNET [44] – artificial neural network software, which receives all necessary data from SOFiSTiK and FReET via the FReET–SOFiSTiK interface and performs ANN training and simulation; see Section 5.1. This interface is connected to FReET as a dynamic-link library (DLL) and transfers generated samples directly to SOFiSTiK for dynamic analysis. A schematic view of communication between the above-described programmes is depicted in Figure 3.2. Let us note that after successful damage detection has taken
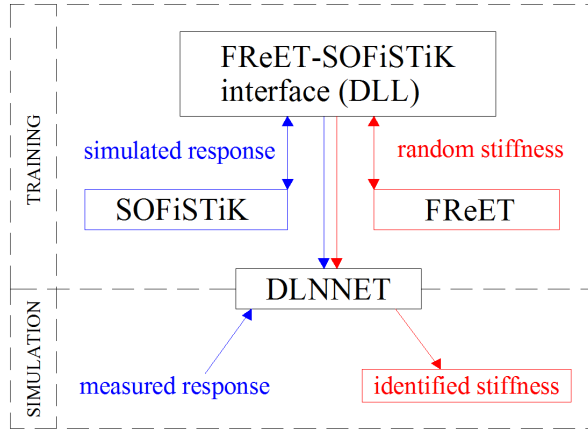
Figure 3.2: Software communication scheme for performing damage detection

place, FReET can be also utilized for the subsequent reliability assessment of the given problem.

3.2 Study of modal properties

In this section the influence of a local decrease in stiffness on modal properties (eigenfrequencies and mode shapes) is studied. The role of the magnitude of damage is examined. The aim is the determination of suitable initial parameters for subsequent inverse analysis. In selected cases, both experimental and numerical evaluations were carried out.

3.2.1 A cantilever beam

Numerical study

A cantilever beam with a constant cross-section has been chosen as the first subject for this study of the suitability of eigenfrequencies and mode shapes for use in damage detection (Figure 3.3). This structural element was selected due to the options for further experimental testing (see below), the existence of an analytical solution and the non-symmetry of this structure (in contrast with, e.g. a simply supported beam). Symmetrical beams have symmetrical and unsymmetrical mode shapes, resulting in ambiguous damage identification. The aim of this study was to discover which eigenfrequencies and mode shapes are affected by a change of stiffness in a certain position within the beam. This kind of information is important for subsequent inverse analysis. It should be mentioned that the evaluation of eigenfrequencies and mode shapes (especially the higher ones) from the experiment is not simple. For the purposes of this study, the first six eigenfrequencies and four mode shapes were
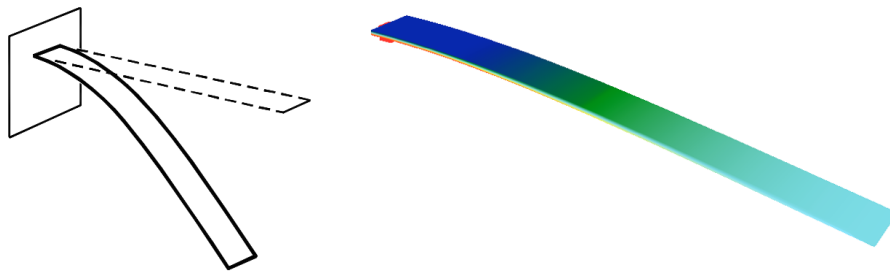
Figure 3.3: A cantilever beam (left) and its model in SOFiSTiK FEM software (right)

considered. The ratio between the first and sixth eigenfrequency was approximately 1:80.

SOFiSTiK FEM software [76] was utilized to prepare the numerical model and perform dynamic and modal analyses (Figure 3.3). The beam was divided into 20 parts, with bending stiffness EI defined for each part (EI_1 to EI_{20}). Initial unit stiffness was considered since relative changes in eigenfrequencies with respect to relative changes in stiffness were being studied. The beam length and some other parameters were considered as unit values too. Damage to the beam in a particular location was modeled by a decrease in bending stiffness to 0.05–0.95 percent of its nominal value. Such damage was applied step by step to all parts of the beam (only one part was damaged at one time).

Figure 3.4 shows the relative changes in eigenfrequencies due to damage position and size. It can be seen that changes in eigenfrequencies correspond in some sense to the mode shapes of the beam – the positions of extreme values correspond to the positions of the amplitudes of the mode shapes. A significant change in eigenfrequencies (more than 10 %) can only be detected for higher degrees of damage (a stiffness of 90 % or less of the nominal value for the first eigenfrequency). The damage in the nodes of the mode shape doesn't affect the corresponding eigenfrequency. It is obvious that for an inverse analysis based only on eigenfrequencies to be efficient a higher number of eigenfrequencies must be considered. This is because the absence of a particular eigenfrequency (e.g. due to damage in the mode shape node) can then be compensated for by the presence of other ones.

The maximum values of the relative change in eigenfrequencies (the first six were considered; see the graduated shading in the figure) are shown in Figure 3.5. The smallest relative change (5 %) under a high level of damage (10 % of the initial stiffness) is at the free end of the cantilever, as was naturally expected. There are also small values in part 8 (a change of 17 %), where the transition between the amplitudes of the first and second mode shapes occurs. The opposite is true in part 5, where the node of the second mode shape is located: this location exhibits maximum change, 27 %, thanks to the first mode shape. The relative changes in higher eigen-
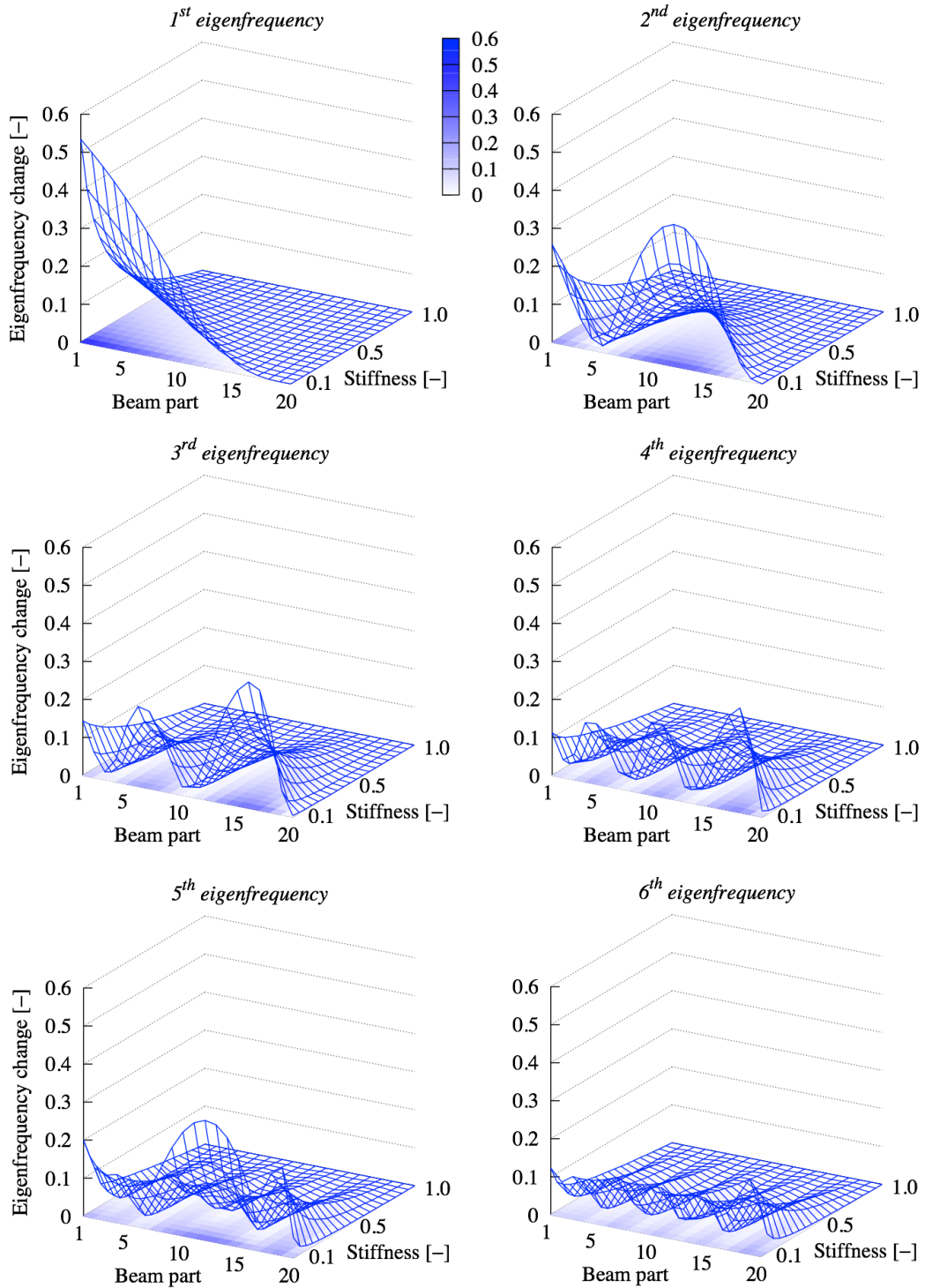
Figure 3.4: Relative changes in eigenfrequencies for different levels of stiffness in particular damaged parts of a cantilever beam
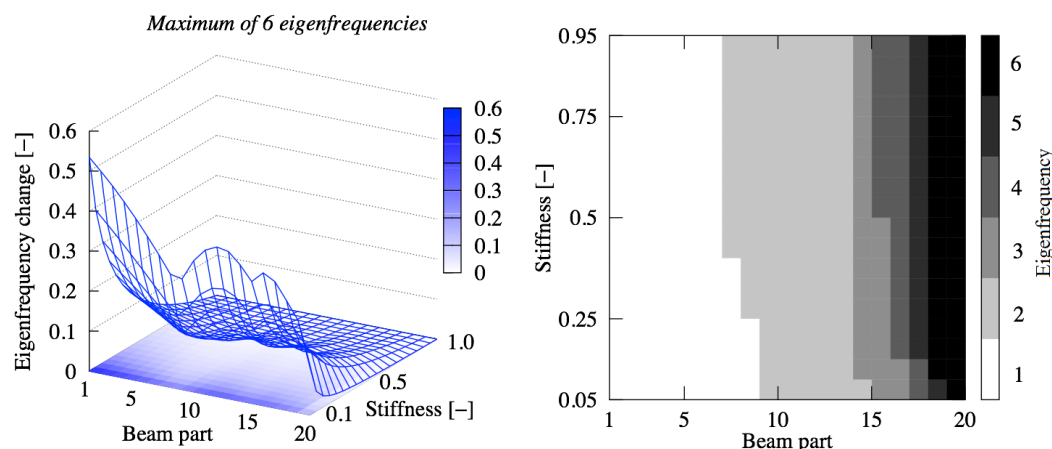
Figure 3.5: Maximum values of relative changes in the first six eigenfrequencies (left), and determination of which eigenfrequency belongs to the specific maximum (right)

frequencies are not so dominant compared to the first and second ones, but their importance increases as we move towards the free end of the cantilever, where the dominance of the first two eigenfrequencies decreases. Damage detection in these parts would thus be very difficult without taking these higher eigenfrequencies into account.

The Modal Assurance Criterion (MAC) was used for the analysis of mode shape changes due to damage in certain parts of the beam. It can be defined for the jth mode shape using the following formula:

$$\text{MAC}(\omega_j) = \frac{|\{\nu_{j\text{v}}^{\text{T}}\}_p\{\nu_{j\text{d}}\}_p|^2}{(\{\nu_{j\text{v}}^{\text{T}}\}_p\{\nu_{j\text{v}}\}_p)(\{\nu_{j\text{d}}^{\text{T}}\}_p\{\nu_{j\text{d}}\}_p)} = \frac{(\sum_p \nu_{j\text{v}}(p)\nu_{j\text{d}}(p))^2}{\sum_p \nu_{j\text{v}}^2(p)\sum_p \nu_{j\text{d}}^2(p)}, \qquad (3.2)$$

where $\nu(p)$ is the ordinate of the $\nu(x)$ curve in point p, index v means the virgin (undamaged) state, and index d means the damaged state. If MAC $= 1$, then the virgin and the damaged curve are the same – exact agreement was achieved.

Figure 3.6 shows a change in the MAC for different levels of damage located at individual parts of the beam. In contrast with eigenfrequencies, the higher mode shape means a higher change in the MAC. This leads to the conclusion that for efficient damage detection, higher mode shapes have to be taken into account. The first mode shape shows only a negligible change, which is not useful for inverse analysis. For complex identification, as many mode shapes as possible should be considered in order to cover the whole structure as shown in Figure 3.7. Here, the MACs of all four analyzed mode shapes are depicted for the extreme case of 90 % stiffness reduction. Note that in practical cases, obtaining higher mode shapes from ambient vibration measurements is not an easy task.
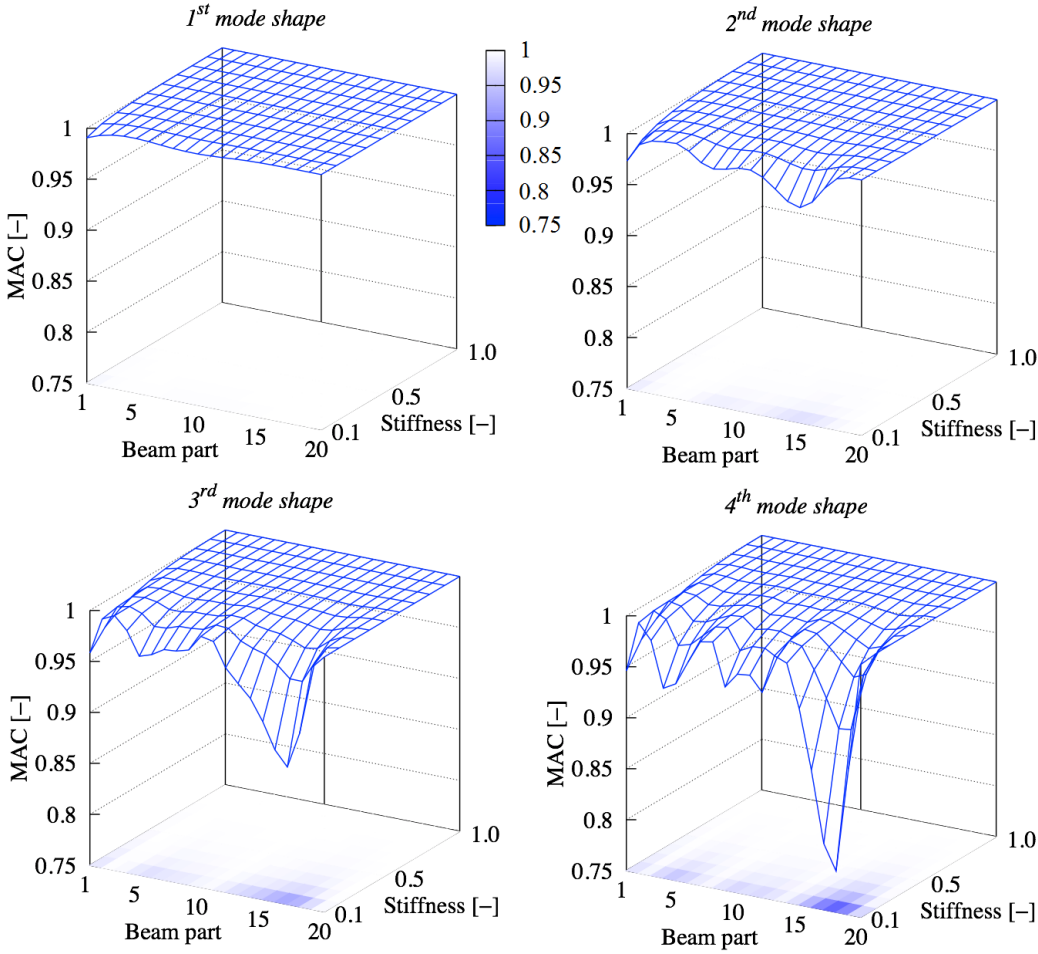
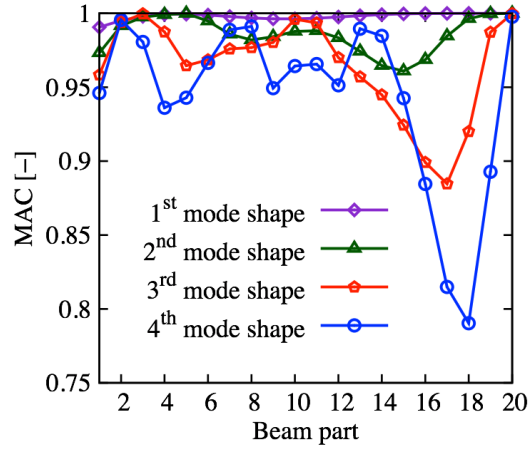Figure 3.6: The MAC of four mode shapes for different levels of stiffness in a particular damaged part

Figure 3.7: Comparison of the MAC of all four mode shapes for stiffness reduction 90 % in a particular damaged part
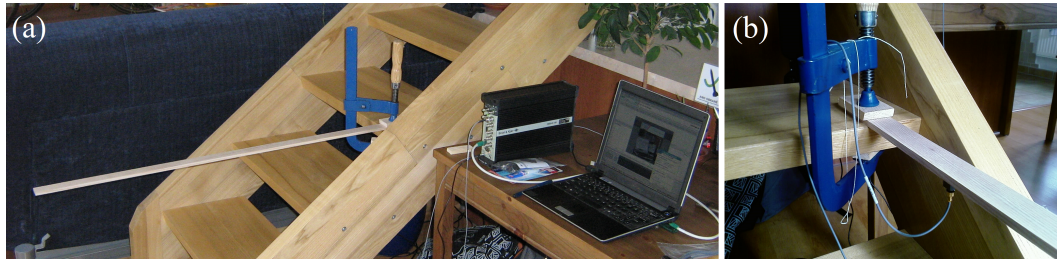

Figure 3.8: Cantilever beam: a) testing configuration, b) the fixed support

Experimental study

A dynamic laboratory experiment was carried out on the cantilever beam to verify the proposed damage detection methodology and extend the numerical study. Five specimens (c11, ... ,c15) made of ash wood were tested. The dimensions of the specimen were as follows: length $= 1\,\text{m}$, width $= 30\,\text{mm}$, and height $= 7\,\text{mm}$. Fixed support was provided by gripping the beam in a vice 100 mm from one end of the beam; the resulting free length of the cantilever beam was 900 mm (Figures 3.8 and 3.9).

First, the dimensions (length, width, height) and weight of all specimens were measured. The modulus of elasticity E of each specimen was determined from the following equation:

$$E = \frac{4f_1^2 m l^3 \pi^2}{1.875^4 I},\tag{3.3}$$

where f_1 is the first eigenfrequency, m is the beam weight, l is its length and I is the moment of inertia of the cross-section. Equation (3.3) was created by modifying the theoretical formula for calculating the eigenfrequencies of the cantilever beam
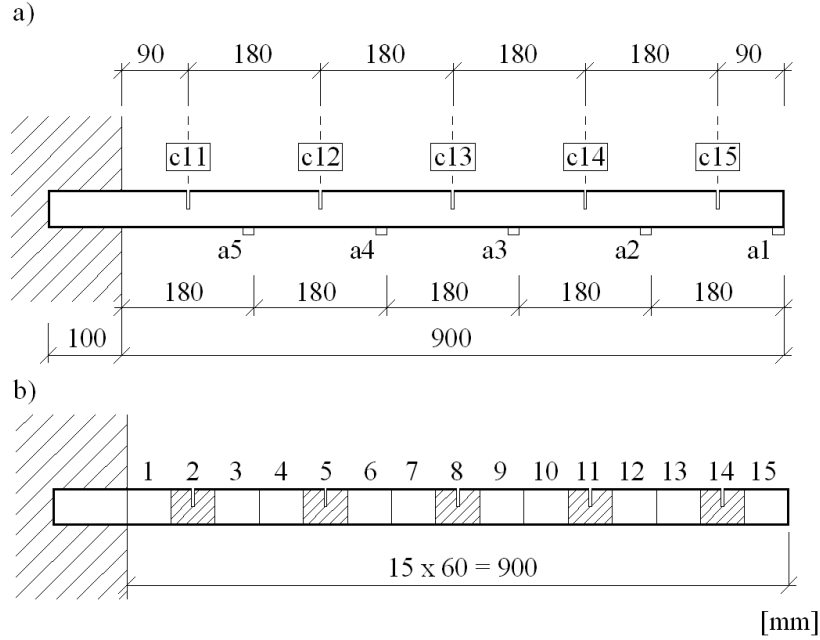
a)

b)

[mm]

Figure 3.9: a) A schematic view of the cantilever beam – positions of accelerometers and cuts for all five specimens; b) numerical model divided into 15 parts

with constant cross-section while neglecting the influence of the deformation energy of shear forces and rotational inertia (Euler-Bernoulli theory, see Brepta et al. [6]):

$$f_m = \frac{\lambda_m^2}{2\pi}\sqrt{\frac{EI}{ml^3}}, \quad \cos\lambda_m.\cosh\lambda_m = -1, \tag{3.4}$$

where λ_m is the eigenvalue corresponding to the mth mode shape and eigenfrequency f_m. If $\lambda_m < \lambda_{m+1}$, then $f_m < f_{m+1}$ for every integer m. Here, the first eigenfrequency f_1 and the first eigenvalue $\lambda_m = 1.875$ were used. The arithmetic mean of the elastic modulus obtained for all five specimens was $15.5\,\mathrm{GPa}$, and the coefficient of variation was 0.10. Note that when determining the modulus of elasticity, the influence of the added mass of accelerometers was eliminated so that the results were not affected by them. However, for the damage detection, corrections were not performed because the accelerometer positions remained the same for all undamaged as well as damaged beams. Consequently, neither the obtained results from the study of modal properties nor those from damage identification are affected by added mass. However, the numerical model in SOFiSTiK [76], which was used for the verification of the measured data, the aforementioned correction, and for damage identification, includes the added mass of accelerometers.

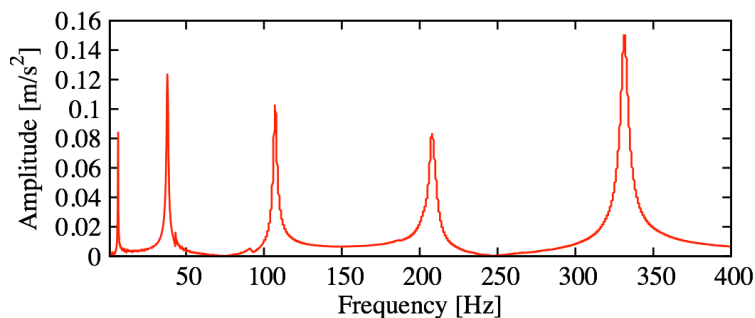Vibration measurements were recorded using five Brüel & Kjær 4508-B-001 ac-

Figure 3.10: Frequency spectrum of undamaged specimen c12 obtained from data recorded by accelerometer a3, which was placed 360 mm from the free end

celerometers which were connected to a Brüel & Kjær 3560-B-140 analyzer. Figure 3.8 shows the testing configuration and how the fixed support was provided. Loading was imposed with a view to attaining repeatability using a plastic projectile with 6 mm diameter and 0.25 g weight, which was dropped from a height of about 32 cm onto the free end of the cantilever beam. The measurement was only accepted if the bullet touched the beam just once.

Dynamic measurement was first carried out using a set of undamaged beams. The recorded time series of accelerations were analyzed using the fast Fourier transform (FFT) method and values were obtained for eigenfrequencies and corresponding mode shapes; see the example of a frequency spectrum in Figure 3.10. Then, every individual specimen was cut in a certain part – see a schematic view in Figure 3.9. Each beam had only one single cut. All five damaged beams were once again tested and their modal properties were evaluated. A comparison of the eigenfrequencies for undamaged and damaged beams is introduced in Table 3.1. The last column of the table shows their relative changes due to damage. These are depicted in Figure 3.11 and compared with those changes obtained from numerical simulation. A comparison of mode shapes in the form of MACs is depicted in Figure 3.12. The displayed boundaries in both figures correspond to relative stiffnesses of 0.4 and 0.6. Let us note that each damage position corresponds to a different test sample – each specimen had a slightly different stiffness, there were minor deviations in the depths of notches, etc. Nevertheless, the experimental results are in good agreement with the numerical ones. The relative changes in eigenfrequencies correspond well with the mode shapes in both cases. The changes in mode shapes are too small compared to the changes in eigenfrequencies, and therefore those were not utilized for damage detection as described in Section 3.3.1.

Table 3.1: Comparison of the results of dynamic measurements for undamaged and damaged beams

| Specimen	Eigenfrequency [Hz]	Undamaged beam	Damaged beam	Relative change [%]
	f_1	5.191	4.923	5.15
	f_2	33.712	33.090	1.84
c11	f_3	96.663	94.188	2.56
	f_4	185.738	184.363	0.74
	f_5	303.588	299.263	1.42
	f_1	6.319	6.047	4.32
	f_2	38.062	37.387	1.77
c12	f_3	107.212	101.938	4.92
	f_4	208.112	205.312	1.35
	f_5	331.512	329.412	0.63
	f_1	6.060	5.955	1.72
	f_2	35.040	33.638	4.00
c13	f_3	96.562	96.837	-0.28
	f_4	186.337	180.112	3.34
	f_5	302.037	303.137	-0.36
	f_1	6.060	6.057	0.04
	f_2	36.014	34.662	3.75
c14	f_3	100.262	94.563	5.68
	f_4	193.662	191.012	1.37
	f_5	312.712	309.062	1.17
	f_1	5.944	5.932	0.20
	f_2	36.136	36.111	0.07
c15	f_3	100.837	99.313	1.51
	f_4	193.662	187.112	3.38
	f_5	313.862	302.812	3.52
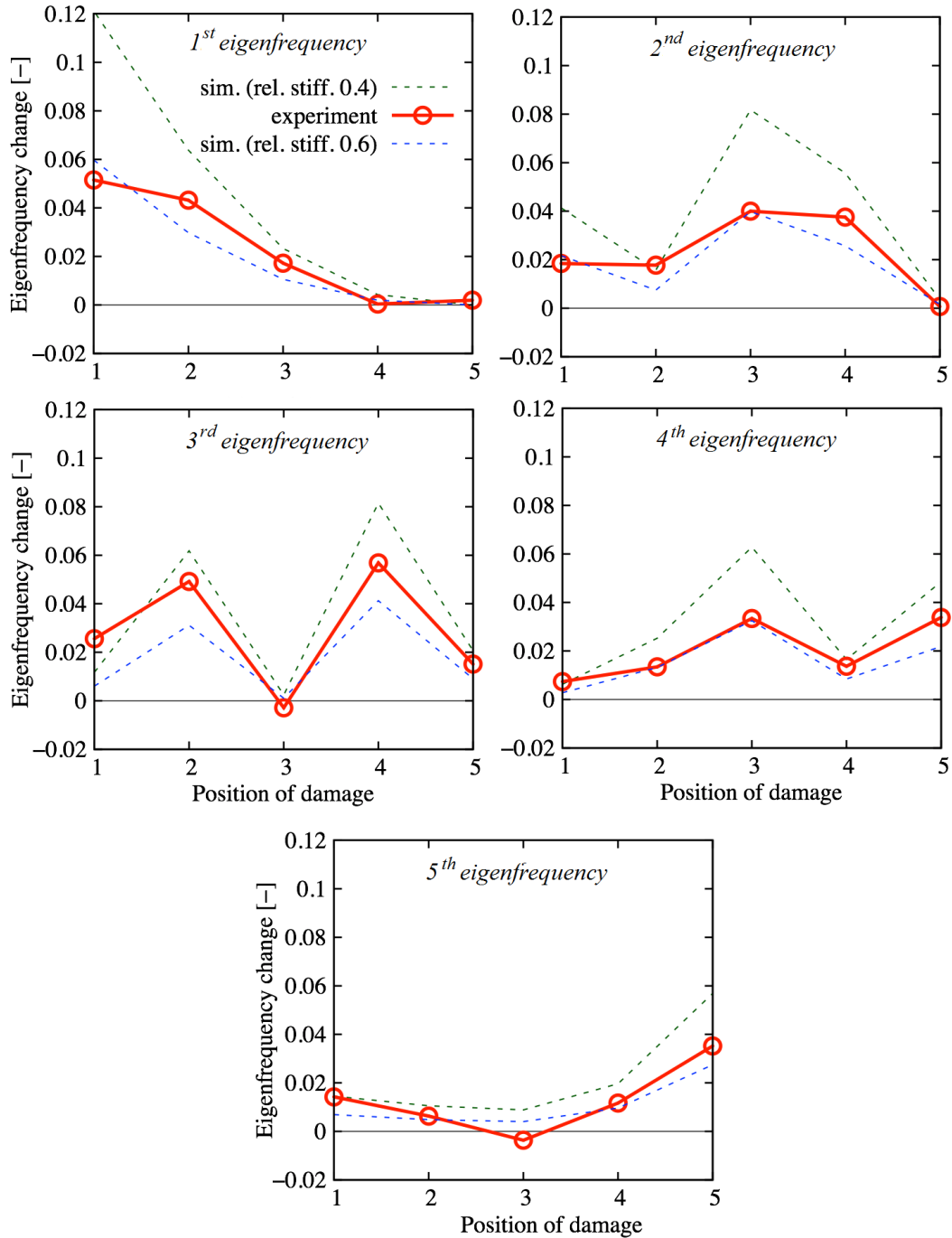
Figure 3.11: Relative changes in eigenfrequencies for different damage positions: experiment vs. numerical simulation with relative stiffnesses of 0.4 and 0.6 in damaged parts
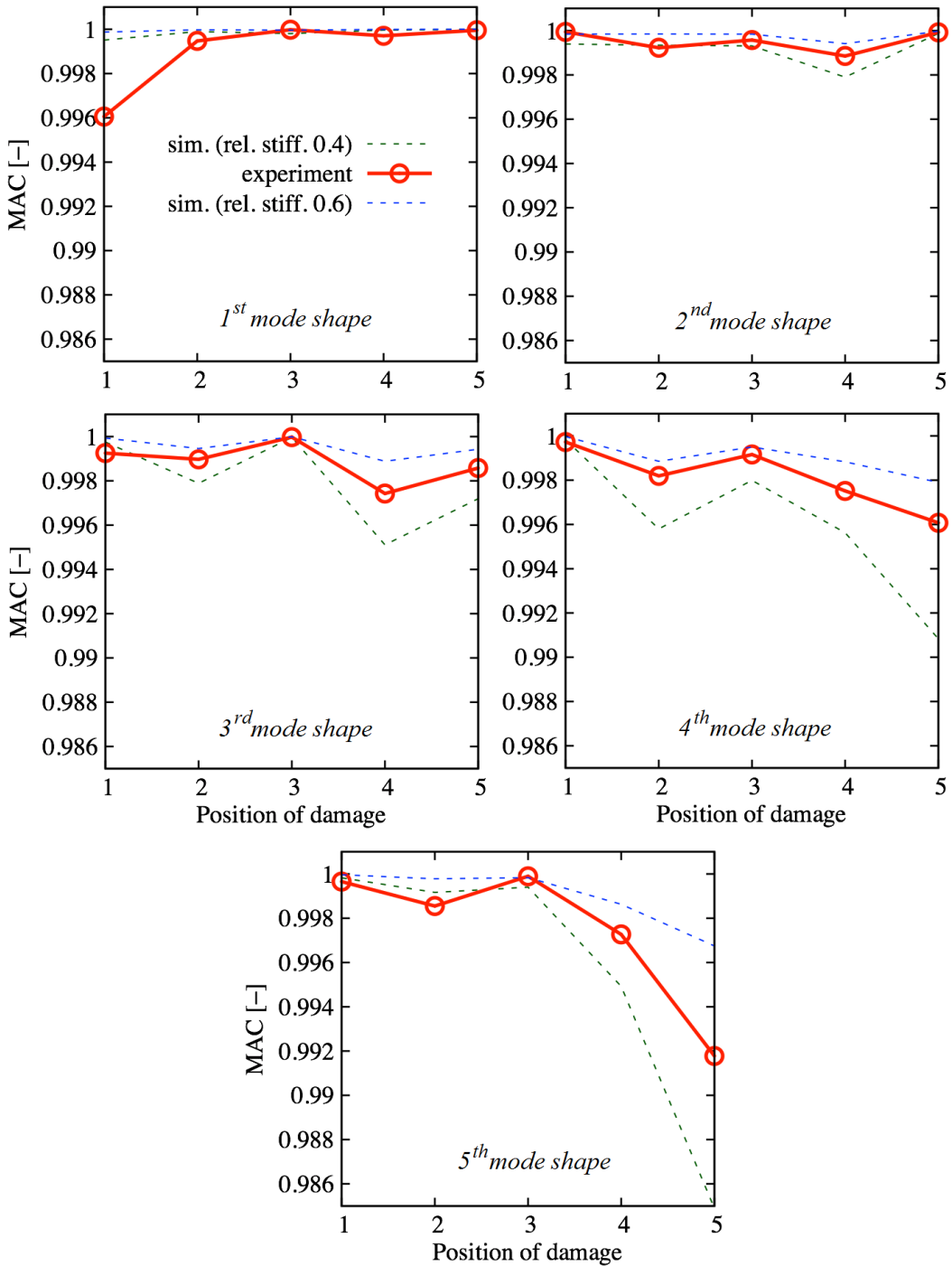
Figure 3.12: MAC for different damage positions: experiment vs. numerical simulation with relative stiffnesses of 0.4 and 0.6 in damaged parts

3.2.2 Two-span continuous beam

Detailed dynamic analysis and damage detection were carried out on reinforced concrete beams together with the fracture–mechanical parameter testing of said beams in cooperation with the Institute of Structural Engineering (IKI) at BOKU University in Vienna, Austria. Changes in modal properties (eigenfrequencies, mode shapes) were investigated for various levels of damage. In total, nine reinforced concrete two-span continuous beams (as depicted in Figure 3.13) were cast and tested at the IKI laboratory; see Figure 3.14. Two loading configurations were tested: (1) symmetric loading by forces in the middle of both spans, and (2) asymmetric loading by a single force in the middle of one span. In this work, the second configuration is analyzed in order to test the ability of the method to detect asymmetric damage.

Initial dynamic testing was performed using an undamaged beam followed by static loading until the initiation of the first visible cracks occurred. Then, dynamic testing was carried out using the damaged beam. This procedure was performed several times for increasing load levels until the ultimate capacity of the beam was reached. The greatest attention was paid to precise vibration measurements and the evaluation of modal properties. For that reason, a laser vibrometer was employed for the direct measurement of the modal deflection of the beam. Several accelerometers were placed on both sides of the beam underneath the connection to one actuator in order to control the torsion of the beam. Furthermore, these accelerometers allowed possible changes in excitation to be controled and considered during the measurements. Dynamic measurements were only conducted for the first two eigenmodes because the realistic adjustment of the excitation to higher modes with only two available actuators was impossible. More details on beam instrumentation and measurement can be found in Hoffmann et al. [22].

Before damage detection, which is described in Section 3.3.2, a numerical study of modal properties was carried out. With respect to measurements, the first four eigenfrequencies and mode shapes were taken into account. The ratio between the first and fourth eigenfrequency was approximately 1:5. The numerical model in SOFiSTiK software and its parameters were tuned with respect to the experimental measurements. A comparison between the first two eigenfrequencies obtained from the experiment and the numerical model for the undamaged beam can be found in Table 3.2 (Section 3.3.2). The beam was divided into 12 parts with independent bending stiffness in each. Damage to the beam in each particular part was modeled by a decrease in its bending stiffness to 0.01–0.90 of its nominal value. Such damage was applied step by step for all parts (only one part was damaged at one time).

Results in the form of relative changes in eigenfrequencies depending on the size of the damage are depicted in Figure 3.15. It is clear that the shape of changes again corresponds to the mode shapes of the bridge. The maxima of the relative changes across all eigenfrequencies are shown in Figure 3.16, together with an indication as to which eigenfrequency is responsible for a particular maximum: see the graduated
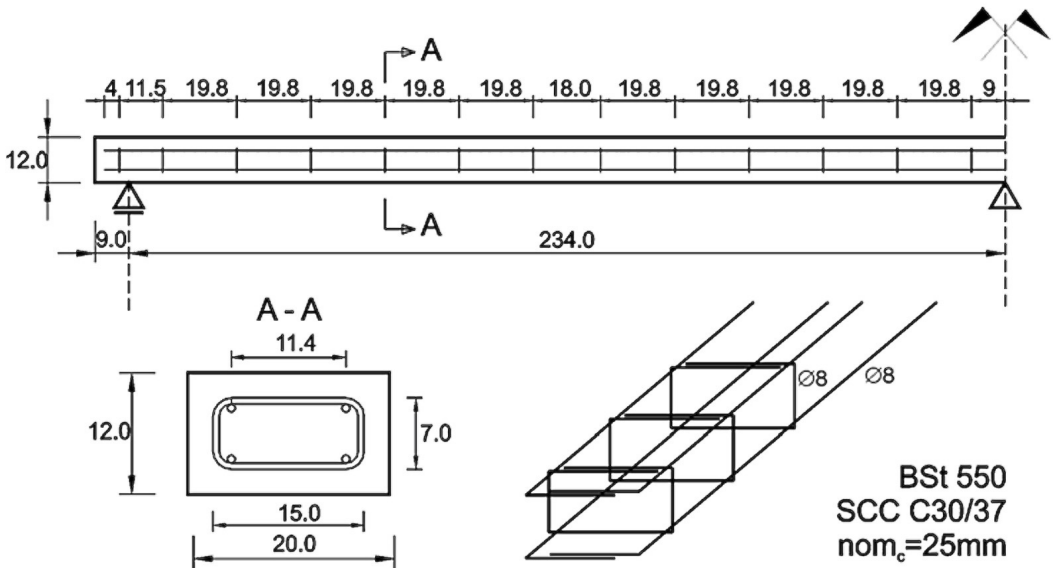
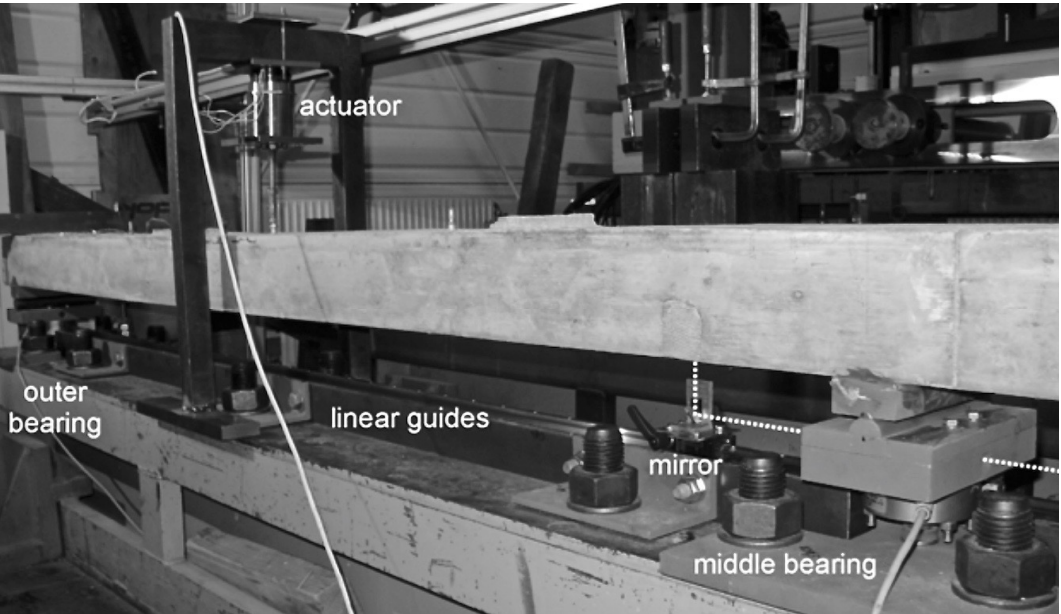Figure 3.13: A schematic view of the tested beam (dimensions in centimeters, adopted from [22])

Figure 3.14: Testing configuration: beam excited by moving coil actuators and measured by a laser vibrometer, accelerometers and force transducers (adopted from [22])
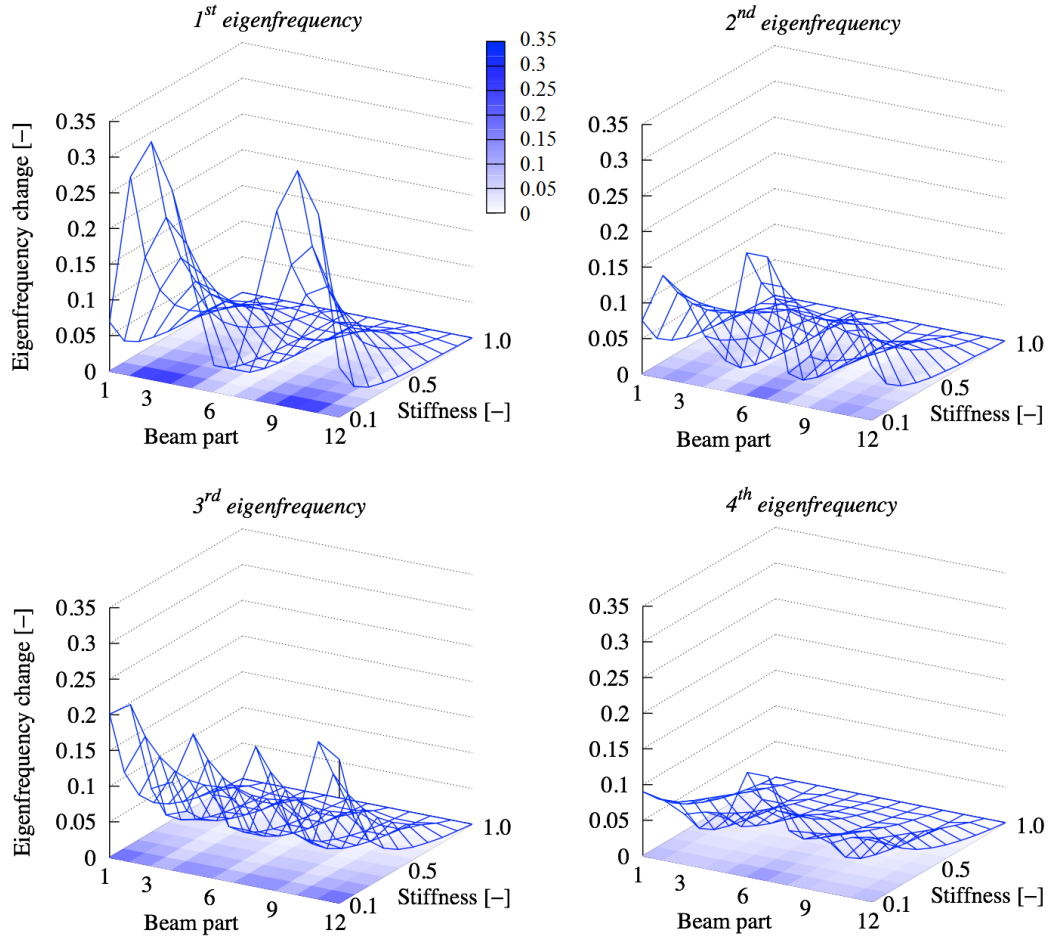
Figure 3.15: Relative changes in eigenfrequencies for different levels of stiff-
ness in a particular damaged part of a continuous beam

shading on the right side of the figure. It is visible that the dominant eigenfrequency
changes with the position of damage on the beam; close to the end supports it also
changes with the size of the damage. Figure 3.17 shows a change in the MAC for a
90 % stiffness reduction if the damage is moved along the girder from one part to
another. It can again be seen that the higher mode shapes are much more affected
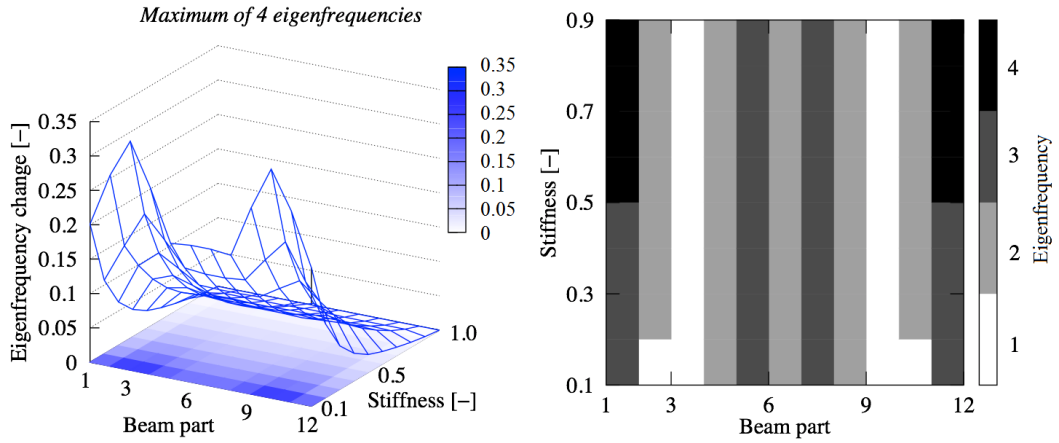compared to the eigenfrequencies.

Figure 3.16: Maximum values of relative changes of the first four eigenfrequencies (left), and the determination of which eigenfrequency belongs to the specific maximum (right)
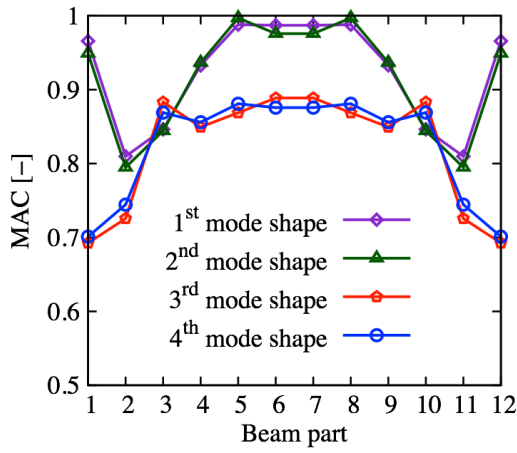

Figure 3.17: Comparison of the MAC of all four mode shapes for a stiffness reduction of 90 % in a particular damaged part of a continuous beam

3.2.3   Bridge Z24

The same study as that conducted on the laboratory beams was performed on the Z24 Bridge in Switzerland, which connects Koppigen and Utzenstorf. The bridge is a A1 highway overpass, which links Bern and Zürich. The Z24 Bridge is a prestressed bridge with three spans, two lanes and an overall length of 60 m. A schematic view of the bridge is shown in Figure 3.18. The bridge was subjected to various damage scenarios in 1999. The modal data are available so the subsequent damage detection can be verified with good knowledge of the damage induced during previous experiments.

First, a computational model in SOFiSTiK was developed and tuned according to experimental measurements (stiffness, eigenfrequencies and mode shapes). Equivalent values were calculated for the cross-section area and the bending and torsional moments of inertia of the box section of the main girder. For the purposes of this study, the girder was divided into twenty parts, each with independent bending and torsional stiffness. The girder has higher stiffness above the supporting piers because of the higher thickness of the bottom and top slabs. Examples of mode shapes are depicted in Figure 3.19. The first and fifth modes are pure bending, while the third and fourth are a combination of bending and torsion. Since the second mode shape is pure horizontal bending, it was excluded from further analyses.

For the parametric study, the same level of damage was considered for both bending and torsional stiffness. Comparative studies in which only one type of stiffness (bending or torsional) was changed were also carried out, but since these cases are not very relevant to the detection of real bridge damage, the results are not discussed here. The results of the study have shown that rotational stiffness only affects combined mode shapes (3rd and 4th); on the other hand, bending stiffness affects all four mode shapes. For the 4th mode shape the combination is very important and the results are not a simple summation of bending and torsion (as is the case with the 3rd mode shape). The real behavior lies somewhere between these extremes. For this reason, a statistical correlation between bending and torsional stiffness was imposed during damage detection.

Results in the form of a relative change in eigenfrequencies depending on the size of the damage are depicted in Figure 3.20. It is clear that the shape of the changes again corresponds to the mode shapes of the bridge. The maximum values of the relative change in eigenfrequencies (see the graduated shading in the figure) are shown in Figure 3.21. Figure 3.22 shows the change in the MAC for a 90 % stiffness reduction if the damage is moved along the girder from one part to another. It can be seen again that the higher mode shapes are much more affected compared to eigenfrequencies. Unfortunately, as was already mentioned, obtaining the higher mode shapes experimentally is a complicated task.
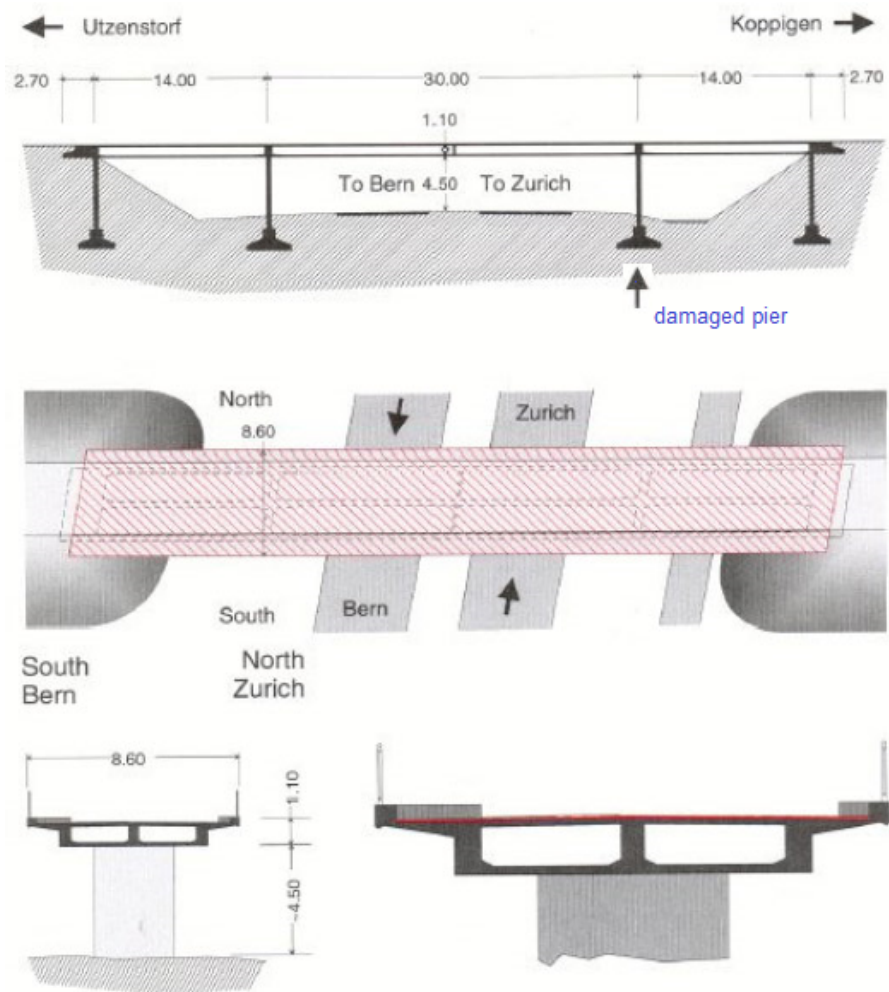
Figure 3.18: A schematic view of the Z24 Bridge – side view, top view, and cross-section (adopted from [52])

1st mode shape

3rd mode shape

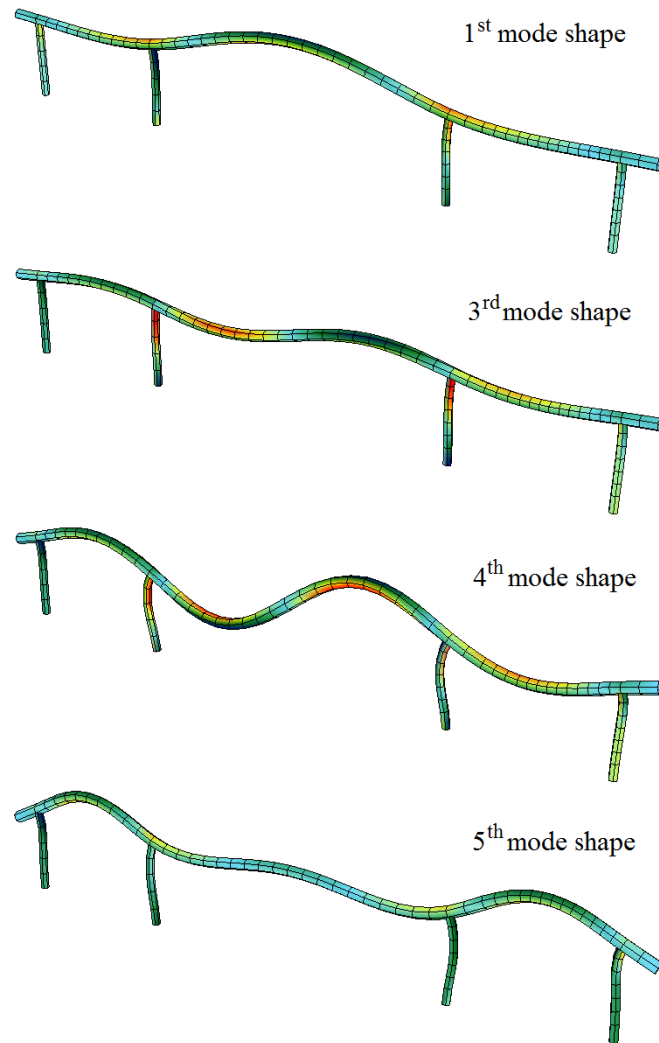4th mode shape

5th mode shape

Figure 3.19: Four mode shapes of the Z24 Bridge which were considered
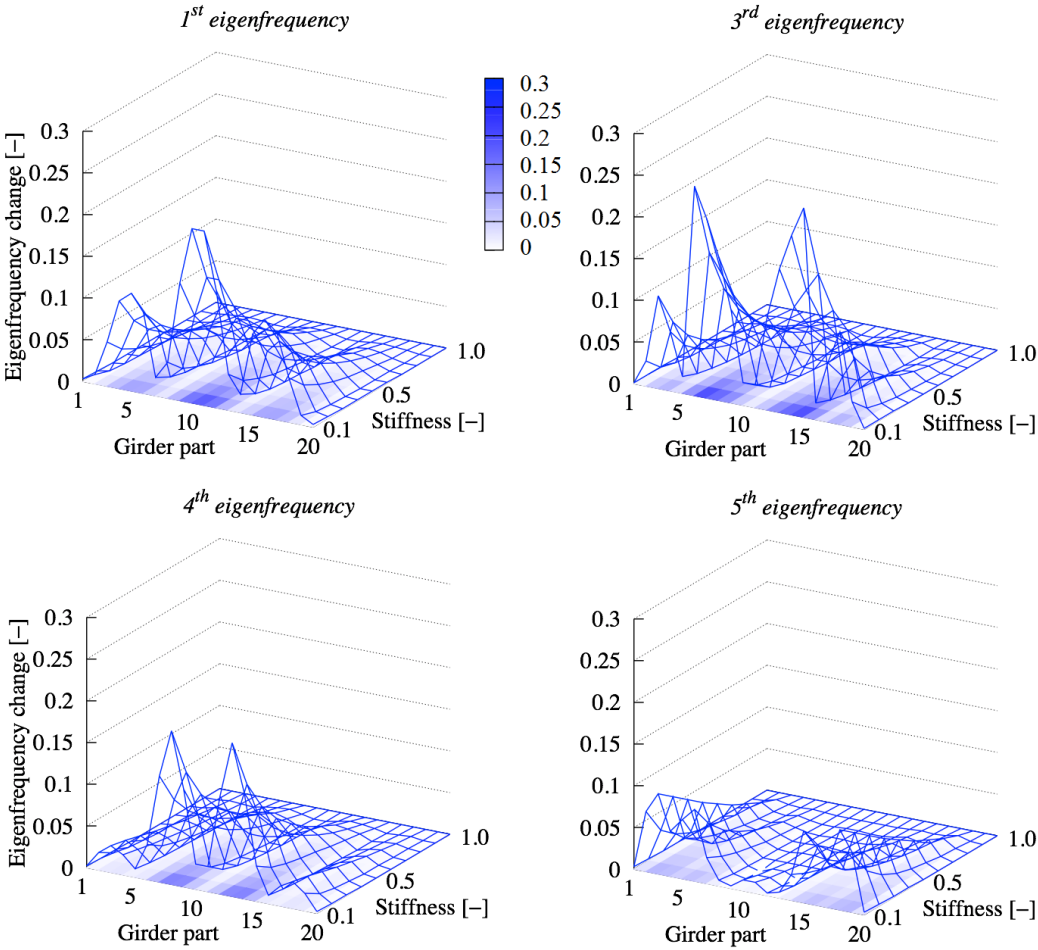for parametric study and subsequent damage detection

Figure 3.20: Relative change in eigenfrequencies for different levels of stiffness in a particular damaged part of the Z24 Bridge
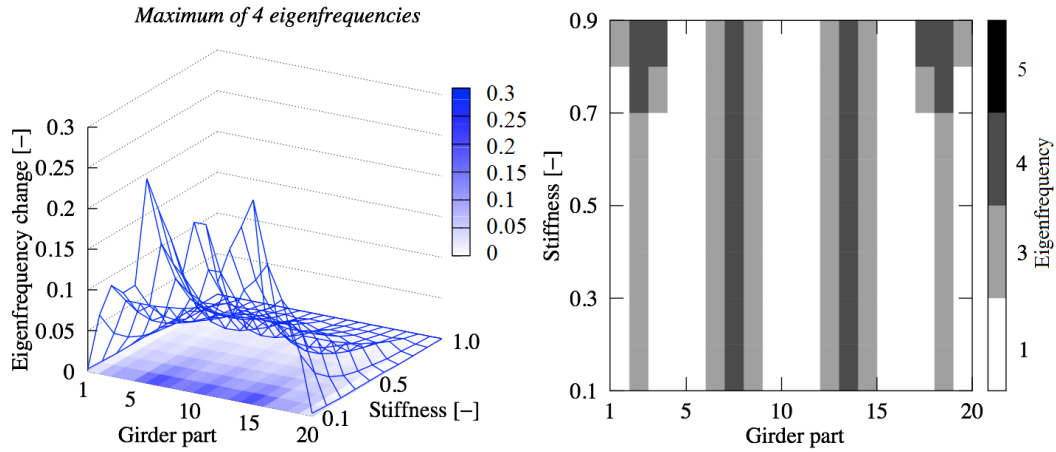
Figure 3.21: Maximum values of relative changes in the first four eigen-
           frequencies (left), and determination of which eigenfrequency
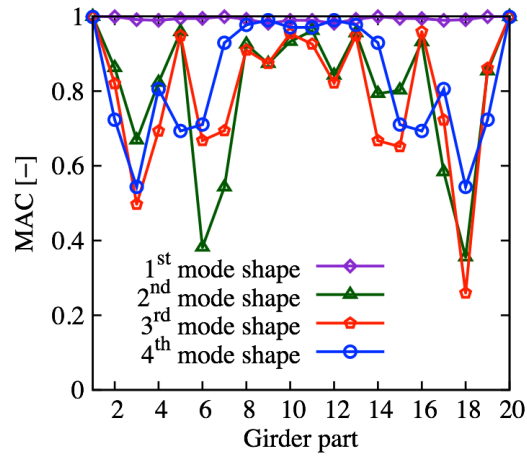   belongs to the specific maximum (right)

Figure 3.22: Comparison of the MAC of all four mode shapes for a stiffness
           reduction of 90 % in a particular damaged part of the Z24
           Bridge

3.3 Example of damage detection

3.3.1 Cantilever beam

Following the numerical and experimental study of the cantilever beam, damage detection was carried out. The relative changes in the five eigenfrequencies were used as inputs for inverse analysis. Mode shapes were not included due to the smallness of the changes that affected them; see Section 3.2.1. For damage detection, the beam model was divided into 15 parts with independent bending stiffness $EI_1, ..., EI_{15}$ (see Figure 3.9). Its values were randomly generated from the $\langle 0.2, 1 \rangle$ interval and corresponding eigenfrequencies were calculated. The training set contains 120 samples and was divided into two parts – 115 samples were used directly for training the network, while 5 samples were employed in the testing of network overfitting.

The employed ANN consists of 1 hidden layer with 10 nonlinear neurons (hyperbolic tangent transfer function) and an output layer with 15 linear neurons (15 stiffness values). There are also 5 inputs to the network (5 eigenfrequencies); see Figure 3.23. After the network was trained using the gradient descent method with momentum, the eigenfrequencies obtained from the experimental testing of damaged beams were introduced to the ANN as an input signal. After the ANN simulation, the spatial distribution of stiffness along the girder was obtained (15 values; see Figure 3.24). Because of the inconsistency between the experimental and numerical results of specimen c11, which was probably caused by some testing errors along
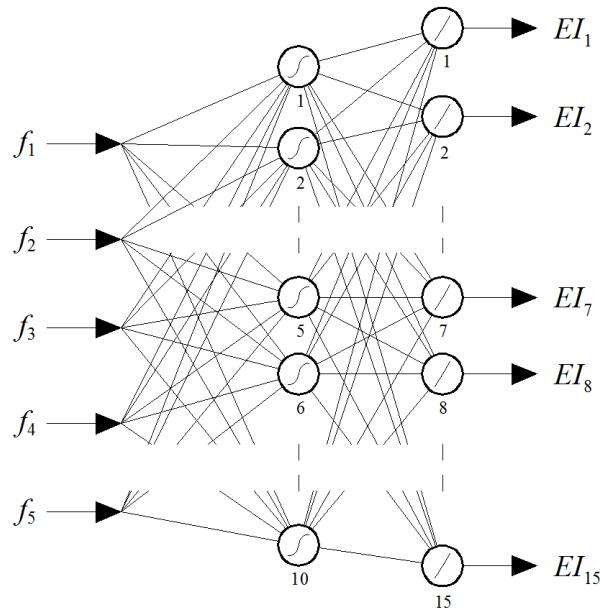
Figure 3.23: A schematic view of the ANN for the detection of damage in a cantilever beam
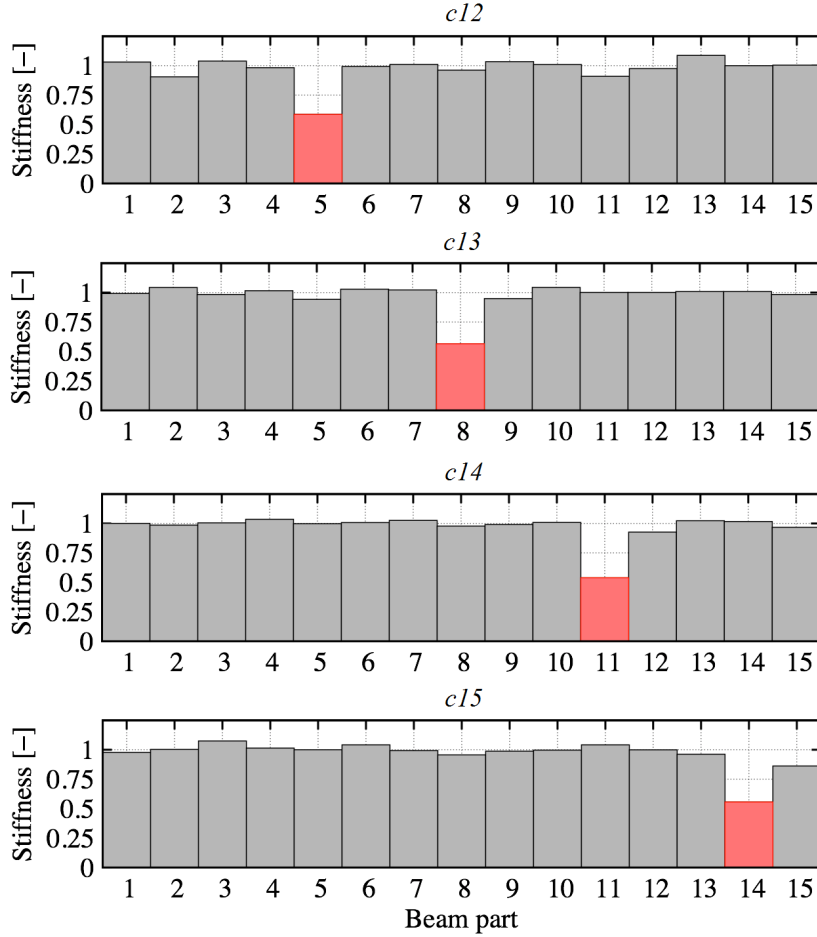
Figure 3.24: Stiffness distribution after the performance of damage detection on cantilever beams (the red elements correspond to the parts where the beams were cut)

with high vibration sensitivity to damage located close to the fixed end of the cantilever beam, this specimen was omitted from damage detection. The performance of inverse analysis for the remaining four specimens resulted in very clear and correct indications of where all beams were cut (the red parts in Figure 3.24) and how great the damage was.

3.3.2 Two-span continuous beam

Damage detection was performed on a continuous beam loaded by single force in one span using modal data obtained from experimental testing. The beam model was once again divided into 12 parts with independent bending stiffness. Since laboratory dynamic measurements were only conducted for the first two eigenmodes, the first two eigenfrequencies were taken into account for damage detection in the first step. Unfortunately, due to the symmetry of the beam, this kind of input information is not sufficient for the successful identification of asymmetric damage caused by asymmetric loading; see the crack pattern in Figure 3.26c. The identified stiffness distribution was more or less symmetric (Figure 3.26a). Nevertheless, verification showed that the eigenfrequencies obtained from the numerical model were in good agreement with those determined experimentally. It was obvious that the inverse problem itself was ill-posed and that inverse analysis had found one of the possible solutions related to the selected input data. However, when comparing mode shapes, the discrepancy between experiment and simulation is noticeable (Figure 3.27a). Therefore, in the second step, in addition to the first two eigenfrequencies, the maximal amplitudes of both mode shapes measured in the unloaded field were utilized as a new input data.

In the second step, the ANN consists of 1 hidden layer with 12 nonlinear neurons (hyperbolic tangent transfer function) and an output layer with 12 linear neurons (12 stiffness values). There are also 4 inputs to the network (2 eigenfrequencies and 2 amplitudes of mode shapes); see Figure 3.25. In order to prepare the training set, the relative stiffness values were randomly generated from the $\langle 0.25, 1.25 \rangle$ interval and corresponding eigenfrequencies and mode shapes were calculated. The training set contains 500 samples and was divided into two parts – 450 samples were used directly for training the network, while 50 samples were employed in the testing of network overfitting.

After the network was trained using the gradient descent method with momentum, the eigenfrequencies and mode shape amplitudes obtained from the experimental testing of the damaged beam were introduced to the ANN as an input signal. After the ANN simulation, the spatial distribution of stiffness along the girder was obtained (12 values, see Figure 3.26b). To achieve verification, these values were utilized in the numerical model, and corresponding eigenfrequencies and mode shapes were calculated; see their comparison with the experimental results in Table 3.2 and Figure 3.27b. It can be concluded that the identified stiffness is now in much better agreement with the experimental crack pattern than in the first step when it was detected using only eigenfrequencies. Also, asymmetric mode shapes were correctly identified.

Table 3.2: Eigenfrequencies for the continuous beam in an undamaged and
damaged state: experiment vs. identification

	Eigenfrequencies [Hz]			
Mode shape	Undamaged state		Damaged state	
	Experiment	Model	Experiment	Model
1st	34.99	34.42	27.24	28.02
2nd	51.34	53.77	42.31	44.58
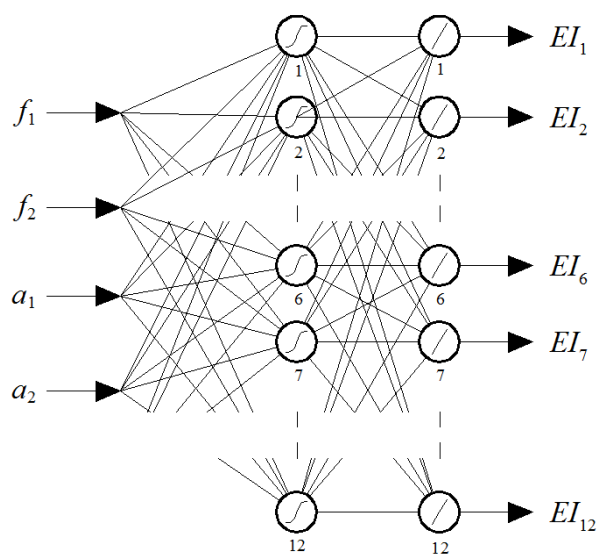
Figure 3.25: A schematic view of the ANN for damage detection in a con-
tinuous beam
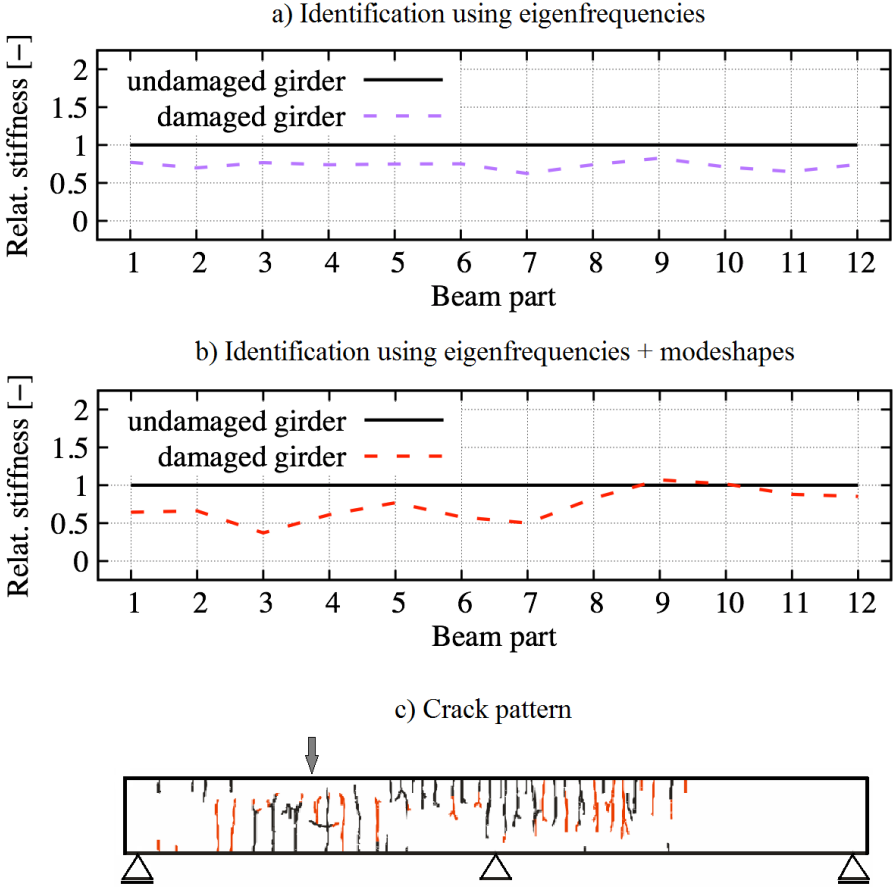
Figure 3.26: Identified bending stiffness of the continuous beam using: a) eigenfrequencies, and b) eigenfrequencies and amplitudes of mode shapes; c) experimental crack pattern at ultimate capacity

a) Identification using eigenfrequencies

b) Identification using eigenfrequencies + mode shapes

Figure 3.27: Comparison of mode shapes obtained from experimental measurements and numerical analyses with stiffness identified using: a) eigenfrequencies, and b) eigenfrequencies and amplitudes of mode shapes

3.3.3 Bridge Z24

Damage detection was carried out on the Z24 Bridge. A computational model in SOFiSTiK was developed and tuned according to experimental measurements, as mentioned in Section 3.2.3. For the purpose of damage detection, the girder was divided into twenty parts with independent values for bending 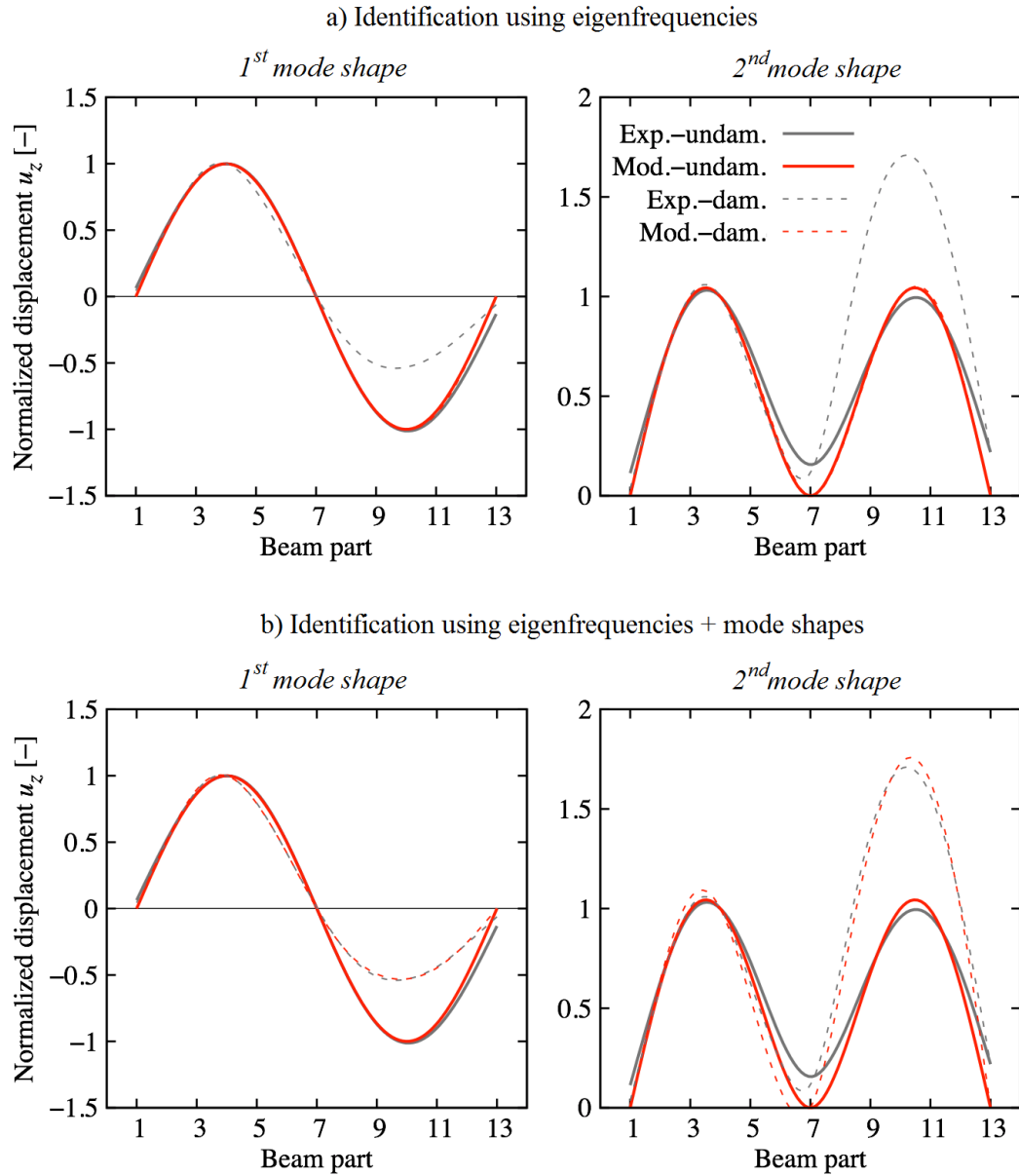stiffness EI and torsional stiffness GI_{t} . The girder has higher stiffness above the supporting piers due to the higher thickness of the bottom and top slabs. A comparison of eigenfrequencies for the undamaged state obtained from the experiment and numerical model is in Table 3.3.

The bridge was subjected to various controlled damage scenarios in 1999. The modal data are easily available so the results of modeling and inverse analysis can be verified with the results from experiments. For the purpose of damage detection the scenario with inner right pier lowering was used (see Figures 3.18 and 3.29). Corresponding experimental eigenfrequencies measured after damage occurred are in Table 3.3. Because of bridge symmetry and the high number of unknowns (20 parts with 2 stiffness values in each), damage detection was restricted to the right half of the bridge, where pier lowering was applied. Finally, 18 stiffness values were identified (9 parts, each with both bending and rotational stiffness). Based on the results of the study of modal properties and experience with the detection of damage in cantilever and continuous beams, only eigenfrequencies were considered as an input for inverse analysis (see Table 3.3).

The neural network used for inverse analysis consists of 1 hidden layer with 8 nonlinear neurons (hyperbolic tangent transfer function) and an output layer with 18 linear neurons (18 stiffness values). Stiffness varied from 25 % to 125 % of the original stiffness (undamaged girder). There are also 4 parameters as inputs to the network (4 eigenfrequencies); see Figure 3.28. The training set was generated using 500 simulations of the LHS method and was divided into two parts – 450 simulations were used directly for training the network, while 50 simulations were employed for testing network overfitting. After the network was trained using the gradient descent method with momentum, the eigenfrequencies from the experimental testing of the damage state were used for the ANN simulation. The output of the ANN is a spatial distribution of stiffness along the girder (18 values, one half of the girder). The final modal analysis in SOFiSTiK was performed using identified stiffness values in order to obtain corresponding mode shapes and eigenfrequencies.

Figure 3.30 shows bending and rotational stiffness distribution along the girder for undamaged (reference) and damaged (after pier lowering) states. The stiffness for the damaged state is the result of identification. The resulting eigenfrequencies are presented in Table 3.3. A comparison of the experimental and numerical mode shapes obtained from the simulation with both bending and torsional stiffness being identified, respectively, for the bridge in a damaged state is shown in Figure 3.31. The results of identification using four eigenfrequencies have again shown the

Table 3.3: Eigenfrequencies for the bridge in an undamaged and damaged
         state

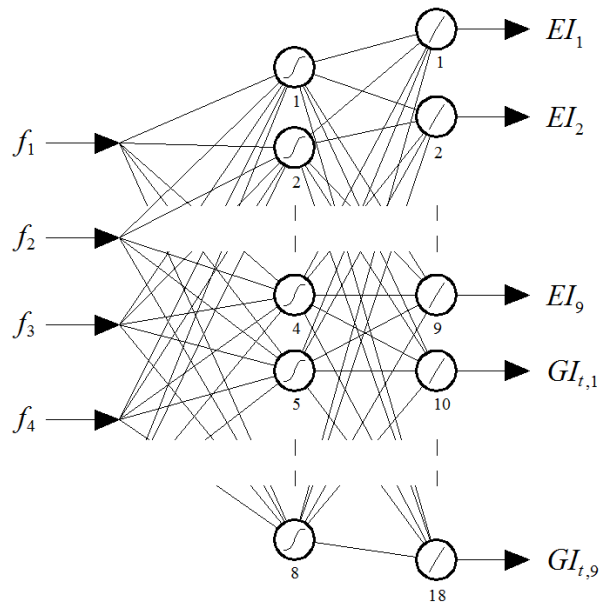| Mode shape | Eigenfrequencies [Hz] | | | |
| | Undamaged state | | Damaged state | |
	Experiment	Model	Experiment	Model
1st	3.89	3.87	3.67	3.75
3rd	9.80	9.81	9.21	9.38
4th	10.30	10.42	9.69	9.95
5th	12.67	12.60	12.03	12.26

Figure 3.28: A schematic view of the ANN for damage detection in the Z24
         Bridge

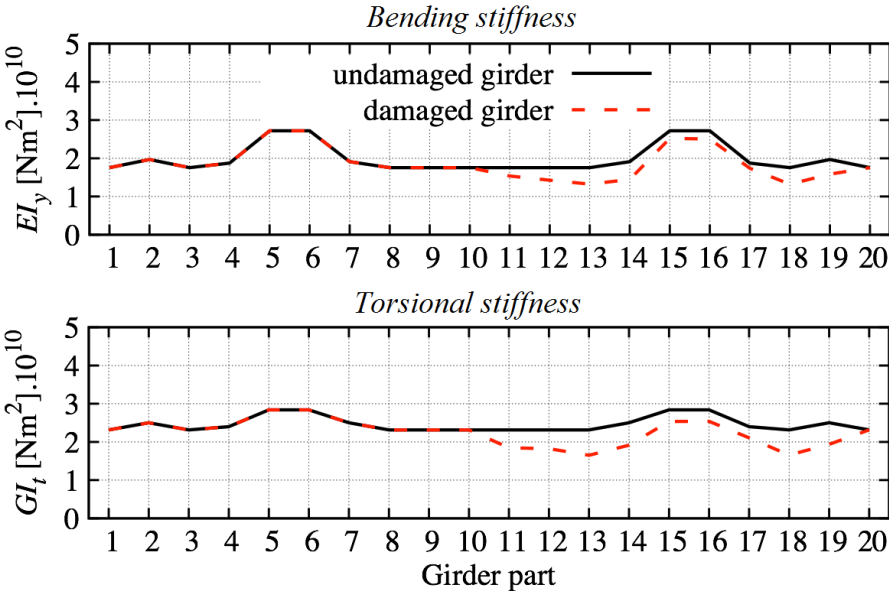Figure 3.29: Bridge Z24: damage of the inner right pier

Figure 3.30: Bending and torsional stiffness of the girder in an undamaged and damaged state

potential of the proposed identification technique and this type of input information.

3.4   Summary

The identification of damage affecting existing structures while in use is a very topical and challenging issue. The proposed ANN-based inverse analysis method seems to be a promising one. Its efficiency was verified using laboratory experiments as well as a real bridge. Beyond the presented examples, verifications were carried out using several other structures, resulting in similar outcomes, e.g. Strauss et al. [80], Lehký et al. [36]. Let us mention one of the important advantages of the proposed method – after initial stochastic calculations, ANN setup and training, it can be easily implemented in the permanent monitoring system of a particular bridge, providing real-time damage detection based on measured data.

The most critical part of the whole damage detection procedure is the appropriate selection of input information. Tested examples have shown the ability of an ANN to correctly detect damage using several eigenfrequencies. However, let us note that in all cases the size of the damage was relatively great. With smaller amounts of damage, eigenfrequency changes are relatively minor and damage detection would be much more difficult. This is in agreement with the findings of other researchers (e.g. Sinou [74], Wenzel and Pichler [87]). The same situation will occur in the case of mode shapes or criteria derived from them. Fortunately, this is not a limitation of the proposed method but of the whole concept of damage detection based on structural health monitoring data. Therefore, the main aim of future research in this field must be to find a more relevant type of input information which will allow the detection of relatively small amounts of damage, will not be sensitive to environmental and operational conditions, such as changing ambient temperature or sensor placement and, on the other hand, can be easily extracted from ambient vibration data.
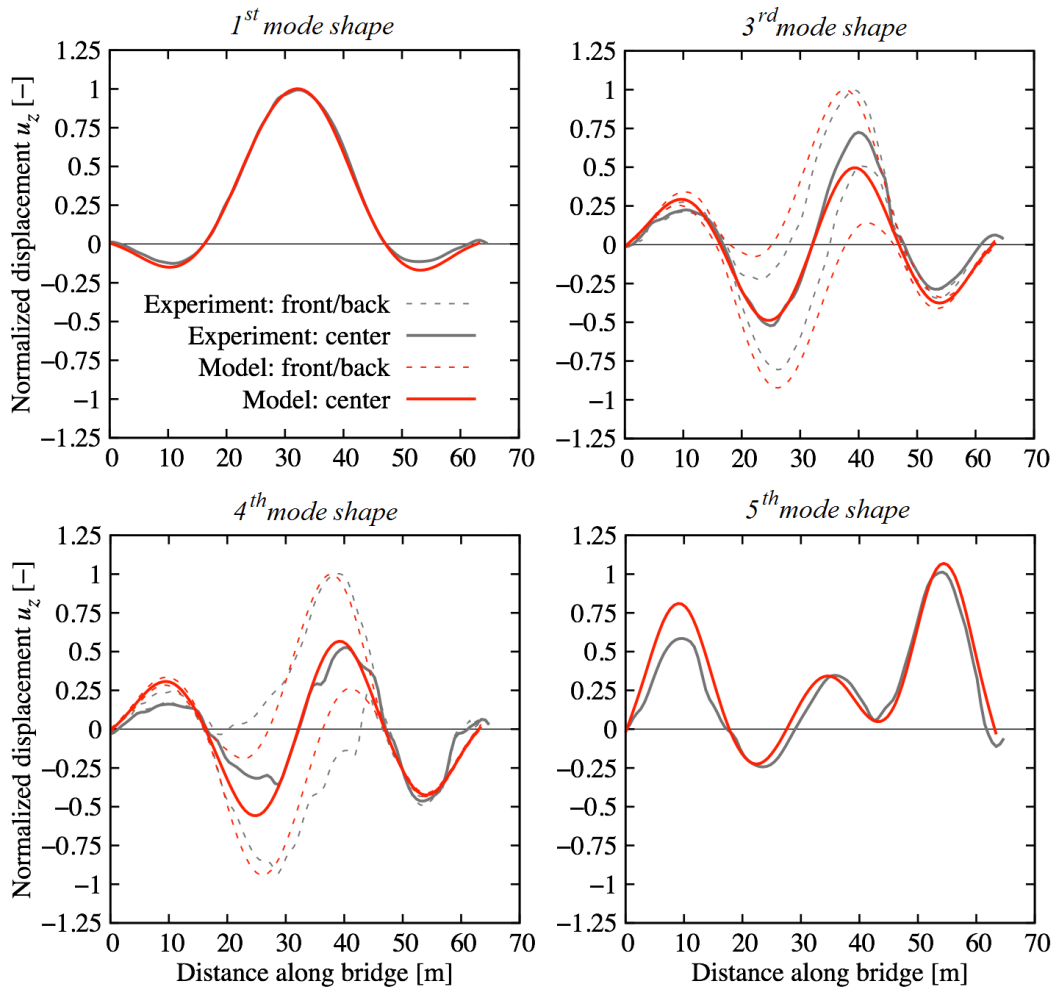
Figure 3.31: The Z24 Bridge in a damaged state: Comparison of mode shapes obtained from experimental measurements and a numerical model with identified bending and shear stiffness (The first and fifth are pure bending modes, while the third and fourth are combined bending and torsional modes)

Chapter 4

Material parameter identification

The last type of inverse problem discussed in this work is an identification of fracture–mechanical parameters of concrete and other quasi-brittle materials using results of laboratory fracture experiments. Their knowledge is fundamental for deterministic and stochastic nonlinear computational modeling of structures made of these materials. Standard experimental testing, often performed in the form of compression tests on cubic specimens, provides incomplete information about fracture–mechanical parameters. The lack of information often necessitates the use of engineering judgment or information from the literature. Information regarding the parameters of constitutive laws for nonlinear fracture mechanics analysis is of crucial importance, particularly fracture energy, tensile strength, and softening function, etc. Data for such parameters is still insufficient today even though they play a key role in the modeling of fracture, crack development and the ultimate load bearing capacity of structures.

A great deal of attention has been devoted to the development of inverse methods to determine the quasi-brittle fracture behavior of concrete (Planas et al. [64]). One possibility is to obtain computational model parameters indirectly – based on a combination of fracture tests and inverse analysis. This chapter describes a methodology of acquiring such parameters using experimental data from three-point bending test and ANN-based inverse analysis method introduced in this work. The proposed methodology for parameter identification combining nonlinear simulations with the training of an artificial neural network is relatively time-consuming and of high complexity (Novák and Lehký [58]). Therefore, the whole procedure has been implemented in the software tool FraMePID–3PB, described in details in Section 5.3.

A key parameter of concrete structure modeling using nonlinear fracture mechanics is the specific fracture energy, which is the subject of research by many authors, e.g. Bažant and Planas [4], Karihaloo [29]. Other important parameters of concrete

are modulus of elasticity, tensile strength, and compressive strength. Crack propagation resistivity is described by e.g. effective crack elongation or effective fracture toughness (Karihaloo [29]). Determination of the values of such parameters can be performed using two techniques – (i) direct evaluation from an experimental load–deflection diagram via the effective crack model and the work-of-fracture method; (ii) inverse analysis using ANN-based method.

Depending on the sample size of the statistical set, the basic statistical characteristics (mean values and standard deviations) of material parameters can be determined using two approaches:

1. The "one by one" approach – the parameters of each specimen are identified separately and the final statistics are calculated from the set of all values for each parameter;

2. the "direct" approach – in the case of a larger statistical set it is more efficient not to identify each specimen one by one but to identify the whole statistical set for all specimens together based on the random response of fracture tests (Lehký and Novák [37], [39]).

4.1   Laboratory test

Fracture–mechanical parameter values should be determined using the results of fracture tests in suitable configurations (three-point bending test, wedge splitting test, etc.). In our case, due to the relative simplicity and availability of testing equipment, a three-point bending test (3PB test) of specimens with a central notch is used, see a schematic view in Figure 4.1. The specimens are of the nominal size $100 \times 100 \times 400 \, \mathrm{mm}$. The loading span is $300 \, \mathrm{mm}$. In the center of the beam the notch is cut to a depth of about $1/3$ of the depth of the specimen using a diamond blade saw. An example of a test specimen is shown in Figure 4.2a.

The testing machine has to be stiff enough to perform a stable test. A test can be regarded as stable if the load and deflection change slowly and without any sudden jump during the whole test. Whenever there are problems in running the test in
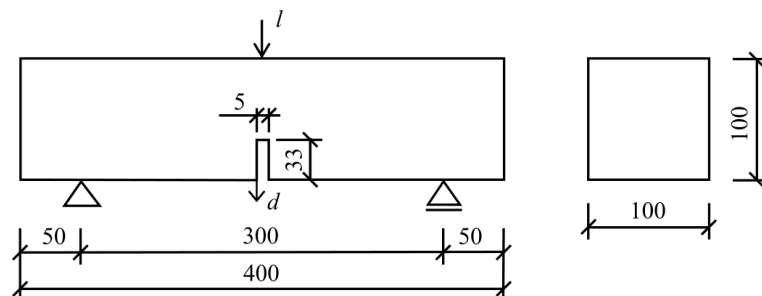

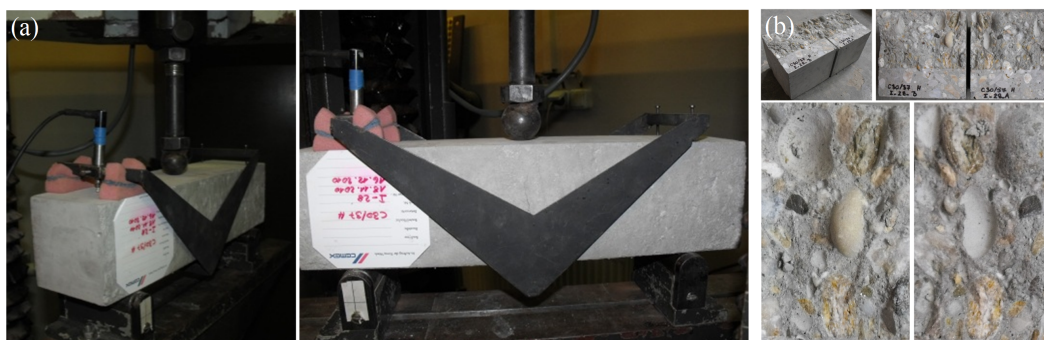Figure 4.1: A schematic view of the tested beam

Figure 4.2: (a) Selected specimen tested in a three-point bending configuration and (b) the fractured parts/surfaces after testing

a stable manner, crack mouth opening displacement shall be used as the control value for deformation rate. The supports and loading arrangements should be such that the forces acting on the beam are statically determinate. The deflection of the center of the beam shall be determined with regard to a line between two points on the beam above the supports. Alternatively the deformation of the load-point with respect to the support may be measured if the load-application and supports are arranged in such a way that non-elastic deformations at these points are less than 0.01 mm. The deformations shall be measured with an accuracy of at least 0.01 mm.

The test is performed with an approximately constant rate control displacement, which is chosen so that the maximum load is reached within a few minutes after the start of the test. The deflections of the center of the beam and the corresponding load are registered until the beam is completely separated into two halves. The outcome of the test is a load–deflection diagram (l–d diagram), which is subsequently used for fracture–mechanical parameter determination.

In order to enlarge the set of material parameters by including compressive strength data, which is not directly obtained from 3PB testing, compression tests are also performed. These are carried out using the two halves of the fractured beams obtained after completion of the 3PB tests. Each part is cut to the nominal size of $100 \times 100 \times 100$ mm using a diamond blade saw (Figure 4.3).

An important step before evaluating the parameters from the obtained l–d diagram is to verify that the whole loading process has been quasi-static, i.e. there is no loss of stability in the measured data which can lead to the so-called snap–down effect (Figure 4.4a, Bažant and Cedolin [3]). This effect is caused by insufficient stiffness of the test setup (the frame of the testing machine and load cell sensor) with regard to the stiffness of the specimen. Such a loss of stability can be detected from a deflection time series (Figure 4.4c). If loss of stability occurs, the time derivative of the deflection significantly exceeds the rate of the control displacement setting (Figure 4.4d). Such a part of the measured data is incorrect and cannot be used for the identification of parameters. It has to be removed and could be replaced by a
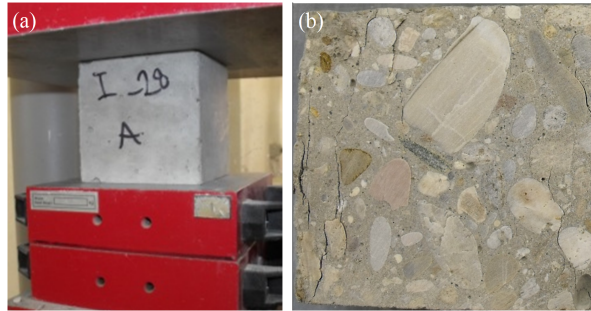
Figure 4.3: (a) Compression test on cubic samples cut from the fractured specimens and (b) the shape after destruction
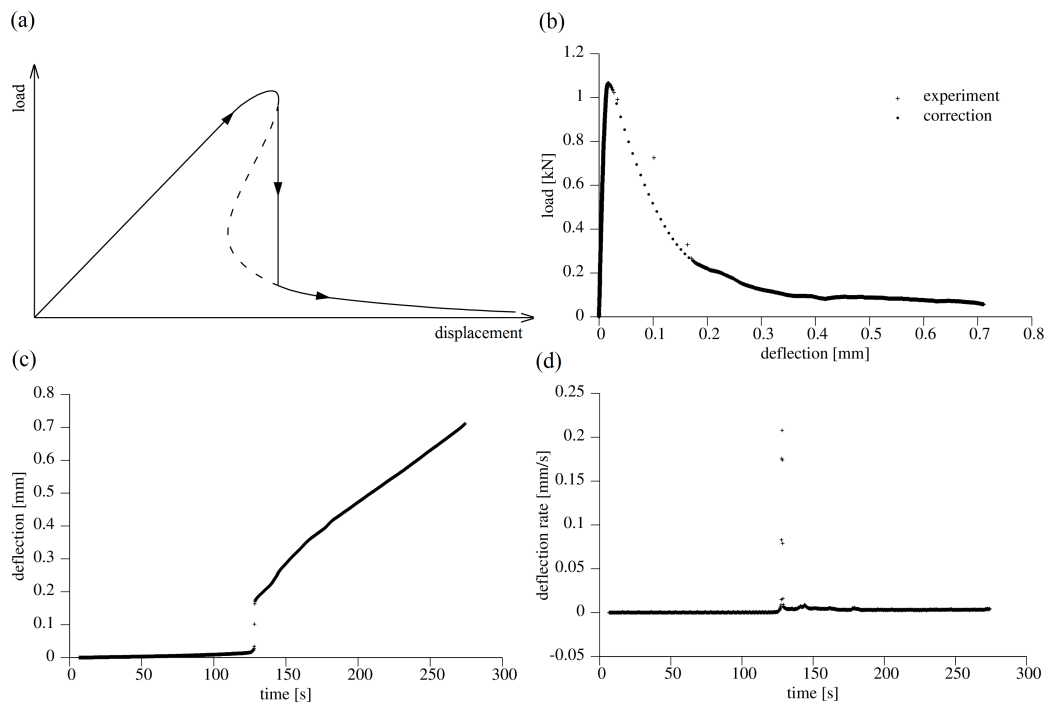

Figure 4.4: (a) Snap–down effect; (b) l–d diagram with distinct loss of stability – "wrong" data is replaced by a quadratic approximation; (c) measured time series of deflection and (d) its time derivative

suitable approximation (Figure 4.4b, Frantík et al. [17]).

4.2 Effective crack model

In the case of the effective crack model (Karihaloo [29]), a fracture in a real concrete structure originates when the stress intensity factor K_{I} (for the opening mode) corresponding to the effective crack length a_{e} reaches the critical value K_{Ice}. This model combines the linear elastic fracture mechanics and equivalent elastic crack length approaches. The energy dissipated in the so-called fracture process zone is considered equal to the energy needed for creating a fictitious crack – the effective (or the equivalent) crack a_{e}. In practice, this length is not determined from the energy equivalence but from the equivalence of the effective stiffness. For the calculation of a_{e} and K_{Ice} only two points from the l–d diagram are needed: the first is from the initial linear–elastic part, the second from the peak (or just before the peak). The Young modulus E is evaluated using just the first point from the initial linear–elastic part and the initial crack length a_0.

As presented in Karihaloo [29] the effective critical stress intensity factor K_{Ice} determined for a geometry dependent effective crack length a_{e} from the effective crack model can be used to identify the onset of unstable fracture. For the three point bending test it follows from

$$K_{\mathrm{Ice}} = \frac{6M_{\max}}{BW^2} Y_1\left(\frac{a_{\mathrm{e}}}{W}\right) Y_2\left(\frac{a_{\mathrm{e}}}{W}, \frac{S}{W}\right) \sqrt{a_e}, \tag{4.1}$$

where $M_{\max}$ is the maximum moment at the mid span, and S, W, and B are the support distance (equal to $300\,\mathrm{mm}$ for our particular specimen size), and height and width of the specimen, respectively. Specific forms of the polynomial geometry functions Y_1 and Y_2 are available, e.g. in [29].

To estimate elastic Young modulus the following formula can be adopted:

$$\begin{aligned}
E &= \frac{l_{\mathrm{i}}}{4Bd_{\mathrm{i}}}\left(\frac{S}{W}\right)^3\left[1 + \frac{5qS}{8l_{\mathrm{i}}} + \left(\frac{W}{S}\right)^2\left(2.70 + 1.35\frac{qS}{l_{\mathrm{i}}}\right) - 0.84\left(\frac{W}{S}\right)^3\right] \\
&+ \frac{9l_{\mathrm{i}}}{2Bd_{\mathrm{i}}}\left(1 + \frac{qS}{2l_{\mathrm{i}}}\right)\left(\frac{S}{W}\right)^2 F_1(a_0/W), \tag{4.2}
\end{aligned}$$

where q is the specimen self-weight per unit length, $(l_{\mathrm{i}}, d_{\mathrm{i}})$ are the corresponding pairs of values from the initial elastic range of the loading curve, and

$$F_1(a_0/W) = \int_0^{a_0/W} xY^2(x)\,\mathrm{d}x. \tag{4.3}$$

The geometry function $Y(x)$ for the three-point bending test is available, e.g. in [29].

4.3 Work–of–fracture method

The fracture behavior of concrete is often characterized by the fracture energy G_f. For its determination a technique referred to as the work–of–fracture method has been developed (RILEM [65]). This method is based on the cohesive (or fictitious) crack model (Hillerborg et al. [20], Hillerborg [21]). According to RILEM recommendation, the specific fracture energy is evaluated from the whole *l–d* diagram by dividing the total applied energy with projected ligament area. Therefore, for a specimen with the width B, depth W and the initial crack length a_0, the G_f is given by:

$$G_f = \frac{1}{B(W - a_0)} \int_0^\infty l(d) \mathrm{d}d, \tag{4.4}$$

where l is the applied load, and d is the deflection at the loading point. Obviously, Equation (4.4) represents an average of the energy required to separate the ligament area.

Assuming that most energy required for crack growth is consumed within the fracture process zone, the fracture energy can be related to the tensile softening or cohesive (crack–bridging) stress–crack opening ($\sigma_b - w$) curve by Hillerborg et al. [20]:

$$G_f = \int_0^{w_c} \sigma_b(w) \mathrm{d}w, \tag{4.5}$$

where w_c is the critical crack opening above which, there is no more cohesive stress transferred. Equation (4.5) defines the specific fracture energy as the area under the strain–softening curve $\sigma_b - w$ that is a material property for the material considered. Obviously, G_f defined in Equation (4.4) is a material constant only if the $\sigma_b - w$ relationship remains unchanged during the entire crack growth process. If a single $\sigma_b - w$ relationship can be used to describe the fracture process at any location along the ligament ($W - a_0$), the "locally defined" G_f in Equation (4.5) has to be the same as the "average" G_f in Equation (4.4).

4.4 Inverse analysis

Along with the classical evaluation of fracture–mechanical parameters from fracture tests, it is convenient to perform identification of parameters using the ANN-based inverse method (Novák and Lehký [58]). This approach is based on matching the laboratory measurements and the results found by reproducing the same test numerically. The ANN is used here as a tool to drive the associated optimization problem. Conveniently, the ATENA finite element program (Červenka et al. [8]) is exploited to simulate the fracture test numerically. A 3D Non Linear Cementitious 2 material model was selected to govern the gradual evolution of localized damage.
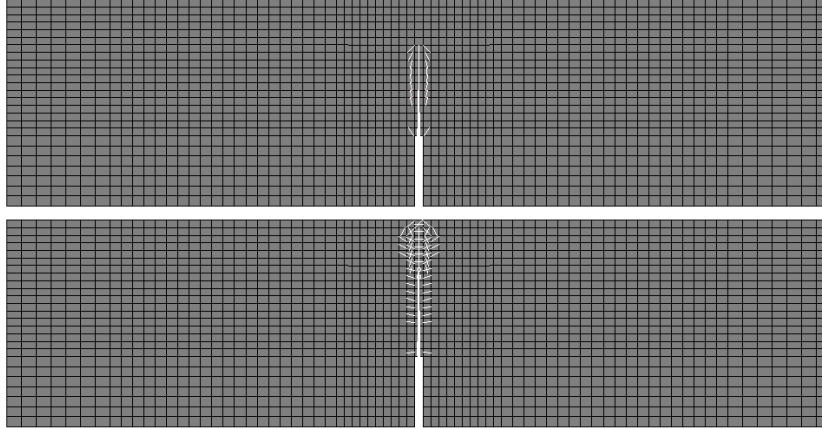
Figure 4.5: FEM model adopted in numerical simulations including damage distribution at peak load (top) and at failure (bottom)

The model is formulated in the total format assuming additive decomposition of small strains and initial isotropy of the material. The tensile behavior is governed by the Rankine-type criterion with exponential softening according to Hordijk [23], while for the behavior in compression the Menétrey–Willam yield surface with hardening and softening phases is used [54]. The fracture model employs the orthotropic smeared crack formulation and the rotational crack model with the mesh adjusted softening modulus both in tension and compression. The analysis is performed under plane stress conditions.

The cornerstone of the inverse method is the ANN which transfers the input data – response in the form of l–d diagram obtained from the fracture test – to the desired material parameters. The following three fundamental parameters of concrete are subject of identification: modulus of elasticity E, tensile strength f_t, and specific fracture energy G_f. Other parameters of the material model, e.g. compressive strength, were omitted from identification based on sensitivity analysis. Here, Spearman's nonparametric rank-order correlation was used (Novák et al. [56]).

The set for training of ANN is prepared numerically by the utilization of a FEM model (Figure 4.5) which simulates a three-point bending test with random realizations of material parameters. Rectangular probability distribution is once again utilized to generate random samples as the lower and upper limits represent the bounded range of physical existence of the parameters. The realizations of parameters are generated using LHS method. The random responses from the computational model and the corresponding random realizations of parameters serve as input–output elements of the ANN training set.

After training the ANN is ready to solve the main task, which is to provide the best material parameters in order that the numerical simulation will result in the best agreement with the experiment. This is performed by means of the simulation

of a network using measured responses as an input. This results in a set of identified material parameters. The last step is result verification – calculation of the computational model using the identified parameters. A comparison with the experiment will show the extent to which the inverse analysis was successful.

The proposed inverse method is general and can be employed for parameter identification of various types of concrete and other quasi-brittle composites. On the other hand, it is very time-consuming. In order to automate the whole difficult process of material parameter identification the FraMePID–3PB software tool has been developed. Preliminary identifications using various types of concrete mixtures tested at different ages showed that the structure of the ANN used for identification in this testing configuration is almost the same in all cases. Thanks to that, and to using a standardized test, the time needed for inverse analysis can be significantly reduced because only one single robust network with applicability to a wide range of concretes is created, trained, tested and implemented into the FraMePID–3PB system. Therefore, the time-consuming preparation of the training set using stochastic nonlinear analysis and training of the network using a suitable optimization technique is performed only once.

The structure of the ANN implemented within the FraMePID–3PB system is as follows (see Figure 5.8 in Section 5.3): 3 inputs, 1 hidden layer having 5 neurons with a nonlinear transfer function (hyperbolic tangent) and 1 output layer having 3 neurons with a linear transfer function. Each of the output neurons correspond to one of the identified material parameters, and each of the inputs corresponds to one parameter extracted from l–d diagram. More details on the FraMePID–3PB software can be found in Section 5.3.

Let's note that the proposed methodology of fracture–mechanical parameters determination of concrete and other quasi-brittle materials using results of laboratory fracture experiments presented in previous sections has undergone officially certification, see Novák et al. [62].

4.5 Examples

4.5.1 Standard concrete mixtures from a concrete plant

An extensive experimental campaign in co-operation of Brno University of Technology, University of Natural Resources and Life Sciences in Vienna, Austria, and the concrete company Franz Oberndorfer GmbH & Co KG, Gunskirchen, Austria was carried out with the aim of determination of fracture–mechanical parameters of selected standard concrete types. Concrete specimens were tested in parallel at laboratories in Brno and Vienna. The testing program involved standard compression tests, three-point bending tests and wedge splitting tests. Since one of the aims was to study the evaluation of fracture–mechanical parameters and their statistics over time, testing was carried out at 1, 7, 28, and 126 days of hardening. On each

Table 4.1: Selected statistical parameters of C50/60 concrete obtained using the effective crack method + the work-of-fracture method (ECM+WFM), and inverse analysis

Parameter of concrete/model	ECM+WFM		Inv. analysis	
	Mean	CoV [%]	Mean	CoV [%]
Modulus of elasticity [GPa]	32.6	14.3	34.8	10.6
Tensile strength [MPa]	–	–	3.9	10.6
Compressive strength [MPa]	77.0	6.4	–	–
Specific fracture energy [J/m^2]	241.8	16.8	219.8	12.8
Effect. frac. toughness [MPa.m$^{1/2}$]	1.414	12.9	–	–

testing day, 7 specimens made of one concrete type were tested in each testing configuration. Note that the studied concretes are used in industry for the production of prefabricated concrete elements. Specimens were stored in conditions equivalent to those present during the storage of a structural components (storage condition 1); moreover, beams were also tested after 28 days of hardening in conditions according to the relevant normative standard (storage condition 2, with a higher humidity than storage condition 1).

The results for 6 specimens (one was destroyed during transport) of C50/60 concrete strength class stored at standard conditions (storage conditions 1) and tested in three-point bending configuration at 28 days of hardening are presented here. Testing was performed using a Heckert FPZ 100/1 mechanical press. Loading was applied continuously with a constant increment of displacement of 0.1 mm/min in the center of the span. Deflection of the center of the beam was recorded using inductive sensor with an accuracy of 0.001 mm. Two fractured parts of an original specimen were also tested in compression. The values of selected fracture–mechanical parameters obtained from all 6 specimens using both the effective crack method + the work-of-fracture method as well as the inverse analysis method implemented within the FraMePID–3PB tool were statistically evaluated. Their mean values and coefficients of variation (COV) are shown in Table 4.1. There is a significant advantage in the case of using inverse analysis – the tensile strength value of the concrete can also be determined. A comparison of the experimentally measured loading curves from a three-point bending test and those derived numerically using identified parameters are shown in Figure 4.6. For more detailed results of the selected concrete class as well as the other concrete classes, see Řoutil et al. [66] and Novák et al. [61].

Let's note that statistical characteristics of fracture–mechanical parameters of all concretes tested within this testing campaign were stored into material database implemented in FReET probabilistic software (Novák et al. [63]). Such database serves as the source of material parameters for a realistic nonlinear modeling and reliability assessment of structures made of tested concretes.
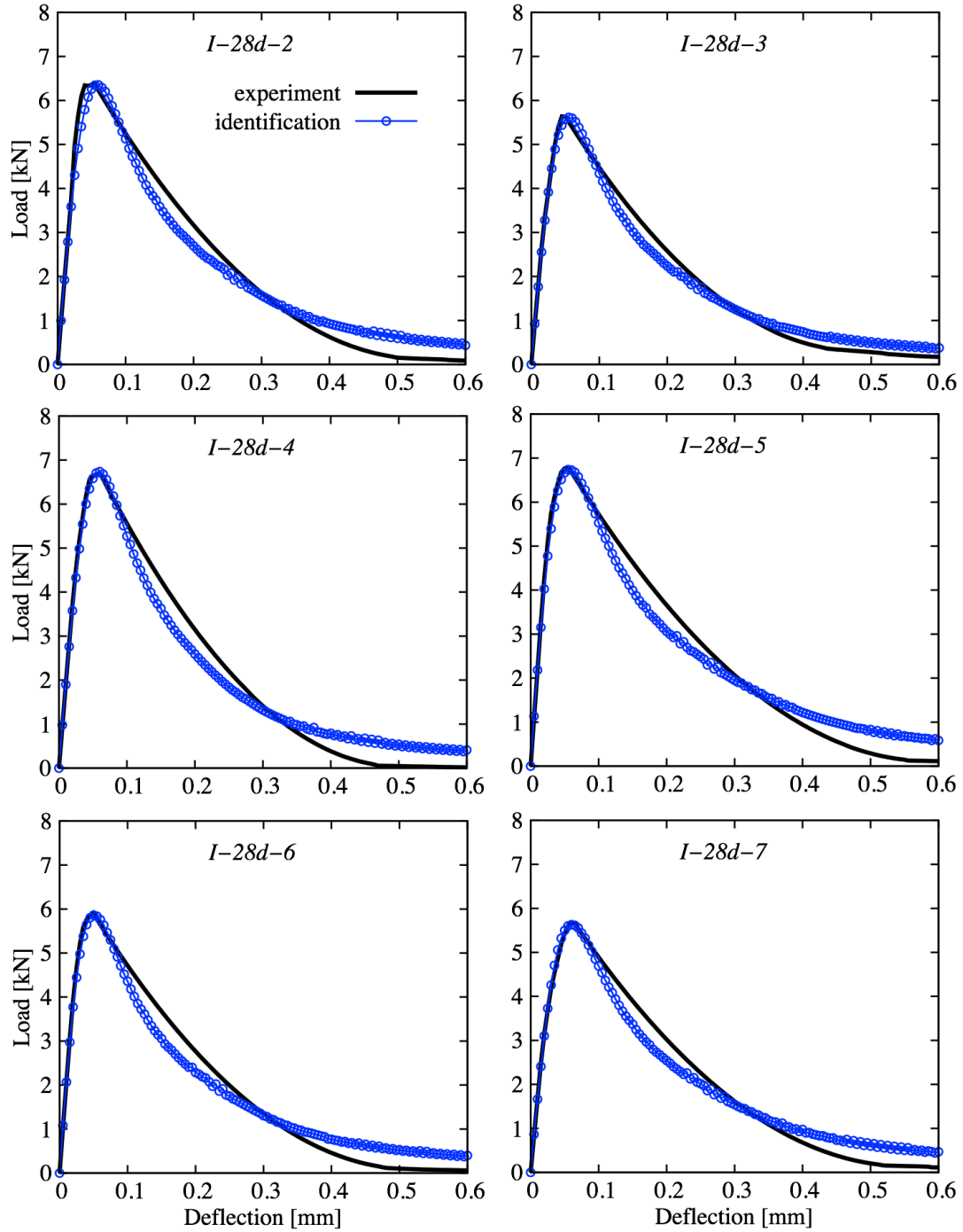
Figure 4.6: Load vs. midspan deflection diagrams of C50/60 concrete spec-
            imens measured and numerically derived from identified param-
            eters

Table 4.2: Selected statistical parameters of FAC1 mixture obtained using the effective crack method + the work-of-fracture method (ECM+WFM), and inverse analysis

Parameter of concrete/model	ECM+WFM		Inv. analysis	
	Mean	CoV [%]	Mean	CoV [%]
Modulus of elasticity [GPa]	34.0	6.5	36.2	2.0
Tensile strength [MPa]	–	–	4.0	14.4
Compressive strength [MPa]	76.7	1.3	–	–
Specific fracture energy [J/m^2]	247.4	10.9	250.3	7.8
Effect. frac. toughness [MPa.m$^{1/2}$]	1.642	4.3	–	–

4.5.2   Concrete mixtures with fly-ash additive

Using fly ash as an admixture in cements is now common in many applications since the massive increase in CO_2 emission in recent years has supported a considerable effort towards the replacement of ordinary Portland cement by alkali-activated aluminosilicate materials. One of the possible applications of these mixtures is in the production of the segments of lining used in tunneling. In cooperation with the Department of Mechanics of the Czech Technical University and the Klokner Institute in Prague, Czech Republic extensive experimental measurements were performed to evaluate the fracture–mechanical parameters of several concrete mixtures with partial or full replacement of cement by fly-ash (Šejnoha et al. [69]). The results of a set consisting of 3 specimens made of FAC1 mixture where 30 % of ordinary Portland cement was replaced by low-calcium fly-ash are presented here.

The testing setup as well as the evaluation using both methods was the same as in the case of the standard concrete mixtures described in the previous section. The values of selected fracture–mechanical parameters obtained for all 3 specimens (once again using both methods) were statistically evaluated, and their mean values and coefficients of variation (COV) are shown in Table 4.2. A comparison of the experimentally measured loading curves from a three-point bending test and those derived numerically using identified parameters are shown in Figure 4.7. For more information about the results for the FAC1 mixture as well as the other mixtures containing fly-ash, see Šejnoha et al. [69], Keršner et al. [31] and Lehký et al. [40].

4.6   Summary

The knowledge of fracture–mechanical parameters is fundamental not only for nonlinear computational modeling of structures made of quasi-brittle materials, but also for the evaluation of newly developed materials. In many cases, attention is focused on improving the properties associated with resistance to crack formation and propagation, rather than on the maximum strength of the material. The proposed
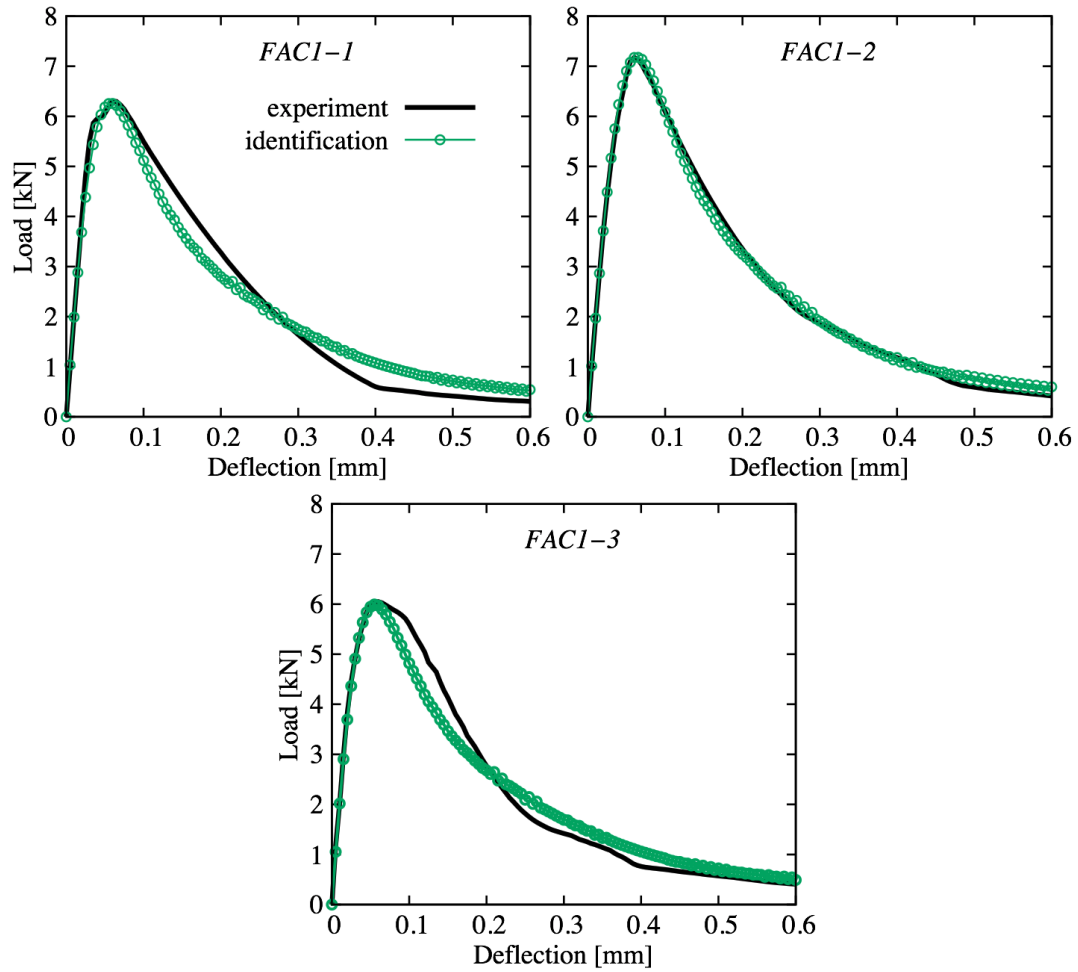
Figure 4.7: Load vs. midspan deflection diagrams of FAC1 specimens measured and numerically derived from identified parameters

identification method combines experimental response of fracture test with ANN and LHS, which helps to significantly reduce the number of simulations needed for training the ANN and therefore allows to perform the inverse analysis also for the time-consuming FEM applications. An efficiency of the method is clearly shown for both tested materials – standard concrete mixtures and concrete mixtures with fly-ash additive. The l–d diagrams obtained from numerical simulations of all specimens with identified parameters show very good agreement with those derived from experiments. The significant advantage is that the inverse analysis additionally provides values for the tensile strength of concrete. The results can serve efficiently as input data for the stochastic nonlinear simulation of studied concretes.

The developed software FraMePID–3PB, discussed in the following chapter, is designed for routine application to a wide range of standard concrete mixtures as well as concrete mixtures including additives such as fly-ash, etc. The proposed identification method itself is general and goes beyond identification of above mentioned fracture–mechanical parameters using fracture test in three-point bending configuration. It can easily be used for identification of almost any material or model parameters and for different kinds of experimental or numerical response.

Chapter 5

Software

The proposed general inverse analysis methodology discussed in previous chapters combines several mathematical models and methods: artificial neural networks, small-sample simulation methods, reliability and optimization methods, FEM, etc. In order to fully automate the whole process, several software tools must be combined. Software which has been developed exclusively by the author is presented in this chapter. It includes:

1. DLNNET artificial neural network software,

2. IRel inverse reliability software, and

3. the FraMePID–3PB fracture–mechanical parameter identification tool.

Another important piece in the overall puzzle is FReET software – a program for the statistical, sensitivity and reliability analysis of engineering problems. It has been developed at the author's institute and is easy to use in combination with other programs. More details about FReET can be found in Novák et al. [59] and [60]. ATENA software [8] was employed for the static analysis of structures made of concrete and other quasi-brittle materials. As regards the dynamic and modal analysis of structures, SOFiSTiK software [76] was utilized.

Besides the above-mentioned major programs, several minor tools have also been developed. These include:

a) DLSENS for sensitivity analysis,

b) the FReET–SOFiSTiK interface for direct communication and data transfer between stochastic and FEM programs, and

c) ANNRSMDLL for connecting an ANN-based response surface to FReET software for reliability analysis.

5.1   DLNNET

The cornerstone of all the inverse analyses presented in this work is an ANN. The same status applies to DLNNET software (Lehký [44]) for ANN creation, training and simulation, as this tool is an essential part of the whole system. It has been written in the Delphi 2010 programming environment using Object Pascal. All graphical components of the application (form, buttons, graphs, etc.) are taken from the Delphi Visual Component Library (VCL). A new set of classes has been defined for all ANN components (net, layers, interlayers, neurons, synapses). The relations among the ANN components are depicted in Figure 5.1.

DLNNET enables complex work with feed-forward multilayer neural networks. In the first step the ANN is created, i.e. the number of layers and corresponding neurons are defined (Figure 5.2). Then, for each layer, an appropriate type of transfer function (binary, linear, nonlinear) is selected depending on the type of analyzed problem. More details about ANN design are mentioned in Section 1.2.2.

The second window of the program is dedicated to network simulation (Figure 5.3). Here, the number of input sets needs to be adjusted (the program allows simulation for more than one input set during one run) and input data must be assigned to network inputs. Then, network parameters – biases and synaptic weights – must be assigned to individual neurons and connections. This can be done by loading data from an external file or adjusting the data automatically if ANN training has already been performed. During network simulation the output results of
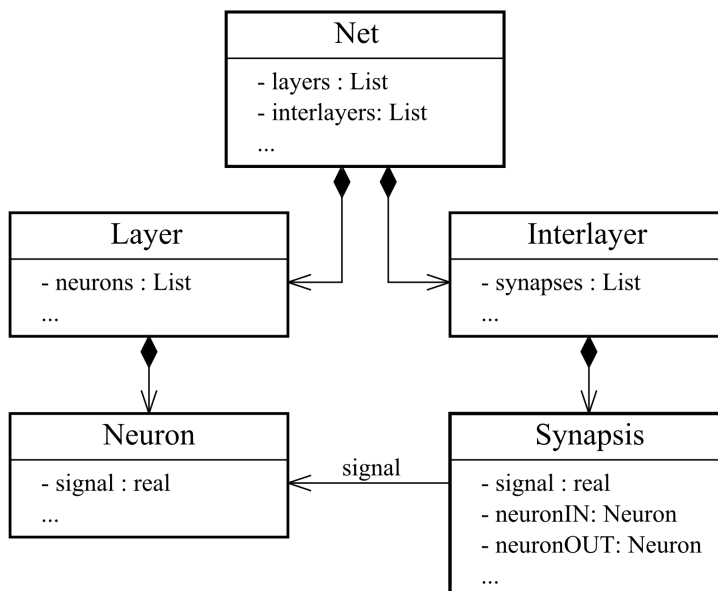

Figure 5.1: Diagram of the relations among the ANN components

individual neurons are listed in the right pane of the window and also stored to the `output.txt` file.

The last window is related to ANN training (Figure 5.4), i.e. the optimization of synaptic weights and biases in such a way that the real output of the ANN for a given input is as close as possible to the desired output. At first, it is necessary to specify the size of the training set, i.e. the number of input–output elements, and load the values of training elements from external files. Then, the network parameters must be initiated. This is mostly done randomly, allowing training convergence to be tested and improved via multiple initiations of parameters, which leads to different paths when searching for a global minimum. Another option is to retrieve specific initial parameter values from an external file. This is useful if we want to start the optimization process from a certain point, e.g. if the results of a previously trained network need to be refined. During training, the values of the synaptic weights and biases are stored to the `trainweights.txt` file.

Several optimization methods are available for the training process: the gradient descent method (with or without momentum), evolution strategies, simulated annealing, and genetic algorithms. Every method has its own set of parameters. Their default values are adjusted when a particular method is selected. If needed, these parameters can be changed during the training process. The progress of network error during training is displayed in a new window in order to check the speed and convergence of the optimization process (Figure 5.5). The optimization is performed until a predefined number of epochs have finished or the desired accuracy has been reached. The resulting values from the network outputs are stored to the `trainweights.txt` file and can be compared to the desired output values from the training set. Optimized ANN parameters are stored in computer memory for future use in network simulation.

The structure of the ANN, as well as all data related to simulation and training, can be saved to a `*.dln` file. It is a structured text file which, if needed, can be easily modified in an arbitrary text editor. This is the only file needed to archive and restore the task. Other files are just temporary files, which can be useful in various cases depending on the user's needs.
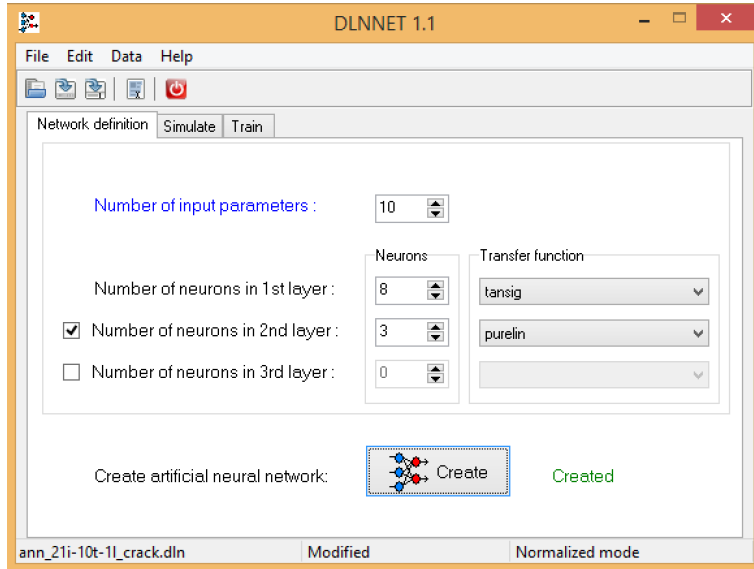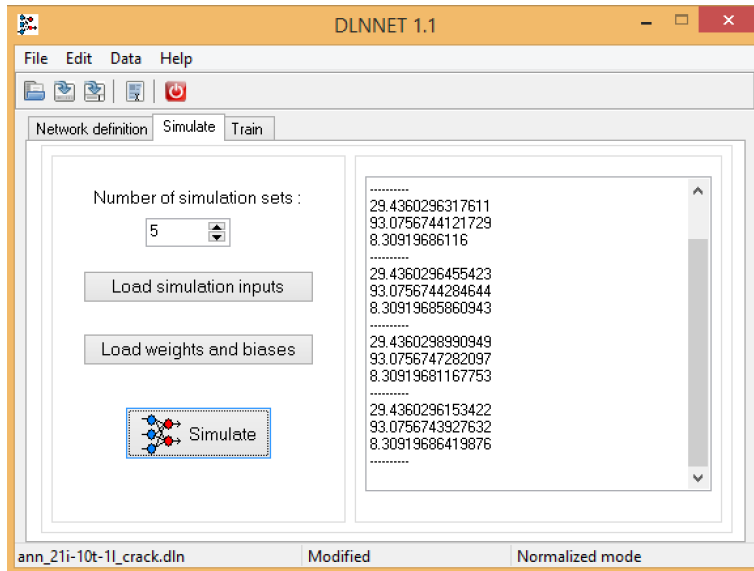
Figure 5.2: DLNNET: ANN design
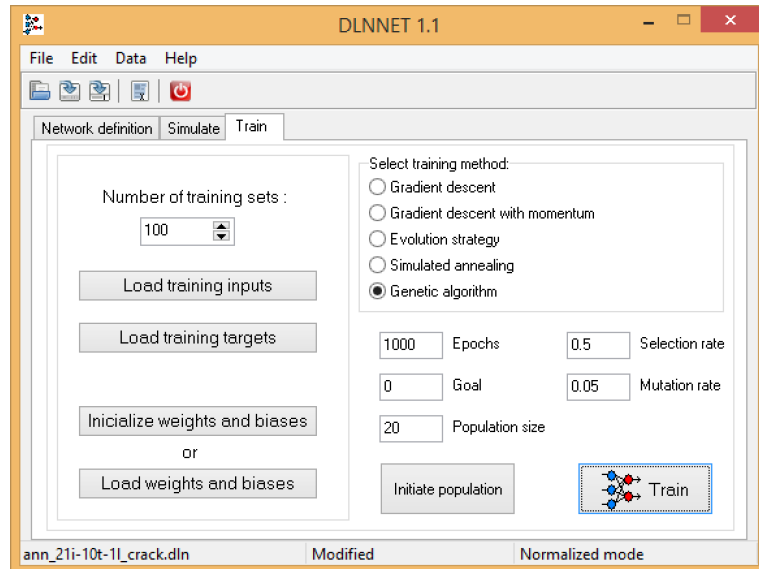

Figure 5.3: DLNNET: ANN simulation
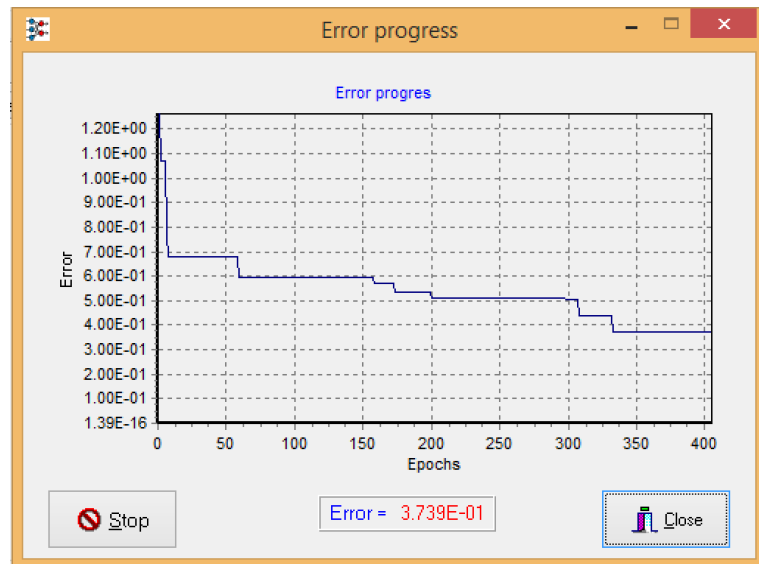
Figure 5.4: DLNNET: ANN training

Figure 5.5: DLNNET: Training error progress

5.2   IRel

IRel software (Lehký [45], Figure 5.6) is primarily concerned with inverse reliability analysis, a process which is described in Chapter 2. The whole procedure requires the performance of multiple stochastic analyses, so IRel has been developed in order to integrate FReET software for statistical, sensitivity and reliability analysis with DLNNET artificial neural network software in order to automate this time-consuming task. If DLNNET is the heart of the software system, IRel is the head, as it controls all communication and transfers data between programs. It has been written in the Delphi 2010 programming environment using Object Pascal.

First, a stochastic model has to be created in FReET software. If the model has already been prepared outside the program, the corresponding `*.fre` file can be placed in the working directory and the model will be automatically loaded. The limit state functions of the analyzed problem can be implemented directly in FReET software via the equation editor or developed as a more complicated function defined in a dynamic-link library (.dll) and linked to FReET. Limit state functions can be integrated into the software as third-party programs too. Statistical correlation can be considered in small-sample simulations using a simulated annealing algorithm (Vořechovský and Novák [86]). Finally, the parameters of the stochastic model are transferred back to IRel.

In the second step, the desired design parameters are selected from the stochastic model. A new stochastic model of the design parameters is created and random realizations of the design parameters are generated using FReET and the LHS simulation technique. The number of simulations defines the size of the ANN training set. Let us note that a double stochastic analysis is needed for training set preparation. Random sampling of the design parameters is represented by the outer loop. The inner loop represents the reliability calculation for one particular realization of design parameters. Here, the first order reliability method or response surface approximation method are recommended due to their relatively low computational demands, as Monte Carlo-type simulation techniques require a very high number of simulations for small failure probabilities (thousands, millions).

The results of individual reliability calculations – failure probability or reliability index can be calculated – are then transferred together with generated realizations of design parameters via a text file to DLNNET, where an appropriate ANN is created, trained and simulated. The desired design parameter values are obtained from the outputs of the ANN.
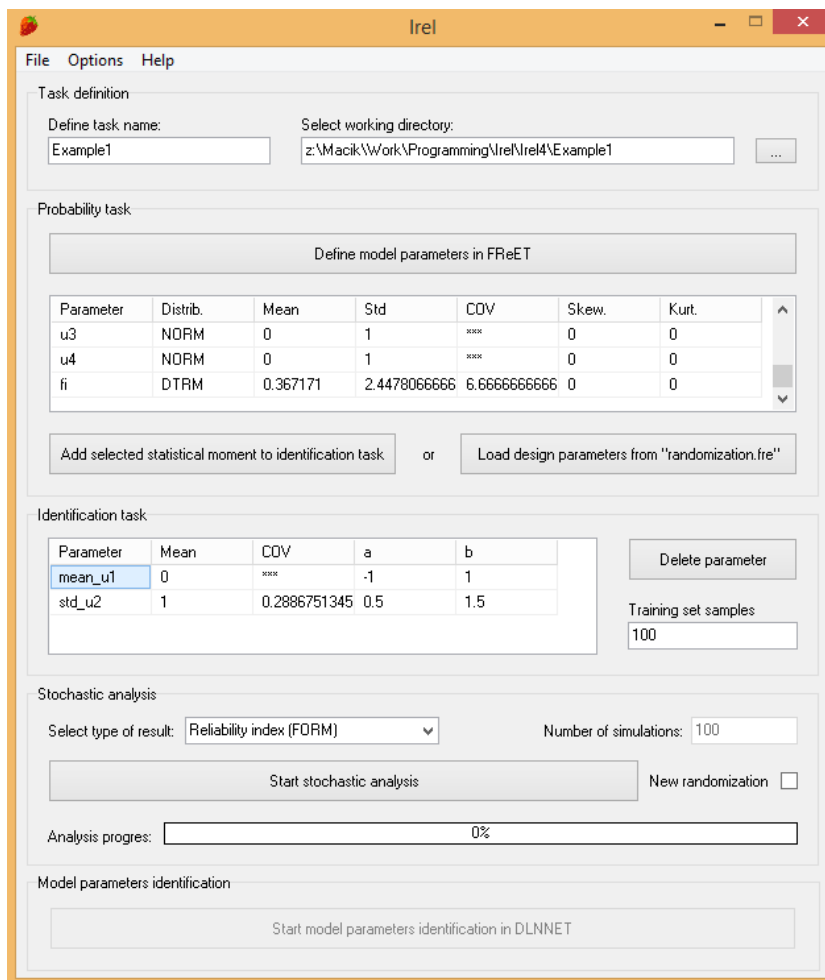
Figure 5.6: Inverse reliability problem definition – IRel software

5.3   FraMePID–3PB

In order to automate the time-consuming process of material parameter identification described in Chapter 4, FraMePID–3PB software (Lehký et al. [42] and Lehký [47]) has been developed fully in compliance with the certified methodology (Novák et al. [62]). The code has been written in the Delphi 2010 programming environment using Object Pascal. The main aim of the software is to reduce time and computational effort when identifying the fracture–mechanical parameters of standard concrete and related quasi-brittle composites. Its range of application is approximately from concrete strength class C15/20 to C70/85.

During training set preparation the material parameters were randomized. Here, large variability was used on purpose in order to create a rather general network capable of covering the identification of concrete parameters of various strengths and ages. The mean values were $40\,\mathrm{GPa}$ for modulus of elasticity, $4.5\,\mathrm{MPa}$ for tensile strength and $200\,\mathrm{J/m^2}$ for specific fracture energy. Coefficients of variation were 0.2 for modulus of elasticity, 0.25 for tensile strength and 0.4 for specific fracture energy. The training set was set up to have 100 samples generated using the LHS method. Training of the network was carried out using the Levenberg–Marquardt method (Singh et al. [73]) and genetic algorithms (Schwefel [72]).

The structure of the neural network implemented within the FraMePID–3PB system is as follows (see Figure 5.8): 3 inputs, 1 hidden layer with 5 neurons and a nonlinear transfer function (hyperbolic tangent), and 1 output layer with 3 neurons and a linear transfer function. Each of the output neurons corresponds to one of the identified material parameters, and each of the inputs corresponds to one parameter extracted from an l–d diagram.

The procedure of material parameter identification using the trained neural network stored in FraMePID–3PB software can be summarized as follows:

1. The l–d diagram obtained from the fracture test is loaded into FraMePID–3PB. It is possible to choose between two input file formats: (i) deflection–load; the file contains two columns, namely the deflection of the center of the beam, and applied load; (ii) time–load–deflection; the file contains three columns, namely measured time, applied load and the deflection of the center of the beam. From the loaded data, the inputs of inverse analysis are extracted and prepared for the ANN (Figure 5.7). This procedure means averaging thousands of points of the l–d diagram obtained from the experiment into 120 equidistant intervals along the deflection axis. It is necessary for numerical calculation of the work of fracture, which is one of the input parameters. Other input parameters are maximum load and load corresponding to a deflection of the center of the beam equal to 0.01 mm. All three input parameters are then normalized to the $<\text{-}1;1>$ interval with regard to the range of the parameters within the training set.

2. The input signal is transmitted through the neural network and the best set of material parameters is obtained from the output layer of the network. This step is possible because the neural network is trained in advance and remains the same for the identification of parameters of various concretes (Figure 5.8). Let us emphasize that no new nonlinear fracture mechanics calculations are needed to prepare the training set – the network is ready to use and implemented in FraMePID–3PB. It was created and trained for a relatively wide range of concrete strength classes – approximately from C15/20 to C70/85, as mentioned above. The utilization of l–d diagrams obtained from the testing of such concretes avoids the use of input data which violates their upper/lower bounds. Note that, for example, in the case of higher strength concrete another ANN should be created, trained and implemented into the software.

3. The verification of identified parameters is performed. The obtained material parameters are used in the computational model and numerical analysis is carried out. In the current version (1.0) this is done in a semi-automatic manner by exporting the identified material parameters together with the fixed ones to a `*.ccm` file (ATENA materials) and then importing the file into ATENA software. It is intended that in the next version ATENA software will be linked with FraMePID–3PB to enable direct data transfer via COM interface. The resulting numerical l–d diagram is compared with the experimental one, which will show the extent to which the inverse analysis was successful.

At present, FraMePID–3PB software operates with a "basic" configuration of experiment and model. Nevertheless, it was designed more generally with respect to future extensions for other configurations, e.g. specimens with various notch depths, other concrete softening models (linear, multilinear, etc.), additional testing configurations (compressive test, wedge splitting test), etc. This will facilitate the routine identification of material parameters for various research and practical tasks.
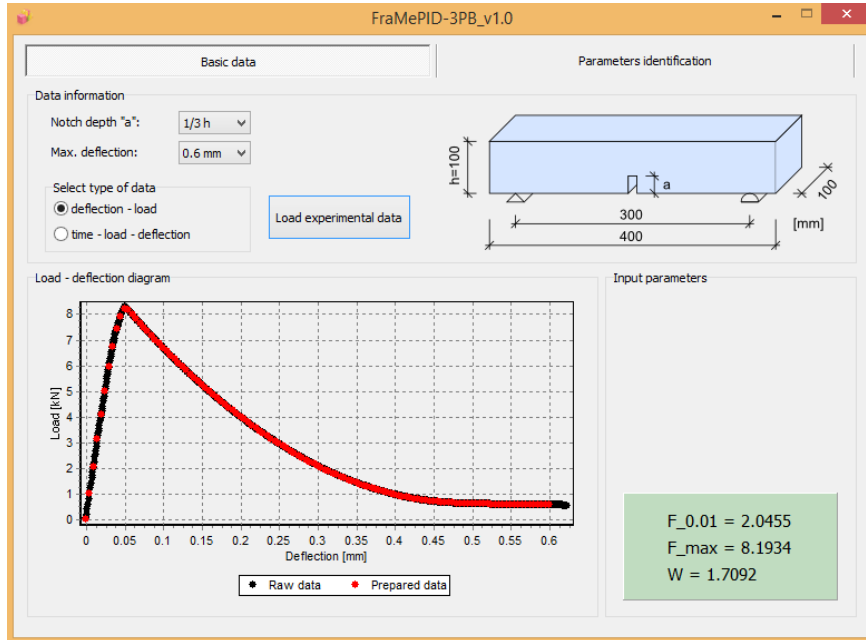
Figure 5.7: FraMePID–3PB: selection of input data file format, experimental data loading and preparation of the input signal for the artificial neural network
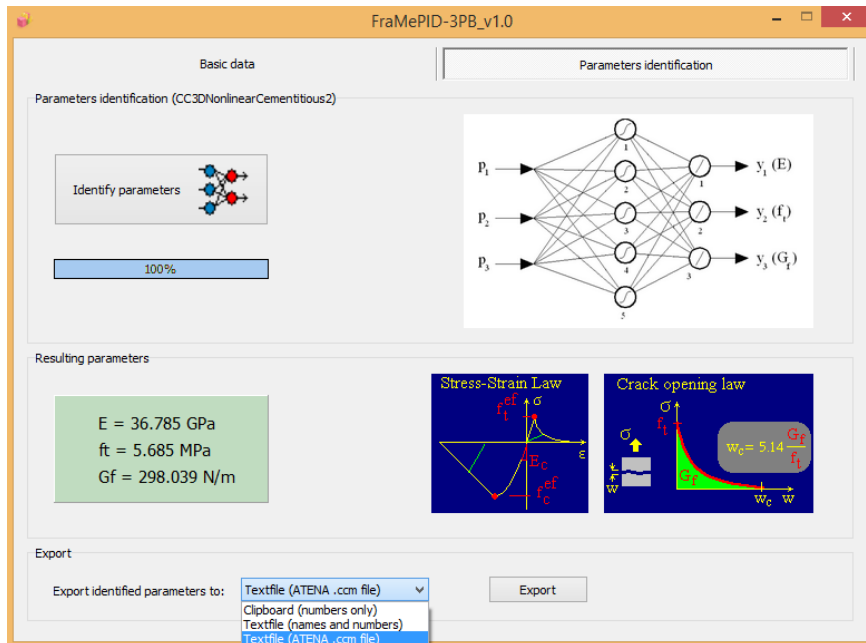

Figure 5.8: FraMePID–3PB: neural network structure and material parameter identification

Conclusion

Solving inverse problems is a common task in civil and structural engineering. In the present work three specific types of inverse problems were presented: (1) the identification of design parameters in order to reach a desired reliability level defined by reliability indicators, (2) damage detection based on changes in structural vibration, and (3) the identification of fracture–mechanical parameters based on the results of laboratory tests. All three fall into the category of complex problems whose solution is computationally intensive and time-consuming, thus rendering the utilization of a trial-and-error procedure impossible or ineffective. In order to solve this kind of inverse problem the soft computing-based methodology of inverse analysis has been proposed. The methodology is general and (with certain modifications) can be utilized to solve a variety of inverse problems.

Due to the complexity of the methodology and the inclusion of a number of advanced mathematical models and methods, several software tools have been developed and combined in order to provide a user-friendly experience during analysis. All programs enable the solution of the presented inverse problems in a routine way, as was demonstrated via the presented examples. All of the results confirmed the potential and ability of the proposed methodology and software to successfully perform inverse analysis with the required accuracy within an acceptable time. Nevertheless, performing inverse analysis and utilizing software can be slightly difficult for practicing engineers, since it requires a basic knowledge of ANNs, optimization methods and simulation techniques.

This problem can be partially reduced by the preparation of ANNs and their default parameters in advance, before the processing of inverse analysis tasks is required. But still, at least some elementary knowledge is required because the default setting is very often not the best one and so needs to be adjusted by the user with respect to the analyzed problem. The software which is the most user-friendly from this point of view is FraMePID–3PB, in which a trained ANN has already been implemented and is ready to use. This also helps to significantly reduce time and computational effort.

Future work

Artificial intelligence and soft computing methods have become very popular in recent years, and in combination with traditional mathematical methods offer great potential to those solving time-consuming and computationally intensive tasks such as inverse analysis. The future work in this field should be focused on two main targets: (1) Improving the existing methodology and software, especially toward improved user-friendliness that will also enable its routine application by practicing engineers, and (2) the implementation of advanced models and methods for solving other – more complex – types of inverse problems, e.g. time-dependent inverse analysis.

The first-mentioned target also involves expanding the options for connecting the utilized software to other FEM programs, e.g. ANSYS, RFEM, DIANA, etc., that are commonly used by engineers in practical design. Another important aspect is the reduction of computational time via parallelization. This can be done during training set preparation, where individual FEM deterministic analyses are carried out in parallel, and during the optimization of ANN parameters during ANN training. The former depends mainly on FEM software developers, while the latter is related to DLNNET software and is under preparation.

The second target includes the utilization of other types of ANNs such as recurrent neural networks (RNNs), where connections between neurons form a directed cycle. An RNN performs the same task for every element of a sequence, with the output being dependent on the previous computations. Another way to think about RNNs is that they have a "memory" which captures information about what has been calculated so far. They exhibit inherent dynamic behavior, and can thus be used to construct empirical models for dynamic systems, load prediction systems, etc.

This is the general outlook regarding future work related to soft computing techniques and inverse analysis. Now let us focus on the particular analyses discussed in this work. In the case of inverse reliability analysis, some practical problems are very often ill-posed, leading to multiple solutions. In order to provide a unique solution related to a selected objective function an optimization loop must be added to inverse reliability analysis. The latter is performed to provide equality constraints which can be eliminated by substituting them into the objective function. Any general optimization method, e.g. the Quasi-Newton method, the quadratic approximation method, the simplex and complex method, the aimed multi-level sampling method, or any of the many stochastic and evolutionary algorithms, can be used to obtain the needed independent design parameters by performing optimization. The optimum results will meet both equality and reliability constraints, as well as the minimization requirement.

As far as damage detection is concerned, major attention must be paid to the evaluation of other possibilities for the use of input data extracted from in-situ

measurements supported by numerical analyses. Such input information should allow the detection of relatively small amounts of damage and should not be sensitive to environmental and operating conditions such as changing ambient temperature or sensor placement. On the other hand, it should be easy to extract from ambient vibration data. The implementation of such software in the permanent monitoring system run by a bridge operator will also help to provide them with real-time damage detection based on measured data for a particular bridge.

As regards fracture–mechanical parameter identification, future research will mainly be focused on expanding the usability of FraMePID–3PB software by including additional ANNs for the identification of other types of quasi-brittle composites, e.g. cement composites without aggregates, fiber-reinforced concretes, etc. Consequently, the testing of other specimen sizes will then be required. The intention is also to include other test configurations such as the wedge splitting test, and the compression test. From the theoretical point of view, attention will be paid to the identification of size-independent properties using specimens of various sizes.

Bibliography

[1] ANTÓNIO, C., HOFFBAUER, L. Uncertainty propagation in inverse reliability-based design of composite structures. *International Journal of Mechanics and Materials in Design*, 6 (1), 2010, 89–102.

[2] ARMON, D., BEN-HAIM, Y., BRAUN, S. Crack detection in beams by rank-ordering of eigenfrequencies shifts. *Mechanical Systems and Signal Processing*, 8 (1), 1994, 81–91.

[3] BAŽANT, Z.P., CEDOLIN, L. *Stability of structures, elastic, inelastic, fracture, and damage theories*. New York: Oxford University Press, 1991.

[4] BAŽANT, Z.P., PLANAS, J. *Fracture and size effect in concrete and other quasibrittle materials*. Boca Raton, Florida: CRC Press, 1998.

[5] BAŽANT, Z.P., BECQ-GIRAUDON, E. Statistical prediction of fracture parameters of concrete and implications for choice of testing standard. *Cement and Concrete Research*, 32 (4), 2002, 529–556.

[6] BREPTA, R., PŮST, L., TUREK, F. *Mechanické kmitání*. Technický průvodce 71, Sobotáles, Prague, Czech Republic, 1994 [in Czech].

[7] CICHOCKI, A., UNBEHAUEN, R. *Neural networks for optimization and signal processing*. John Wiley & Sons Ltd. & B.G. Teubner, Stuttgart, 1993.

[8] ČERVENKA, V., JENDELE, L., ČERVENKA, J. *ATENA program documentation – Part 1: theory*. Cervenka Consulting, Prague, Czech Republic, 2016.

[9] ČSN EN 1992-1-1: *Eurocode 2: Design of concrete structures – Part 1: General rules and rules for buildings*. Czech Office for Standards, Metrology and Testing, Prague, Czech Republic, 2006 [in Czech].

[10] ČSN EN 1992-2: *Eurocode 2: Design of concrete structures – Part 2: Concrete bridges – Design and detailing rules*. Czech Office for Standards, Metrology and Testing, Prague, Czech Republic, 2007 [in Czech].

[11] ČSN 736222: *Load bearing capacity of road bridges.* Czech Office for Standards, Metrology and Testing, Prague, Czech Republic, 2013 [in Czech].

[12] DEIX, S., GEIER, R. Updating FE-models using experimental modal analysis for damage detection and system identification in civil structures. *Third European Conference on Structural Control (3ECSC)*, Vienna, Austria, 2004.

[13] DER KIUREGHIAN, A., ZHANG, Y., LI, C.C. Inverse reliability problem. *Journal of Engineering Mechanics*, ASCE, 120 (5), 1994, 1154–1159.

[14] EN 1995-1-1. *Eurocode 5: Design of Timber Structures – Part 1.1: General Rules and Rules for Buildings.* European Committee for Standardization, Brussels, Belgium, 2004.

[15] FANG, X., LUO, H., TANG, J. Structural damage detection using neural network with learning rate improvement. *Computers and Structures*, 83, 2005, 2150–2161.

[16] FELTRIN, G. Temperature and damage effects on modal parameters of a reinforced concrete bridge. *5th European Conference on Structural Dynamics (EURODYN)*, Munich, Germany, 2002.

[17] FRANTÍK, P., PRŮŠA, J., KERŠNER, Z., MACUR, J. About stability loss during displacement–controlled loading. *Fiber concrete 2007*, Prague, Czech Republic, 2007.

[18] GURNEY, K. *An introduction to neural networks.* CRC Press, Taylor & Francis Group, Boca Raton, FL, USA, 1997.

[19] HASOFER, A.M., LIND, N.C. Exact and invariant second-moment code format. *Journal of Engineering Mechanics*, ASCE, 100 (1), 1974, 111–121.

[20] HILLERBORG, A., MODÉER, M., PETERSSON, P.E. Analysis of crack formation and crack growth in concrete by means of fracture mechanics and finite elements. *Cement and Concrete Research*, 6, 1976, 773–782.

[21] HILLERBORG, A. The theoretical basis of method to determine the fracture energy G_f of concrete. *Materials and Structures*, 18 (4), 1985, 291–296.

[22] HOFFMANN, S., WENDNER, R., STRAUSS, A. Comparison of stiffness identification methods for reinforced concretestructures. *Proceedings of the 6th International Workshop on Structural Health Monitoring*, Stanford University, Stanford, USA, 2007.

[23] HORDIJK, D.A. *Local approach to fatigue of concrete.* Ph.D. thesis, Delft University of Technology, Delft, Netherland, 1991.

[24] HUNTINGTON, D.E., LYRINTZIS, C.S. Improvements to and limitations of Latin Hypercube Sampling. *Probabilistic Engineering Mechanics*, 13 (4), 1998, 245–253.

[25] HUTH, O., FELTRIN, G., MAECK, J., KILIC, N. AND MOTAVALLI, M. Damage identification using modal data: Experiences on a prestressed concrete bridge. *Journal of Structural Engineering*, ASCE, 131 (12), 2005, 1898–1910.

[26] CHENG, J., ZHANG, J., CAI, C.S., XIAO, R.C. A new approach for solving inverse reliability problems with implicit response functions. *Engineering Structures*, 29 (1), 2007, 71–79.

[27] CHENG, J., LI, Q.S. Application of the response surface methods to solve inverse reliability problems with implicit response functions. *Computational Mechanics*, 43 (4), 2009, 451–459.

[28] JOINT COMMITEE ON STRUCTURAL SAFETY. *JCSS Probabilistic Model Code*. Technical University of Denmark, Kongens Lyngby, Denmark, 2007, http://tinyurl.com/h3rfzpa.

[29] KARIHALOO, B.L. *Fracture mechanics of concrete*. New York: Longman Scientific & Technical; 1995.

[30] KERAMAT, M., KIELBASA, R. Efficient average quality index of estimation of integrated circuits by modified Latin Hypercube Sampling Monte Carlo (MLHSMC). *Proceedings of IEEE Symposium on Circuits and Systems*, Hong Kong, Vol. 3, 1648–1651.

[31] KERŠNER, Z., KUCHARCZYKOVÁ, B., ŠIMONOVÁ, H., FRANTÍK, P., LEHKÝ, D., DANĚK, P., BEDÁŇ, J. *Vyhodnocení lomových experimentů těles z kompozitů FAC1, FAC1-O a S343 (Evaluation of fracture experiments of specimens made of FAC1, FAC1-O and S343 composites)*. Report No. 20120806, Institute of Structural Mechanics, Faculty of Civil Engineering, Brno University of Technology, Brno, Czech Republic, 2012 [in Czech].

[32] KOEHLER, J.R., OWEN, A.B. Computer experiments. *Handbook of Statistics*, 13, 1996, 261–308.

[33] KOH, B.H., DYKE, S.J. Structural health monitoring for flexible bridge structures using correlation and sensitivity of modal data. *Computers and Structures*, 85, 2007, 117–130.

[34] KRAL, Z., HORN, W., STECK, J. Crack propagation analysis using acoustic emission sensors for structural health monitoring systems. *The Scientific World Journal*, Vol. 2013, Article ID 823603, 13 pages, 2013.

[35] KŮRKOVÁ, V. Kolmogorov's theorem and multilayer neural networks. *Neural Networks*, 5 (3), 2009, 501–506.

[36] LEHKÝ, D., NOVÁK, D., FRANTÍK, P., STRAUSS, A., BERGMEISTER, K Dynamic damage identification of Colle Isarco viaduct. *4th International Conference on Bridge Maintenance, Safety and Management (IABMAS 2008)*, Seoul, Korea, 2008, 2549–2556.

[37] LEHKÝ, D., NOVÁK, D. ANN inverse analysis in stochastic computational mechanics. *Artificial Intelligence: New Research*, Nova Science Publishers, Hauppauge, NY, USA, 2009, 323–350.

[38] LEHKÝ, D., NOVÁK, D. Neural network based damage detection of dynamically loaded structures. *Proceedings of the 11th International Conference on Engineering Applications of Neural Networks (EANN 2009)*, London, UK, 2009, 17–27.

[39] LEHKÝ, D., NOVÁK, D. Statistical material parameters identification of fibre-reinforced concrete. *Proceedings of the 9th International Symposium on High Performance Concrete – Design, Verification & Utilization (HPC 2011)*, Rotorua, New Zealand, 2011, 38 + CD (8p).

[40] LEHKÝ, D., KERŠNER, Z., KUCHARCZYKOVÁ, B., ŠIMONOVÁ, H., FRANTÍK, P., DANĚK, P., BEDÁŇ, J. *Identifikace materiálových parametrů těles z kompozitů FAC1, FAC1-O a S343 (Identification of material parameters of specimens made of FAC1, FAC1-O and S343 composites)*. Report No. 20120820. Institute of Structural Mechanics, Faculty of Civil Engineering, Brno University of Technology, Brno, Czech Republic, 2012 [in Czech].

[41] LEHKÝ, D. Early warning system of roofs overloaded by snow based on measurements and inverse analysis. *The 3rd International Symposium on Life-Cycle Civil Engineering – Life-Cycle and Sustainability of Civil Infrastructure Systems (IALCCE 2012)*, Vienna, Austria, 2012, 2175-2181.

[42] LEHKÝ, D., KERŠNER, Z., NOVÁK, D. FraMePID-3PB Software for Material Parameters Identification Using Fracture Test and Inverse Analysis. *Advances in Engineering Software*, 72, 2014, 147–154.

[43] LEHKÝ, D., SLOWIK, O., NOVÁK, D. Double-Loop Optimization and Soft Computing Based Inverse Analysis Approaches for Performing Reliability-based Design. In *Proceedings of the Fourth International Conference on Soft Computing Technology in Civil, Structural and Environmental Engineering*, Civil-Comp Press, Stirlingshire, UK, Paper 6, 2015. doi:10.4203/ccp.109.6.

[44] LEHKÝ, D. *DLNNET – Program Documentation: Theory and User's Manual*. Brno, Czech Republic, 2016. (in preparation)

[45] Lehký, D. *IRel – Program Documentation: User's Manual.* Brno, Czech Republic, 2016, http://www.fce.vutbr.cz/STM/lehky.d/irel/irel.html.

[46] Lehký, D. *FraMePID–3PB – Program Documentation: User's Manual.* Brno, Czech Republic, 2016, http://www.fce.vutbr.cz/STM/lehky.d/framepid-3pb/framepid-3pb.html.

[47] Lehký, D., Šomodíková, M. Reliability calculation of time-consuming problems using a small-sample artificial neural network-based response surface method. *Neural Computing and Applications*, 2016, doi:10.1007/s00521-016-2485-3.

[48] Li, H., Foschi, R.O. An inverse reliability method and its application. *Structural Safety*, 20 (3), 1998, 257–270.

[49] Li, H., Foschi, R.O. Response: 'An inverse reliability method and its application'. *Structural Safety*, 22 (1), 1998, 103–106.

[50] Link, M. Updating of analytical models – basic procedures and extensions. *Modal Analysis and Testing*, NATO Science Series, Kluwer Academic Publ., 1999.

[51] Linton, J. *Copy of Neuroscience*, Haiku Deck, online (17. 2. 2016), https://www.haikudeck.com/copy-of-neuroscience-education-presentation-eRxEMffFWR.

[52] Maeck, J., de Roeck, G. Damage assessment using vibration analysis on the Z24-bridge. *Mechanical Systems and Signal Processing*, 17 (1), 2003, 133–142.

[53] McKay, M.D., Conover, W.J., Beckman, R.J. A comparison of three methods for selecting values of input variables in the analysis of output from a computer code. *Technometrics*, 21 (2), 2009, 239–245.

[54] Menetrey, P., Willam, K.J. Triaxial failure criterion for concrete and its generalization. *ACI Structural Journal*, 92, 1995, 311–318.

[55] Mínguez, R., Castillo, E. Hadi, A.S. Solving the inverse reliability problem using decomposition techniques. *Structural Safety*, 27 (1), 2005, 1–23.

[56] Novák, D., Teplý, B., Shiraishi, N. Sensitivity analysis of structures: a review. 5th *International conference on civil and structural engineering computing*, Edinburgh, Scotland, 1993, 201–207.

[57] Novák, D., Teplý, B., Keršner, Z. The Role of Latin Hypercube Sampling Method in Reliability Engineering. *Proceedings of the International Conference ICOSSAR '97: Structural Safety and Reliability*, Kyoto, Japan, 1998, 403–409.

[58] NOVÁK, D., LEHKÝ, D. ANN inverse analysis based on stochastic small-sample training set simulation. *Journal of Engineering Application of Artificial Intelligence*, 19 (7), 2006, 731–740.

[59] NOVÁK, D., VOŘECHOVSKÝ, M., RUSINA, R. *FReET – Program Documentation: User's and Theory Guides*, version 1.5, Brno/Červenka Consulting, Czech Republic, 2012, www.freet.cz.

[60] NOVÁK, D., VOŘECHOVSKÝ, M., TEPLÝ, B. FReET: Software for the statistical and reliability analysis of engineering problems and FReET-D: Degradation module. *Advances in Engineering Software*, 72, 2014, 179–192.

[61] NOVÁK, D., KERŠNER, Z., LEHKÝ, D., ŘOUTIL, L. *Fracture tests of concrete specimens series I (C50/60) and II (C40/50)*. Research Report, Institute of Structural Mechanics, Faculty of Civil Engineering, Brno University of Technology, Czech Republic, 2014.

[62] NOVÁK, D., KERŠNER, Z., LEHKÝ, D., ŠIMONOVÁ, H., HAVLÍKOVÁ, I., ŘOUTIL, L., FRANTÍK, P., SCHMID, P. *Metodika experimentálně-výpočtového stanovení lomově–mechanických parametrů – 01/2014*. Certified methodology, Institute of Structural Mechanics, Faculty of Civil Engineering, Brno University of Technology, Czech Republic, 2014 [in Czech].

[63] NOVÁK, D., ŘOUTIL, L., NOVÁK, L., SLOWIK, O., STRAUSS, A., KRUG, B. Database of fracture–mechanical concrete parameters and its implementation into reliability software FReET. *Proceedings of the 13th International Probabilistic Workshop (IPW 2015)*, Liverpool, England, UK, 2015, 134–144.

[64] PLANAS, J., GUINEA, G.V., ELICES, M. Size effect and inverse analysis in concrete fracture. *International Journal of Fracture*, 95, 1999, 367–378.

[65] RILEM TC-50 FM. Determination of the fracture energy of mortar and concrete by means of three-point bend tests on notched beams. *Materials and Structures*,18, 1985, 287–290.

[66] ŘOUTIL, L., LEHKÝ, D., ŠIMONOVÁ, H., KUCHARCZYKOVÁ, B., KERŠNER, Z., NOVÁK, D., ZIMMERMANN, T., STRAUSS, A., KRUG, B. Experimental-computational determination of mechanical fracture parameters of concrete for probabilistic life-cycle assessment. *Fourth International Symposium on Life-Cycle Civil Engineering (IALCCE 2014) – Life-Cycle of Structural Systems: Design, Assessment, Maintenance and Management*, Tokyo, Japan, Furuta, Frangopol & Akiyama (Eds.), Taylor & Francis Group, London, UK, 2014, 801–807.

[67] SADOVSKÝ, Z. Discussion on: an inverse reliability method and its application. *Structural Safety*, 22 (1), 1998, 97–102.

[68] Salgado, R., Cruz, P.J.S., Ramos, L.F., Lourenço, P.B. Comparison between damage detection methods applied to beam structures. *Third International Conference on Bridge Maintenance Safety and Management*, Porto, Portugal, 2006.

[69] Šejnoha, M., Brouček, M., Novotná, E., Keršner, Z., Lehký, D., Frantík, P. Fracture properties of cement and alkali activated fly ash based concrete with application to segmental tunnel lining. *Advances in Engineering Software*, 62–63, 2013, 61–71.

[70] Shayanfar, M.A., Massah, S.R., Rahami, H. An inverse reliability method using networks and genetic algorithms. *World Applied Sciences Journal*, 2 (6), 2007, 594–601.

[71] Sherali, H.D., Ganesan, V. An inverse reliability–based approach for designing under uncertainty with application to robust piston design. *Journal of Global Optimization*, 37 (1), 2007, 47–62.

[72] Schwefel, H.P. *Numerical optimization for computer models*. Wiley, Chichester, 1991.

[73] Singh, V., Gupta, I., Gupta, H.O. ANN-based estimator for distillation using Levenberg–Marquardt approach. *Engineering Applications of Artificial Intelligence*, 20, 2007, 249–259.

[74] Sinou, J.-J. A review of damage detection and health monitoring of mechanical systems from changes in the measurement of linear and non-linear vibrations. *Mechanical Vibrations: Measurement, Effects and Control*, Nova Science Publishers, Inc., 2009, 643–702.

[75] Slowik, O. *Reliability-based Structural Optimization*. Master's thesis, Brno University of Technology, Brno, Czech Republic, 2014. (in Czech)

[76] SOFiSTiK AG. *SOFiSTiK Analysis Programs*, version 21.0, Oberschleissheim, Germany, 2004, http://www.sofistik.com.

[77] Spall, J.C. *Introduction to stochastic search and optimization: Estimation, simulation, and control*. John Wiley & Sons, Inc., Hoboken, New Jersey, 2003.

[78] Spencer Jr., B.F., Gao, Y., Yang, G. Distributed computing strategy for damage monitoring employing smart sensors. *Proceedings of the 2nd International Conference on Structural Health Monitoring of Intelligent Infrastructure (SHMII–2)*, Shenzhen, China, 2005, 35–47.

[79] Strauss A., Lehký, D., Novák, D., Bergmeister, K., Santa, U. Probabilistic response identification and monitoring of concrete structures. *Third European Conference on Structural Control (3ECSC)*, Vienna, Austria, 2004.

[80] STRAUSS, A., BERGMEISTER, K., LEHKÝ, D., NOVÁK, D. Inverse statistical FEM analysis – vibration based damage identification of concrete structures. *International Conference on Bridges*, Dubrovnik, Croatia, 2006, 461–470.

[81] TEUGHELS, A., MAECK, J., DE ROECK, G. Damage assessment by FE model updating using damage functions. *Computers and Structures*, 80 (25), 2002, 1869–1879.

[82] TONG, F., LIU, X.L. On training sample selection for artificial neural networks using number-theoretic methods. *Proceedings of the 4th International Conference on Engineering Computation Technology*, Lisbon, Portugal, 2004, 1–15.

[83] TP 224: *Ověřování existujících betonových mostů pozemních komunikací*. Ministry of Transport, Department for Road Infrastructure, Prague, Czech Republic, 2003 [inCzech].

[84] VOŘECHOVSKÝ, M. Correlation control in small sample Monte Carlo type simulations II: analysis of estimation formulas, random correlation and perfect uncorrelatedness. *Probabilistic Engineering Mechanics*, 29, 2012, 105–120.

[85] VOŘECHOVSKÝ, M. Hierarchical Refinement of Latin Hypercube Samples. *Computer-Aided Civil and Infrastructure Engineering*, 30, 2015, 394–411.

[86] VOŘECHOVSKÝ, M., NOVÁK, D. Correlation control in small-sample Monte Carlo type simulations I: A simulated annealing approach. *Probabilistic Engineering Mechanics*, 24 (3), 2009, 452–462.

[87] WENZEL, H., PICHLER, D. *Ambient vibration monitoring*. John Wiley & Sons Ltd., West Sussex, England, 2005.

[88] WINTERSTEIN, S.R., UDE, T.C., CORNELL, C.A. Environmental parameters for extreme response: inverse form with omission factors. *Structural Safety and Reliability: Proceedings of ICOSSAR'93*, Innsbruck, Austria, 1994, 551–557.

[89] ZADEH, L.A. Soft Computing and Fuzzy Logic. *IEEE Software*, 11 (6), 1994, 48–56.

Curriculum Vitae

Name:	**David Lehký**
Born:	September 14, 1976 in Moravský Krumlov
Address:	Institute of Structural Mechanics
	Faculty of Civil Engineering
	Brno University of Technology
	Veveří 95, 602 00 Brno
phone:	+420 541 147 363
e-mail:	lehky.d@fce.vutbr.cz

Education

- Master degree (Ing.): Brno University of Technology, Faculty of Civil Engineering, specialization *Structures and statics of building*, 1995–2000, master thesis: "Určování součinitele spolehlivosti pro betony z recyklovaného kameniva".

- Doctoral degree (Ph.D.): Brno University of Technology, Faculty of Civil Engineering, Institute of Structural Mechanics, specialization *Theory of structures*, 2000–2006, doctoral thesis: "Inverse stochastic analysis of concrete structures".

Professional positions

- 2001–2003: Structural engineer in K2 project, Ltd. Company, Brno, Czech Republic.

- 2004–now: Lecturer and research fellow at Institute of Structural Mechanics, Faculty of Civil Engineering, Brno University of Technology, Brno, Czech Republic.

Research interests

Inverse analysis, identification, artificial neural networks, genetic algorithms, structural safety and reliability, structural optimization, stochastic computational me-

chanics, Monte Carlo simulation techniques, size effect, quasi-brittle materials, fracture mechanics.

Teaching activities

Institute of Structural Mechanics, Faculty of Civil Engineering, Brno University of Technology:

- *Lectures*: Structural analysis;
- *Tutorial classes*: Basics of Structural Mechanics, Elasticity and plasticity I and II, Statics of structures I and II, Reliability of structures.

Visiting positions and courses abroad

- Bauhaus University, Weimar, Germany – Advanced Studies in Structural Engineering, 2002 (2 weeks);
- University of Natural Resources and Life Sciences, Vienna, Austria – research and teaching activities (Erasmus and Erasmus+, 2004–now), visiting lecturer (2012–now);
- Hohai University, Nanjing, China – research and teaching activities, 2016 (1 week).

Editorships and memberships

- Member of *fib* commission 2 "Safety and performance concepts";
- Member of Scientific Committee of the International Association on Life-Cycle Civil Engineering (IALCCE);
- Reviewer of the international journals: Engineering Intelligent Systems, Applied Mathematics and Computation, Journal of Infrastructure Systems, Neural Computing and Applications.

Awards and scholarships

- Scholarship of Preciosa endowment found, 2003–2004;
- GRAFO found of Brno University of Technology, Brno, Czech Republic, 2008.

International cooperation

- prof. Konrad Bergmeister, assoc. prof. Alfred Strauss, Dipl.-Ing. Dr. Roman Wendner, University of Natural Resources and Life Sciences, Vienna, Austria;
- prof. Maosen Cao, Hohai University, Nanjing, China;

- prof. Johann Kollegger, Vienna University of Technology, Austria
- Dipl.-Ing. Dr. Simon Hoffmann, Mageba, Bulach, Switzerland
- prof. Helmut Wenzel, Wenzel Consulting Engineers GmbH, Vienna, Austria

Academic activities

- Member of organizing committee of international seminar *2nd PhD. Workshop Brno – Weimar – Prague – Wien^{BOKU}*, Institute of Structural Mechanics, Faculty of Civil Engineering, Brno University of Technology, November 2003.
- Member of organizing committee of national conference *Pravděpodobnost porušování konstrukcí (PPK 2004)*, Faculty of Civil Engineering, Brno University of Technology, October 2004.
- Member of organizing committee of international conference *Life Cycle Assessment, Behaviour and Properties of Concrete and Concrete Structures (LC 2004)*, Faculty of Civil Engineering, Brno University of Technology, November 2004.
- Member of organizing committee of international conference *Non-traditional Cement and Concrete (NTCC)*, Faculty of Civil Engineering, Brno University of Technology, 2005, 2008, 2011, 2014.
- Member of organizing committee of *11th International Probabilistic Workshop (IPW11)*, Faculty of Civil Engineering, Brno University of Technology, November 2013.

Research projects

The leader of 2 research projects supported by the Czech Science Foundation, and 1 standard project of Specific University research at Brno University of Technology, member of more than 30 other project teams including 2 international projects.

List of 10 selected projects:

- Project No. 1M6840770001 of Ministry of Education, Youth and Sports of the Czech Republic, Research centre "CIDEAS", 2005–2011, *member of research team.*
- Project No. 103/07/P380 of Czech Science Foundation, "Inverse analysis of dynamically loaded structures using artificial intelligence methods", 2007–2009 (postdoc project), *principal investigator.*
- Project Eurostars No. E!4351, "Risk and Life-time analysis of concrete structures (RLACS)", 2008-2012, *member of research team.*

- Project No. 105/10/1156 of Czech Science Foundation, "Complex modeling of concrete structures: Aspects of nonlinearity, reliability, life-cycle and risk (COMOCOS)", 2010–2012, *member of research team.*

- Project No. 105/11/1385 of Czech Science Foundation, "Inverse structural reliability problems (INSREL)", 2011–2013, *member of research team.*

- Project No. TA01011019 of Technology Agency of the Czech Republic, "Simulation software tools for virtual testing of reliability and service life of concrete structures (SimSoft)", 2011–2014, *member of research team.*

- Project No. 104/13-03662S of Czech Science Foundation, "Fracture–mechanical parameters of quasibrittle materials in simulation of structural response (FRAPA)", 2013–2016, *member of research team.*

- Project No. 105/14-10930S of Czech Science Foundation, "Spatial variability degradation and damage in reliability analysis of concrete structures (SPADD)", 2014–2016, *member of research team.*

- Project No. LH14334 of Ministry of Education, Youth and Sports of the Czech Republic, "Efficient neurocomputing approaches for structural analysis and assessment", 2014–2016, *member of research team.*

- Project No. 105/15-07730S of Czech Science Foundation, "Forward and inverse reliability-based optimization under uncertainties (FIRBO)", 2015–2017, *principal investigator.*

Publications

Author and co-author of 12 papers in journals with impact factor and more than 160 scientific and technical papers, co-author of 1 chapter in book, author of 5 softwares, co-author of 1 functional sample and 1 certified methodology, h-index = 4 (WoS), h-index = 5 (Scopus).

List of 10 selected publications:

- NOVÁK, D., LEHKÝ, D. 2006. ANN Inverse Analysis Based on Stochastic Small-Sample Training Set Simulation. *Engineering Application of Artificial Intelligence*, 19, 731–740.

- LEHKÝ, D., NOVÁK, D. 2008. *Artificial Intelligence: New Research, chapter 7: ANN Inverse Analysis in Stochastic Computational Mechanics.* Randal B. Bernstein & Wesley N. Curtis (eds.), Nova Science Publishers, Hauppauge NY, USA, 323–350.

- LEHKÝ, D., NOVÁK, D. 2012. Solving Inverse Structural Reliability Problem Using Artificial Neural Networks and Small-Sample Simulation. *Advances in Structural Engineering*, 15(11), 1911–1920.

- ŠEJNOHA, M., BROUČEK, M., NOVOTNÁ, E., KERŠNER, Z., LEHKÝ, D., FRANTÍK, P. 2013. Fracture properties of cement and alkali activated fly ash based concrete with application to segmental tunnel lining. *Advances in Engineering Software*, 62–63, 61–71.

- LEHKÝ, D., KERŠNER, Z., NOVÁK, D. 2014. FraMePID-3PB Software for Material Parameters Identification Using Fracture Test and Inverse Analysis. *Advances in Engineering Software*, 72, 147–154.

- STRAUSS, A., ZIMMERMANN, T., LEHKÝ, D., NOVÁK, D., KERŠNER, Z. 2014. Stochastic fracture–mechanical parameters for the performance-based design of concrete structures. *Structural Concrete*, 15(3), 380–394.

- ZIMMERMANN, T., STRAUSS, A., LEHKÝ, D., NOVÁK, D., KERŠNER, Z. 2014. Stochastic fracture–mechanical characteristics of concrete based on experiments and inverse analysis. *Construction and Building Materials*, 73, 535–543.

- ZIMMERMANN, T., LEHKÝ, D. 2015. Fracture parameters of concrete C40/50 and C50/60 determined by experimental testing and numerical simulation via inverse analysis. *International Journal of Fracture*, 192(2), 179–189.

- ŠOMODÍKOVÁ, M., LEHKÝ, D., DOLEŽEL, J., NOVÁK, D. 2016. Modeling of degradation processes in concrete: Probabilistic lifetime and load-bearing capacity assessment of existing reinforced concrete bridges, *Engineering Structures*, 119, 49–60.

- LEHKÝ, D., ŠOMODÍKOVÁ, M. 2016. Reliability calculation of time-consuming problems using a small-sample artificial neural network-based response surface method. *Neural Computing and Applications*, doi:10.1007/s00521-016-2485-3.